Investigation of a Microglia-mediated sex dimorphism in ischemic stroke

Dissertation

zur Erlangung der Würde des Doktors der Naturwissenschaften

Fachbereich Biologie der Fakultät für Mathematik, Informatik und Naturwissenschaften

Universität Hamburg

vorgelegt von Vanessa Roth
geb. am 10.10.1991
in Lich

Hamburg, 2023

Vorsitz der Prüfungskommission: Frau Prof. Dr. Esther Diekhof

Gutachter: Herr Professor Dr. Christian Lohr

Weitere Gutachter der Dissertation: Herr Priv.-Doz. Dr. Mathias Gelderblom

Datum der Disputation: 26.02.2024

Ein Teil der hier präsentierten Ergebnisse wurde in folgenden Fachzeitschriften publiziert:

Häußler, V., Daehn, T., Rissiek, B., **Roth, V.,** Gerloff, C., Arumugam, T., Magnus, T., Gelderblom, M. Intravenous immunoglobulin (IVIg) induce a protective phenotype in microglia preventing neuronal cell death in ischaemic stroke. *Neuromol Med* 22(1), 121-132 (2020)

Piepke, M., Clausen, B., Ludewig, P., Vienhues, J., Bedke, T., Javidi, E., Rissiek, B., Jank, L., Brockmann, L., Sandrock, I., Degenhardt, K., Jander, A., **Roth, V.,** Schädlich, I., Prinz, I., Flavell, R., Kobayashi, Y., Renné, T., Gerloff, C., Huber, S., Magnus, T., Gelderblom, M. Interleukin-10 improves stroke outcome by controlling the detrimental Interleukin-17a response. *J Neuroinflamm* 18(1), 265 (2021)

Table of contents

Abstract

The significance of sex bias in vulnerability to, severity of, and recovery from ischemic stroke is increasingly being recognised. However, knowledge about cellular drivers of sex dimorphism is limited. By implementing a microglia cell-specific CNS depletion via the Cx3Cr1-iDTR system, we confirmed a crucial involvement of female but not male microglia in mitigating tMCAO, an animal model of ischemic stroke. By microglia-specific RNA profiling, we found a pronounced activated phenotype in female cells at early stages, whereas male microglia showed longer latency to adopt an activated phenotype. Notably, female microglia affected both, post-stroke neutrophil infiltration and lesion size. Furthermore, our study implicates distinct metabolic capacities of female and male microglia as a potential mechanism behind the observed sex specific differences in the post-ischemic CNS. Consequently, bolstering the metabolic capacities of male microglia might promote a similar protective phenotype as we were able to observe in females and may hence provide a new therapeutic option in stroke.

Zusammenfassung

Die Bedeutung eines geschlechtsspezifischen Aspekts in der Anfälligkeit, im Schweregrad und der Genesung nach einem ischämischen Schlaganfall wird zunehmend anerkannt. Allerdings ist das Wissen über zelluläre Treiber dieses Geschlechtsdimorphismus aktuell noch sehr begrenzt. Durch die Implementierung einer mikrogliazellspezifischen ZNS-Depletion mittels Cx3Cr1-iDTR-System bestätigten wir eine entscheidende Beteiligung weiblicher, jedoch nicht männlicher Mikrogliazellen an der Linderung von tMCAO, einem Tiermodell des ischämischen Schlaganfalls. Durch mikrogliaspezifisches RNA-Profiling fanden wir in weiblichen Zellen in frühen Stadien einen ausgeprägten aktivierten Phänotyp, wohingegen männliche Mikroglia eine längere Latenzzeit zeigten, um einen aktivierten Phänotyp anzunehmen. Bemerkenswerterweise beeinflussten weibliche Mikroglia nicht nur die Läsionsgröße, sondern auch die Infiltration von Neutrophilen nach einem Schlaganfall. Darüber hinaus deutet unsere Studie darauf hin, dass unterschiedliche Stoffwechselkapazitäten weiblicher und männlicher Mikroglia ein möglicher Mechanismus hinter den beobachteten geschlechtsspezifischen Unterschieden im postischämischen murinen ZNS sind. Folglich könnte die Stärkung der Stoffwechselkapazitäten männlicher Mikroglia einen ähnlichen schützenden Phänotyp fördern, wie wir ihn in weiblichen Tieren beobachten konnten, und somit möglicherweise eine neue Therapieoption bei Schlaganfällen bieten.

1. Introduction

Stroke is the second most common cause of death in Germany (Plass et al., 2014; Busch & Kuhnert, 2017) and a leading cause of death and disability worldwide (Saini et al., 2021). Sex differences and their underlying mechanisms are increasingly being recognised as a crucial aspect in discerning the pathophysiology of various diseases and advancing corresponding treatment options for both, women and men. Currently, an understanding of the cellular mechanisms involved in creating and maintaining sex dimorphism in stroke is lacking. In light of this, our study focussed on elucidating the role of microglia in mediating sex bias during the early post-stroke phase with special emphasis on identifying prospective treatment opportunities.

This introductory chapter serves two main purposes: Firstly, to explicate the pathophysiology of ischemic stroke and known mechanisms underlying sex dimorphism; and secondly, to establish the main aims of this study.

1.1 Ischemic stroke

Based on aetiology, stroke can be broadly subdivided into the following two categories: Haemorrhagic stroke is due to bleeding into the brain by blood vessel rupture; ischemic stroke occurs when blood supply to the brain is corrupted due to acute vessel occlusion by a blood clot. Globally, approximately 70% of all occurring strokes are ischemic in origin (Feigin et al., 2018) and in Germany, 80-85%.

The ischemic stroke unfolds as follows: Upon cessation of blood supply, the hypoperfused central nervous system (CNS) area is rapidly and progressively turned into irreversibly injured tissue commonly referred to as the ischemic core (Mao et al., 2022). The surrounding tissue, the so-called ischemic penumbra, however, is potentially salvageable by reperfusion: If blood supply is reinstated quickly enough, penumbral tissue can recover normal function; otherwise, it will also be irreversibly lost. The amount of sustained initial clinical deficit in stroke patients thus crucially depends on salvaging the penumbra (Baron, 2018). Accordingly, restoring CNS blood supply as quickly as possible is paramount in the treatment of stroke patients. To this end, current treatment options comprise administration of tissue plasminogen activator (tPA) to induce thrombolysis, i.e. medically induced breakdown and dispersion of blood clots, and/or endovascular thrombectomy, i.e. mechanical removal of the thrombus (Qiu & Xu, 2020). However, crucially, for stroke patients to benefit from reperfusion therapy, time is of the essence: To effectively reduce disability, intravenous thrombolysis must be administered within 4.5 h (Emberson et al., 2014) and thrombectomy needs to be performed within 24 h (Olthuis et al., 2023; Sarraj et al., 2023) of stroke onset. Thus, to maximise their therapeutic benefits, both treatment options are critically time-dependent.

Clinically, incurred disability depends on the localisation of infarcted CNS tissue and, thus, the localisation of cerebrovascular occlusion (Fig. 1.1). Most commonly, the middle cerebral artery (MCA) is affected in acute ischemic stroke. Depending on location and occlusion severity, symptoms may vary and comprise contralesional hemisensory loss and hemiparesis of the face, upper and lower extremities, speech impairments (e.g. aphasia), visual disorders, and perceptual deficits.

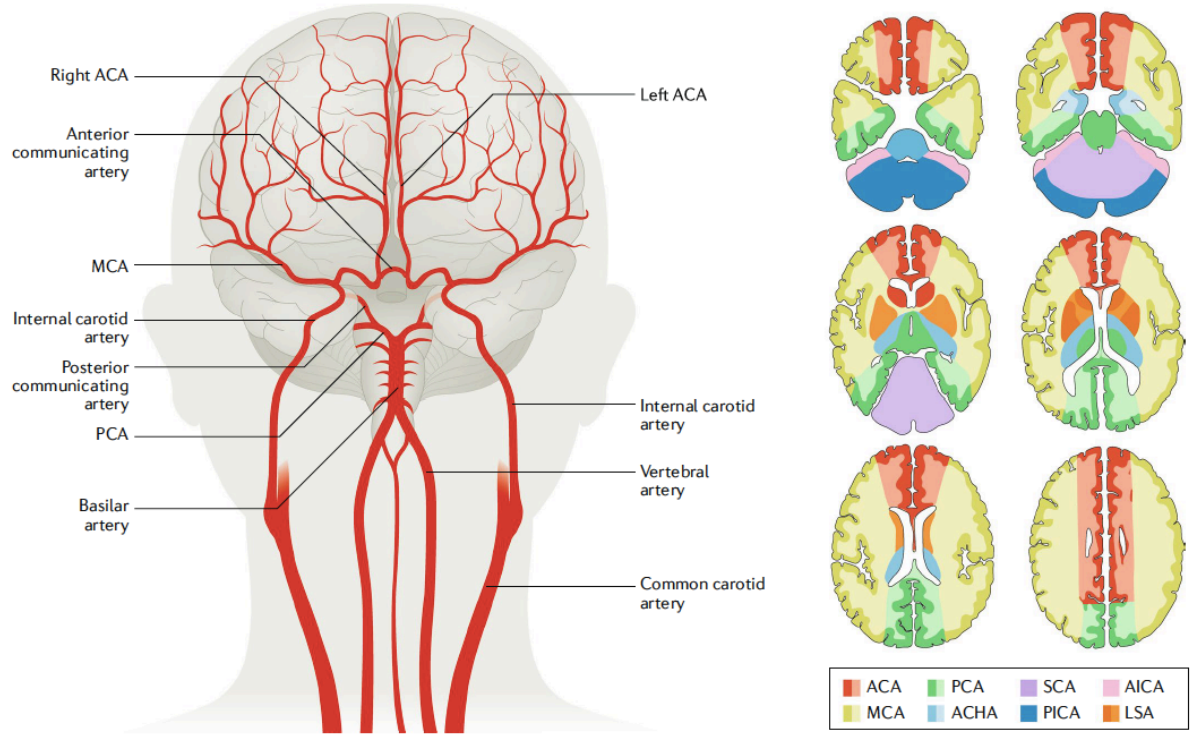

Figure 1.1 | CNS vasculature. A schematic overview of the major cerebral arteries (left) and their respective supply areas (right), illustrating where tissue damage could occur in case of vessel occlusion. ACA, anterior cerebral artery; ACHA, anterior choroidal artery; AICA, anterior inferior cerebellar artery; LSA, lenticulostriate artery; MCA, middle cerebral artery; PCA, posterior cerebral artery; PICA, posterior inferior cerebellar artery; SCA, superior cerebellar artery. Taken from Campbell et al., 2019.

In the following, the pathophysiology of ischemic stroke will be outlined by 1. elucidating the cellular and molecular consequences of glucose and oxygen deprivation, and 2. delineating blood-brain barrier (BBB) disruption and inflammation dynamics in the injured CNS.

1.1a Oxygen and glucose deprivation

As an immediate consequence of ischemic stroke, the affected CNS area is no longer sufficiently supplied with oxygen and glucose, both of which are essential for healthy cellular functioning and survival. In fact, glucose is the main energy source of the mammalian brain, and while the CNS only makes up 2% of the human total body mass, it nonetheless accounts for 20% of total oxygen and

approx. 60% of glucose metabolism, making the CNS the largest source of energy consumption in the human body (Clark & Skololoff, 1999). At the same time, the CNS has only limited capacity for glucose storage and reserve (Ames, 2000), and is thus crucially dependent on its continuous uptake from the blood. Accordingly, disruption in blood supply has dramatic consequences within the CNS: It effectively thwarts the cells' most effective ways of generating energy (Bertram et al., 2006).

The most important form of chemical energy in all cells is the nucleotide coenzyme adenosine triphosphate (ATP), also poignantly referred to as the "molecular unit of currency" in intracellular energy transfer. Upon its consummation in metabolic processes, ATP is converted to either adenosine diphosphate (ADP) or adenosine monophosphate (AMP). On the flip side, ATP can be regenerated from ADP by rephosphorylation via ATP synthase. The most productive way of generating ATP is via cellular respiration, a process which essentially consists of three pathways: glycolysis, the citric acid cycle (also: tricarboxylic acid (TCA) or Krebs Cycle), and oxidative phosphorylation (see Fig. 1.2).

Glycolysis refers to the metabolic pathway that converts glucose to pyruvate in a sequence of enzymatic reactions. It is a catabolic process and the resultant energy is used to generate ATP. Glycolysis can be separated into two phases: an initial investment phase where ATP is consumed, and a subsequent pay-off phase where ATP is generated. The net gain of ATP via glycolysis is two ATP molecules per glucose. Glycolysis occurs in the cytosol of the cell. Glucose is taken up by cells via specialised membrane proteins, so-called glucose transporters, by passive-mediated diffusion. As such, the transport of glucose across the membrane does not require ATP (Wheeler, 1989).

Notably, the fate of pyruvate resultant from glycolysis depends on the presence or absence of oxygen: When oxygen is present, it is converted into acetyl-coenzyme A (acetyl-CoA) which in turn is used as the starting material for the citric acid cycle. The resulting molecules will in turn be used by the electron transport chain to create further ATP by oxidative phosphorylation. On the other hand, in the absence of oxygen, pyruvate will instead undergo fermentation and be reduced into lactate (anaerobic glycolysis; Rivoal & Hanson, 1994).

Oxidative phosphorylation is the process by which most cellular ATP is generated. It takes places in the mitochondria and is energetically coupled to a proton gradient across the inner mitochondrial membrane. These gradients are established by electron transport chains and are used to drive the phosphorylation of ADP for ATP synthesis. Importantly, oxidative phosphorylation relies on the presence of oxygen, and as such, the main source of energy in the cell is only viable under aerobic conditions (Bertram et al., 2006).

In light of this, it becomes apparent why ischemic stroke plays out as a major pathophysiological event in the CNS: On the one hand, stroke-induced hypoxia prevents ATP production by oxidative phosphorylation, thus facilitating and aggravating a situation of unmet cellular energy demands. As a

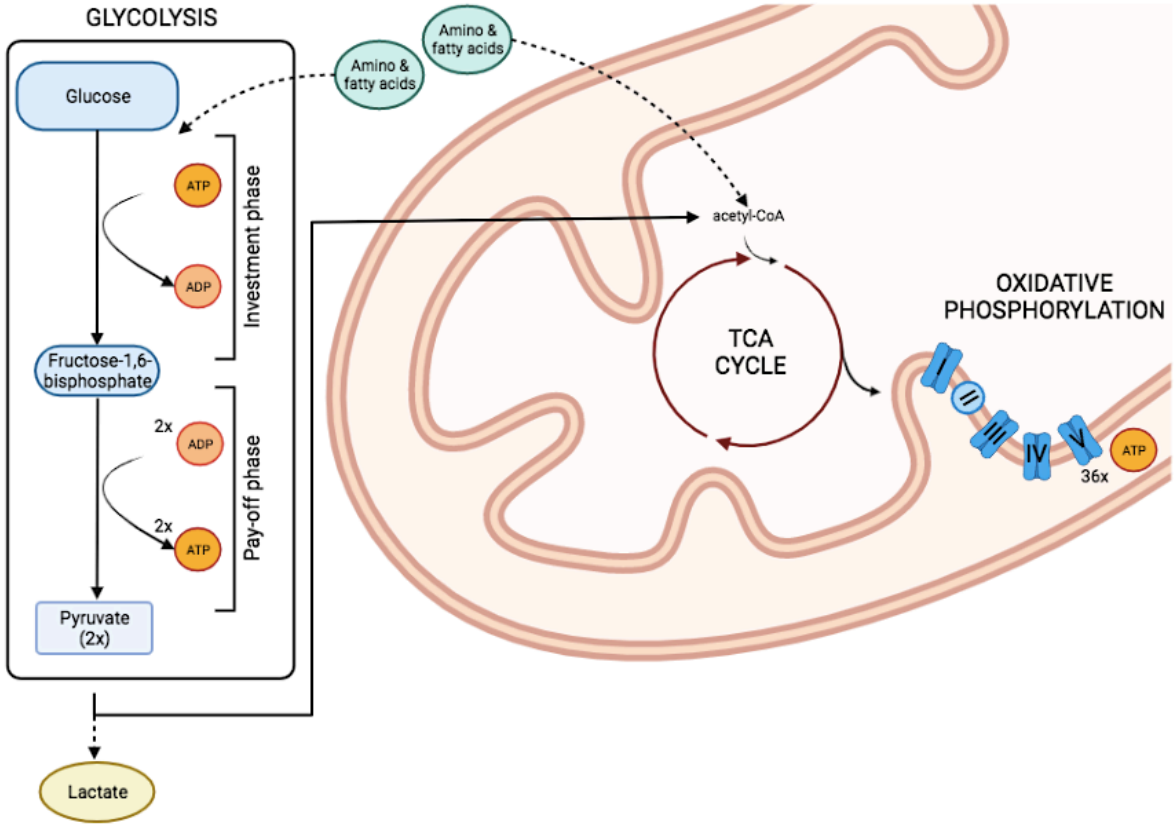

Figure 1.2 | Cellular respiration. Schematic overview of ATP generation by glycolysis (left), TCA cycle and oxidative phosphorylation (right), illustrating main checkpoints, end and/or intermediate products, and supplementing fuel sources in cellular respiration. acetyl-CoA, acetyl-Coenzyme A; ADP, adenosine diphosphate; ATP, adenosine triphosphate; TCA, tricarboxylic acid.

response, an option to generate ATP in the absence of oxygen is anaerobic glycolysis. However, while anaerobic glycolysis allows for upkeep of ATP synthesis, it is less efficient than cellular respiration, generating only two ATP molecules per consumed glucose. Nonetheless, despite its inefficiency, it is a rapid process and will generate ATP approx. 100 times faster than oxidative phosphorylation (Pfeiffer et al., 2001). Accordingly, in situations of acute energy demand, anaerobic glycolysis can present a viable option to synthesise ATP. In the long run, however, cellular energy demands will exceed ATP generation rates by anaerobic glycolysis, thus, eventually, causing cells to undergo cell death (Fricker et al., 2018).

On the other hand, aerobic just as well as anaerobic glycolysis requires the presence of energy metabolites to be used as fuel source, and glucose, the main source in the CNS, is scarce in ischemic stroke. There are, however, some alternative fuel sources to either generate glucose from or substitute other metabolites in the cellular respiration chain to maintain its function: For instance, glycogen can be broken down to generate glucose, and ketone bodies can be used to replace it (Gotoh et al., 2017; García-Rodríguez et al., 2021). Alternatively, pyruvate and acetyl-CoA can be generated from amino or fatty acids and fed into the citric acid cycle, thereby maintaining oxidative phosphorylation (Bertram et

al., 2006). However, amino acid degradation and the depletion of protein stores can also have adverse effects on the cell, especially if prolonged over time (Thiebaut et al., 2019). Consequently, in the absence of glucose, cellular functioning will eventually be corrupted.

Thus, in summary, oxygen and glucose deprivation will challenge cellular energy metabolism in the CNS their own right as well as synergistically: Stroke-induced hypoxia inhibits oxidative phosphorylation, the most potent cellular source of ATP synthesis. Additionally, absence of glucose as the main CNS metabolite for glycolysis forces cells to utilise other cellular substrates to meet their bioenergetic demands. Due to their high energy requirements neurons are especially susceptible to glucose and oxygen deprivation (Watts et al., 2018), but glia and other resident cells are also implicated and affected (Gouix et al., 2014). Ultimately, cells that are not able to generate sufficient ATP will not be able to maintain their cellular functions and a fatal cascade of ionic impalance, chronic membrane depolarization, calcium (Ca^{2+}) overload and abarrent, excitotoxic glutamate release is initiated (Belov Kirdajova et al., 2020). In this way, ischemic stroke causes CNS cells to degenerate and die.

1.1b BBB breakdown and CNS inflammation

The BBB represents a physical and biochemical shield of specialised microvascular endothelial cells (ECs) that prevent non-selective passage of solvents from circulating blood into the CNS. It thus serves as an important barrier between the CNS and its surroundings and helps to establish and maintain the highly sensitive intracerebral ion and substrate homeostasis to ensure proper CNS functioning. The development and continuity of the BBB does not only rely on ECs, but depends on the presence and support of pericytes, astrocytes, neurons, microglia, and basal lamina (also: extracellular matrix, ECM), which are collectively called the neurovascular unit (NVU; see Figure 1.3). Under physiological conditions, the NVU regulates haemodynamics and controls the influx and efflux of substrates in the CNS in response to its needs (Yu et al., 2020).

A major pathophysiological feature of stroke is the disruption of BBB integrity which is initiated by ischemia and aggravates with sustained hypoperfusion. This deterioration is largely due to nutrient and oxygen deprivation and concomitant structural disintegration of tight junctions, endothelial and ECM damage, and constitutively results in an increase in BBB permeability. Elevated permeability occurs within minutes to hours of initial vascular insult (Khatri et al., 2012) and was shown to persist for up to several weeks (Strbian et al., 2008; Meral et al., 2017). The initial breakdown of the BBB is thought occur due to ionic dysbalance and an accumulation of intracellular Na^+ which causes endothelial cells to swell and the BBB to be disrupted (Abdullahi et al., 2018). Additionally, as Na^+ accumulates intracellularly, Ca^{2+} removal from the cell via Na^+/Ca^{2+} exchanger (NCX) breaks down. Concomitant failure of the Ca^{2+} ATPase due to the stroke-associated lack of ATP further exacerbates intracellular

Ca^{2+} accumulation. Elevated levels of intracellular Ca^{2+} concentrations are known to adversely impact mitochondrial function, and facilitate reactive oxygen species (ROS) generation and cell death (Vazana et al., 2016), thus aggravating BBB disruption. Additionally, an overexpression of metalloproteases (MMPs) is also considered a key factor in BBB disintegration as they directly degrade tight junction proteins and ECM components (Yang et al., 2011). Once structural integrity of the BBB is sufficiently lost, CNS entry of macromolecules such as proteins and peripheral cells can no longer be regulated and prevented. Additionally, intracerebral cells such as microglia release pro-inflammatory signals like nitric oxide (NO) and inflammatory cytokines which also increase BBB disruption and permeability and, moreover, attract peripheral immune cells to the CNS (Xing et al., 2012; Liu et al., 2017; Kabba et al., 2018). Thus, a neuroinflammatory cascade is initiated with peripheral immune cells entering the CNS extracellular space. The beneficial and adverse aspects of post-stroke inflammation are currently still controversially debated, but the overall consensus transpires as a net detrimental impact on stroke outcome. In the following, the most important immune cell populations will be introduced and their role in post-stroke neuroinflammation will be elucidated.

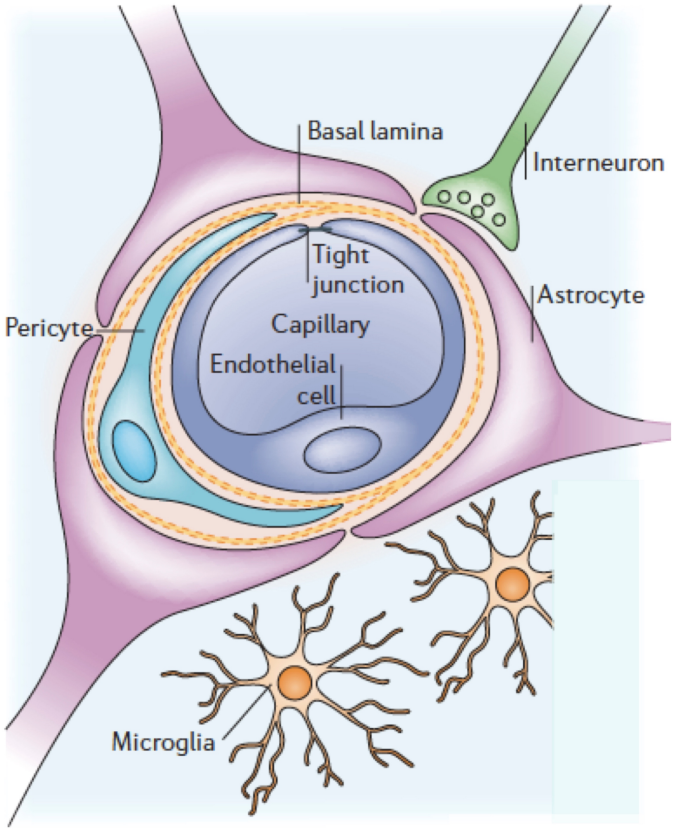

Figure 1.3 | **Neurovascular unit.** Schematic overview of a capillary cross-section showing all relevant cells involved in establishing the NVU: The CNS vessel is lined by endothelial cells that form tight junctions to restrict diffusion and insulate the vessel. A continuous basal lamina surrounds the endothelial layer and interspersed pericytes. Parenchymal astrocytes extend their processes to establish communication with their surroundings, further enclosing the vessel. Interneurons are able to affect vessel tone in accordance with neuronal signals. Microglia continuously survey their environment to quickly sense and respond to perturbances. Taken and adapted from McConnell et al., 2017.

1.1c Inflammation

Immune cells involved in the inflammatory reaction occurring after an ischemic insult can be subdivided into CNS resident and infiltrating populations. Their activation and proliferation dynamics might differ considerably (see Fig. 1.4 for an overview) and their functional involvement in stroke is still not entirely and conclusively unravelled. Nonetheless, the most important cell types and their respective functions shall be introduced.

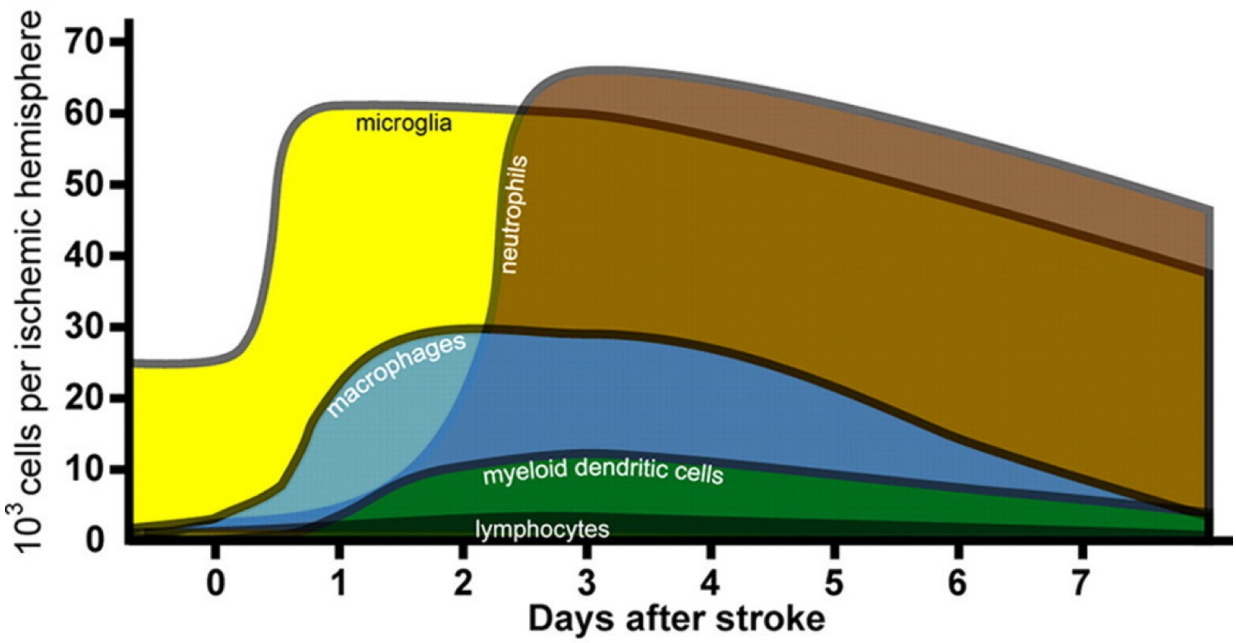

Figure 1.4 | Temporal immune cell dynamics within the first week after stroke. Accumulation of different immune cell populations in the ipsilesional hemisphere at different time points after ischemic stroke. Taken from Gelderblom et al., 2009.

Resident cells

Microglia are the tissue-resident macrophage population of the CNS and the main immune-competent cell type in the brain. They have been shown to arise from the yolk sac during embryonic development (Ginhoux et al., 2010; Kierdorf et al., 2013), while recent studies also highlight the possibility of circulating monocytes to infiltrate the CNS and adopt a microglia-like phenotype (Karlen et al., 2018; Lund et al., 2018). Microglia are remarkably long-lived cells with an annual turnover rate of 28% in humans (Rau et al., 2017) and corresponding low rates in mice (Füge et al., 2017). Their activation can be induced in two ways: Either inhibitory signals from surrounding neurons are lost, or through sensing of damage-associated molecules; both activating mechanisms are possible and prevalent in ischemic stroke (Szepesi et al., 2018; Wang et al., 2018). Once activated, microglia have been shown to serve several different functions throughout both the innate and subsequent adaptive immune response. A main function is to engulf and kill invading microorganisms and to dispose of pathogens, infected cells

and cellular debris, thus serving as an immunological first line of defence (Li et al., 2020). In addition to their phagocytic capacities, they are also known to orchestrate immune responses by inducing inflammation and producing inflammatory mediators that activate and recruit other immune cells to the CNS (Fenn et al., 2014). Their involvement is thus not only critical in providing an immediate protective function via phagocytosis, but also in instigating and mediating an extending immune response.

Infiltrating cells

Neutrophils are the most numerous cells of the innate immune response and have been shown to enter the CNS within the first few hours after ischemic stroke, making them the first peripheral immune cell population to enter the brain. They mature in the bone marrow, and infection or inflammation triggers their increased production and migration into the affected tissue. Their numbers in the CNS peak between 1-3 d after stroke (Cai et al., 2020), but since they are short-lived, they survive only a few hours to days (Brostjan et al., 2020). Their main function is tissue clearance via phagocytosis. However, in stroke, their involvement was shown to be largely detrimental: Neutrophils release neurotoxic substances such as ROS and metalloproteinases (e.g. MMP9), aggravating neuronal demise and BBB disruption (Shimakura et al., 2000; Garcia-Bonilla et al., 2014; Zhu et al., 2018; Chen et al., 2018).

Blood-derived **monocytes** enter the CNS around 3-4 h after ischemic insult (Garcia et al., 1994) and their numbers peak between 2-7 d after stroke. They are able to differentiate into specialised immune cells, namely macrophages and dendritic cells (DCs), but are also able to exert specific functions themselves. Monocytes participate in both innate and adaptive immune responses and their main functions comprise phagocytosis, antigen presentation, and cytokine production. While it was originally believed that the presence of monocytes exacerbated ischemic injury (Chen et al., 2003), more recent studies on monocyte depletion showed an aggravation of tissue damage due to destabilised brain microvasculature (Gliem et al., 2012). In sum, their impact in stroke currently remains ambiguous (Han et al., 2020; Pedragosa et al., 2020; Werner et al., 2020).

DCs start to accumulate in the CNS at 24 h after stroke (Gelderblom et al., 2018; Felder et al., 2010). They are heterogeneous immune cell population with tissue-specific functions (Schlitzer et al., 2015) centering around antigen presentation and facilitating the adaptive immune response. Certain subtypes of DCs were shown to be protective in stroke (Gallizioli et al., 2020), but overall, their distinct involvement remains incompletely understood. DC infiltration reportedly peaks at 72 h after stroke (Gelderblom et al., 2009).

Lastly, as part of both the innate and adaptive immune response, lymphocytes migrate into the CNS after the first 24 h after stroke. Interestingly, certain lymphocyte populations can still be detected even weeks post-stroke (Shi et al., 2021). Lymphocytes can be further subdivided into **T cells**, **B cells**, and

natural killer (**NK**) **cells**; moreover, an additional hybrid population of **NK T cells** exists as well.

As part of the innate immune response, NK cells broadly act as eliminators of pathogens or corrupted cells via their cytolytic capacity. More recently, they were also shown to participate in adaptive immune memory formation (Sun et al., 2009). As suppressing NK cell entry into the CNS was shown to be protective in ischemic stroke (Li et al., 2021), their net involvement in stroke is believed to be detrimental.

B cells, one of the central players of the adaptive immune response, are responsible for humoral immunity. As such, they produce antibodies directed against pathogens and toxins, and can function as antigen-presenting cells. Their role in stroke remains ambiguous: Conflicting studies described both, detrimental (Becker et al., 2016) and ameliorative effects (Doyle et al., 2015; Ortega et al., 2020) of B cells on stroke recovery. Most likely, their specific involvement depends on intricate temporal activation patterns which to date remain insufficiently understood. Broadly, during early post-stroke phases B cells seem to mainly function as cytokine producers and as such, exert ameliorate effects through the release of the anti-inflammatory cytokine interleukin (IL) 10 (Ren et al., 2011; Chen et al., 2012). However, emerging evidence highlights the involvement of B cells in post-stroke cognitive decline during chronic phases, presumably due to B cells producing brain-reactive antibodies disturbing neuronal function (Doyle et al., 2015; Doyle et al., 2017).

The second key player of adaptive immunity is the T lymphocyte population, which can be further subdivided into the $\alpha\beta$ (conventional) and $\gamma\delta$ (unconventional) **T cells** subset according to their respective heterodimeric makeup. $\gamma\delta$ T cells were shown to infiltrate early into the ischemic CNS where they significantly exacerbate tissue damage via the release of the neurotoxic cytokine IL-17 (Gelderblom et al., 2012; Meng et al., 2019). However, $\gamma\delta$ T cells make up only a small subset of the overall T lymphocyte population. More generally, T cells are responsible for cell-mediated immunity; their main functions are either cytotoxicity or facilitation and regulation of immune functions. While certain subtypes of T cells (namely regulatory T cells, Tregs) have indeed been shown to exert protective effect in stroke (Liesz et al., 2009), their overall involvement in stroke is nonetheless believed to be detrimental to stroke recovery (Yilmaz et al., 2006; Kleinschnitz et al., 2010). Importantly, T cells require signals to infiltrate the CNS. These signals may be provided by microglia either directly through the release of pro-inflammatory cytokines, or indirectly through chemoattraction of T lymphocyte-attracting peripheral myeloid cells.

Lastly, as a unique hybrid subset of T cells, **NK T cells** express both the T cell receptor (TCR) as well as NK cell lineage receptors, thus acting as a bridge between innate and adaptive immunity. Since NK T cells are able to rapidly and excessively release cytokines, their role in post-stroke immunomodulation is increasingly being recognised. Mounting evidence points toward an immunosuppressive function of NK

T cells via the release of IL-10 (Wong et al., 2011; Wong et al., 2017). Other studies, however, only reported marginal effects of NK T cells on the ischemic brain during the early post-stroke phase (Kleinschnitz et al., 2010).

In summary, while it is clear that the immune response plays an important role in post-stroke recovery, the intricate and complex dynamics of different cells, their distinct functional subsets and temporal activation patterns complicate our understanding of immune processes in stroke.

1.2 Sex dimorphism in ischemic stroke

Sexual dimorphism of the CNS refers to sex-specific characteristics in female and male brains that differ between the biological sexes. It is currently not sufficiently understood what, exactly, the root cause of sex dimorphism is, but it is most likely the consequence of an interplay between a range of factors including hormonal, cellular, and regional brain differences. Additionally, more recently, the molecular foundation of sex dimorphism has increasingly been recognised and unravelled by gene expression studies. One such study revealed that in the human brain, the cerebellum appeared to be the least sexually dimorphic, whereas hippocampus and spinal cord harboured the strongest sex-related divergence in gene expression of all 13 investigated CNS regions (Oliva et al., 2020). Moreover, sex bias in disease susceptibility has increasingly been noted: Women were observed to be more commonly afflicted by adult-onset disorders such as Alzheimer's disease (AD), multiple sclerosis, or major depressive disorder, whereas men appeared to be more susceptible to developmental onset disorders such as schizophrenia or autism (Lee et al., 2022). In terms of sex bias in treatment response, the literature is thus far not conclusive but tentatively purports sex as an influencing factor on treatment efficacy (Li et al., 2017; LeGates et al., 2019). A potential reason for this observation might be the increasingly recognised sexual dimorphism in immune cells between women and men. For instance, female immune cells mounted a stronger pro-inflammatory response, whereas male immune cells showed stronger accumulation and proliferation of several immune cells (macrophages, neutrophils, DCs) after lipopolysaccharide (LPS) stimulation (Klein et al., 2016). Additionally, a further complication arises due to the more recent observation that age plays an important role in modulating the immune cell-related sex dimorphism: Male immune cells reportedly showed earlier and stronger age-related epigenetic changes compared to the corresponding female cell population (Márquez et al., 2020).

To summarise, sex bias differentially affects not only disease susceptibility but potentially treatment efficacy as well. In light of this, sex dimorphism, its underlying mechanisms on the one hand and impact on pathophysiology on the other, are an increasing focus of interest in recent research. In the following,

sex-specific characteristics of microglia cells and the role of sex bias in stroke will be further illuminated.

1.2a Sex dimorphism and microglia

Microglia play an important role in both, CNS health and disease (Li et al., 2018). They are known to not only interact with neurons and other glia cells, but to also establish and maintain the structural integrity of the developing and adult CNS via their involvement in synaptic pruning, neuronal wiring, myelogenesis and vascularisation. Due to their ubiquitous presence and functional versatility, microglia have attracted more and more attention in recent research. As a result, sex dimorphism in microglia cells has also increasingly been recognised and was observed in cell maturation (Lenz et al., 2015; Hanamsagar et al., 2017), brain colonisation patterns (Schwarz et al., 2012), and response to disease cues (Villapol et al., 2017). Moreover, the role of microglial sex dimorphism in metabolic functioning has lately come into focus as metabolic dysregulation is a central aspect of many CNS pathologies. Interestingly, a recent study was able to demonstrate that microglia are able to utilise different mitochondrial fuel sources to meet their functional energy demands (Bernier et al., 2020). A sex bias in metabolic functioning was described in disease conditions, where microglia from female from AD mice showed an increase in glycolysis with concomitant exacerbation of an activated phenotype (Guillot-Sestier et al., 2021). The pivotal importance of an operational microglia metabolism for CNS functioning was further emphasised by recent studies showing that the reversal and restoration of age-induced metabolic impairments in microglia cells effectively abolished cognitive decline (Lu et al., 2021; Minhas et al., 2021).

1.2b The role of sex dimorphism in stroke

The significance of sex bias in stroke is increasingly being recognised. In both human and animal stroke studies, females were shown to be less severely affected than males as is reflected in smaller infarct sizes and lower incidence in females. Crucially, however, due to the increased life expectancy of women, the prevalence of stroke in patients above the age of 85 increased two- to threefold in women compared to men (Howard et al., 2005). Women were also shown to suffer from poorer stroke outcomes, sustaining more often lasting disability and mood disorders (Di Carlo et al., 2003). On the other hand, and seemingly contradictorily, women were found to benefit more from tissue plasminogen activator (tPA) treatment than men (Kent et al., 2005; Lorenzano et al., 2013). Taken together, we see an increasing need to account for and understand sex dimorphism in disease aetiology as well as treatment options to facilitate individual recovery after stroke. The underlying mechanisms establishing and influencing a sex dimorphism in stroke include genetic, hormonal, anatomic, and immune system-related factors. For instance, gene expression analyses have revealed sex-specific differences in genes

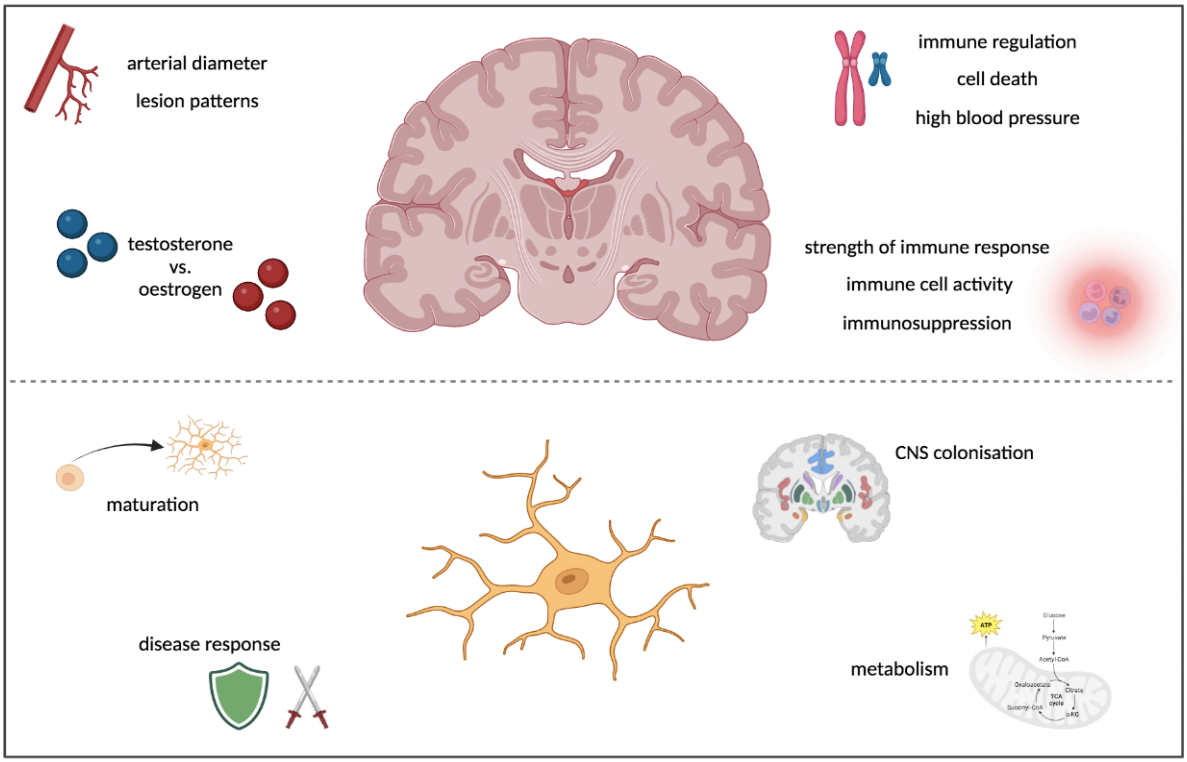

Figure 1.5 | Visual summary of sex dimorphism. Most important aspects of sex dimorphism in the CNS (top) and microglia (bottom).

involved in immune regulation, inflammation, and cell death (Tian et al., 2012). Moreover, high blood pressure, a known risk factor for stroke, was shown to be partially related to genes on the Y chromosome (Charchar et al., 2002).

The most relevant hormonal difference between women and men concerns steroid hormones, i.e. oestrogen, progesterone, and testosterone, typically with higher oestrogen levels in (pre-menopausal) women and higher testosterone levels in men. Oestrogen was shown to influence the CNS circulation system, specifically cerebrovascular flexibility, cerebral blood flow, and BBB function, and was found to ameliorate atherosclerosis (Kavanagh et al., 2009), a main cause for ischemic stroke. Testosterone, on the other hand, was found to increase the expression of genes associated with inflammation, BBB damage, and apoptosis (Cheng et al., 2007).

Anatomic features were also found to differ between the sexes: Generally, women have smaller arteries than men, which puts them at a higher risk for worse stroke outcomes (Davison et al., 2018). In fact, vascular differences might influence a variety of sex-specific phenomena: One recent study found sex-specific lesion patterns in stroke, which were linked to worse stroke recovery in women (Bonkhoff et al., 2021). On the other hand, larger body size naturally correlated with an enlargement of the left cardial atrium, which, in turn, constitutes a risk factor for stroke (Abhayaratna et al., 2006).

Lastly, sex-specific aspect in the immune response of women and men also exert relevant influences on stroke progression and outcome. Animal studies showed a stronger immune response in females, which

resulted in a more efficient CNS clearance, and thus, favourable outcomes (Klein et al., 2012). Concomitantly, different immune cell populations from females were shown to be more functionally active than their male counterparts (Xia et al., 2009). Interestingly, in human studies, the immunosuppressive IL-10 was shown to be higher in women compared to men 24 h after stroke and associated with worse outcomes (Conway et al., 2015).

In sum, the picture of sex dimorphism in stroke to date remains largely incoherent and complex. All discussed factors situate sex dimorphism as a multi-layered phenomenon that is not readily understood. At the same time, seeing as sex bias exerts a relevant effect on stroke incidence, treatment and recovery, disentangling its intricacies remains exceedingly important.

1.3 Aims of this study

Sex dimorphism simultaneously presents as a problem by affecting disease incidence, pathophysiology, and treatment efficacy, but at the same time as an opportunity if accounted for and utilised advantageously. Currently, albeit insufficiently understood, sex dimorphism in the CNS is seen as a multifaceted phenomenon, established and maintained by different genetic, hormonal, anatomic, and cellular mechanisms. In stroke, sex dimorphism has long been noted but to date not been utilised to facilitate treatment. This is where this project draws on: Broadly speaking, our aim was to understand sex dimorphism in stroke in hopes of identifying potential treatment options and facilitating post-stroke recovery. To this end, we first needed to identify and validate a potent mechanistic setscrew of sex dimorphism in stroke. We settled on microglia cells as a viable target as they are not only implicated in sex dimorphism but also crucially involved in stroke pathophysiology. Next, we conducted mechanistic analyses to elucidate how microglia are able to mediate sex bias in stroke outcomes by analysing their role in the post-stroke inflammatory response and, more broadly, their overall functional activity in the early post-stroke phase. Lastly, we attempted to bridge the translational gap by comparing and relating our findings to data generated from human stroke patients.

2. Material and methods

2.1 Material

2.1.1 Laboratory equipment

Table 2.1 | General laboratory equipment

Instrument	Model	Manufacturer
Agilent Bioanalyzer 2100	ImageQuant LAS 4000 Mini	GE Healthcare
Anaesthesia induction chamber	6-2451	neoLab
Centrifuge	5417R 5417C Heraeus Multifuge 3 L	Eppendorf Eppendorf Thermo Electron Corporation
Cryostat	NX50	Thermo Scientific
Electrophoresis Chamber	Wide Sub-Cell GT Systems	Bio-Rad
Electrophoresis power supply	Blue Power 500	SERVA Electrophoresis GmbH
Flow cytometers	LSRFortessa Aria IIIu	BD Biosciences
Homogenisator	Pellet Pestles 749540-0000	Sigma-Aldrich
Incubator	Inc153	Memmert GmbH
LED transilluminator	UVT-14-BE-LED	Carl Roth GmbH
Micropipette	3, 10, 20, 100, 200, 1,000 µl	Sartorius
Microscope	Leica/Wild M3Z Nikon Eclipse Ts2	Leica Microsystems Nikon Instruments
Microwave oven		SHARP
Neubauer haemacytometer	Marienfeld	Henneberg-Sander GmbH
Perfusion system	Pumpdrive 5201	Heidolph Instruments
pH-meter	SevenCompact	Mettler Toledo
Pipetgirl and pipetboy pipette controller		Integra
Piston pump	REGLO-CFP Analog	Ismatec
Pulse oximeter	MouseSTAT	Kent Scientific Corporation
Refrigerators / freezer	4 °C Freezer Liebherr Comfort -20 °C Sanyo VIP -86 °C Series Ultra-Low Temperature Freezer	Robert Bosch GmbH Liebherr International GmbH Panasonic Healthcare Corporation

Rotating Wheel		GLW Storing Systems GmbH
Scale	ME53	Mettler Toledo
Scanner	PJ790	Sony
Shaker	KS125 basic	IKA Labortechnik
Spectrophotometer	NanoDrop 2000 uQuant Microplate Reader	Thermo Fisher Scientific BioTek Instruments Inc.
Sterile hood	Safe 2020	Thermo Fisher Scientific
Thermo Shaker	Eppendorf Comfort 5355	Sigma-Aldrich
Thermocycler	FlexCycler^2 ABI PRISM 7900HT Sequence Detection System	Analytik Jena AG Thermo Fisher Scientific
Vortex mixer	REAX 2000	Heidolph
Water bath	GLS400	Grant
Water purification system	Millipore purification system	Millipore GmbH

2.1.2 Chemicals and reagents

2.1.2a Reagents for animal experiments

Table 2.2 | Chemicals and reagents used in animal experiments

Reagent	Company
Diphtheria toxin	Merck Millipore
Tamoxifen	Sigma-Aldrich
Corn oil	Sigma-Aldrich
Sodium chloride (NaCl)	Braun
Paraformaldehyde (37%)	Carl Roth GmbH
Rompun™	Bayer
Saccharose	Sigma-Aldrich
Ketanest® S	Pfizer Pharma
Isoflurane	Baxter
Tramadol	ALIUD Pharma
Buprenorphine	Arevipharma

2.1.2b Reagents for histology

Table 2.3 | Chemicals and reagents used in histology experiments

Reagent	Company
Hydrogen peroxide (H_2O_2)	Sigma-Aldrich
Normal horse serum	Vector Laboratories
Saccharose	Sigma-Aldrich
Triton X-100	Carl Roth GmbH

2.1.2c Reagents for RNA isolation, cDNA synthesis, and quantitative PCR (qPCR)

Table 2.4 | Chemicals and reagents used in RT-qPCR

Reagent	Company
Beta-mercapto-ethanol	Sigma
Deoxynucleotide triphosphates (dNTPs): dATP, dTTP, dCTP, dGTP	Thermo Fisher Scientific
Ethanol	Carl Roth GmbH
RNase-free DNase	Qiagen
TaqMan Gene Expression Master Mix	Applied Biosystems

2.1.2d Reagents for DNA isolation, PCR and gel electrophoresis

Table 2.5 | Chemicals and reagents used in genotyping

Reagent	Company
QuickExtract®	Biozym
EmeraldAmp GT PCR Master Mix	Takara
GeneRuler 1kb Plus Ladder	Thermo Fisher Scientific
ROTI®Gel stain	Carl Roth GmbH
Tris-(hydroxymethyl)-aminomethan	Carl Roth GmbH
Acetic acid	Carl Roth GmbH
0.5 M EDTA, pH 8.0	Thermo Fisher Scientific
Agarose Standard	Carl Roth GmbH

2.1.2e Reagents for FACS

Table 2.6 | Chemicals and reagents used in FACS experiments

Reagent	Company
Ammonium chloride (NH_4Cl)	Sigma-Aldrich
Bovine serum albumine (BSA)	Sigma-Aldrich
Collagenase II	Roche
Desoxycholic acid	Sigma-Aldrich
DNase I	Roche
0.5 M EDTA, pH 8.0	Thermo Fisher Scientific
FCS	Thermo Fisher Scientific
HCl	Carl Roth GmbH
NaOH	Carl Roth GmbH
Potassium bicarbonate ($KHCO_3$)	Sigma-Aldrich

2.1.3 Consumables

Table 2.7 | Consumables

Product	Manufacturer
Cell Culture Plates, 36-well	Greiner
Cell Strainer, 30 µm, 70 µm	Sysmex
Eppendorf Safe-Lock tubes, 1.5 ml, 2 ml	Sarstedt
Falcon tubes, 15 ml, 50 ml	Greiner
Gloves	Carl Roth GmbH
Microplate, 96-well, 384-well	Applied Biosystems
Needles, 20 G1/2“, 24G 1“,	B. Braun Melsungen AG
Object slide	Carl Roth GmbH
PCR plate sealing tape	Carl Roth GmbH
Pipette tips, 10 µl, 200 µl, 1,000 µl	Sarstedt
Syringes, 2 ml, 5 ml	BD Biosciences

2.1.4 Media, buffers, and solutions

Water for all described preparations had been purified before further use with a Millipore purification system (Millipore GmbH, Schwabach) to the degree of “Aqua bidestillata”. pH was adjusted using 37 % HCl of 1 M NaOH.

Blocking buffer	10 µl Normal Horse Serum (1 %) in 1 ml PBS (1x)
Cell sorting buffer	30 µl 0.5M EDTA (0.03 %) in 10 ml PBS (1x)
Digestion buffer (7x)	1.25 ml DNase I (10 mg / ml) 1.25 ml Collagenase II (70 mg/ml) 200 µl FCS (2 %) in 10 ml RPMI
Erylysis buffer	8.02 g NH_4Cl 1 g $KHCO_3$ 0.0372 g EDTA in ddH_2O, volume adjusted to 1 l; pH 7.2-7.4
FACS buffer	10 g BSA (1 %) 100 µl 0.5M EDTA (0.01 %) in 1 l PBS (1x)
Lavage buffer	20 µl 0.5M EDTA (0.04 %) in 5 ml PBS (1x)
Paraformaldehyde (PFA; 4 %)	4 g PFA in 100 ml PBS (1x)
Permeabilization buffer	3 µl Triton X-100 (0.3 %) 50 µl Normal Horse Serum (5 %) in 1 ml PBS (1x)
Phosphate buffered saline (PBS)	137 nM NaCl 2.7 mM KCl 10 mM Na_2HPO_4 1.8 mM KH_2HPO_4 in ddH_2O; pH 7.4
Quenching buffer	3 µl H_2O_2 (0.3 %) in 1 ml PBS (1x)
Sucrose solution (30 %)	9 g Saccharose

	in 30 ml PBS (1x)
TAE buffer (10x)	48.5 g Tris
	11.4 ml Acetic acid
	20 ml 0.5M EDTA (pH 8.0)
	in ddH_2O; volume adjusted to 1 l

2.1.5 Commercial kits

RNeasy Micro Kit	Qiagen
Vectastain Elite ABC Kit Peroxidase (HRP)	Vector Laboratories
Vector SG Peroxidase Substrate Kit	Vector Laboratories
NEBNext Ultra RNA library prep Kit	New England BioLabs GmbH

2.1.6 Antibodies

2.1.6a Antibodies used in histology

Table 2.8 | Antibodies used in histology

Antibody	Host Species	Application	Manufacturer	Cat. No.
Iba1	rabbit	1:200	Wako	019-19741

2.1.6b Antibodies used in FACS

Table 2.9 | Secondary antibody used in FACS experiments

Fluorochrome	Antigen	Clone	Manufacturer
APC	CD4	RM 4-5	Biolegend
APC	CD11c	N418	eBioscience
APC-Cy7	B220	RA3-6B2	Biolegend
APC-C7	CD45	30-F11	Biolegend
APC-F780	CD4	RM 4-5	eBioscience
APC-F780	CD45	RA3-6B2	eBioscience
FITC	MHC-II	M5/ 114.15.2	eBioscience
BV421	CD3	17A2	Biolegend
BV421	CD4	L3T4	Biolegend

Fluorochrome	Antigen	Clone	Manufacturer
BV421	Ly6G	1A8	Biolegend
BV570	B220	RA3-6B2	Biolegend
BV570	CD8a	53-6.7	Biolegend
BV605	CD4	RM 4-5	Biolegend
BV605	F4/80	BM8	Biolegend
BV650	CD8a	53-6.7	Biolegend
BV650	MHC-II	2G9	BD Bioscience
BV711	Nk1.1	PK136	Biolegend
BV785	B220	RA3-6B2	Biolegend
BV785	CD4	RM 4-5	Biolegend
PE	CD3e	145-2C11	Biolegend
PE	CD4	GK 1.5	eBioscience
PE	F4/80	8M8	Biolegend
PE	Ly6G	1A8	BD Bioscience
PE-Cy5.5	B220	RA3-6B2	eBioscience
PE-Cy7	CD11b	M1/70	Biolegend
PE-Cy7	CD4	RM 4-5	Biolegend
PerCP-Cy5.5	B220	RA3-6B2	Biolegend
PerCP-Cy5.5	Cd11b	M 1/70	BD Bioscience
PerCP-Cy5.5	TCRgd	GL3	Biolegend

All antibodies were used in a 1:100 concentration.

2.1.7 PCR Assays

2.1.7a Assays used for genotyping

Table 2.10 | Primers used for genotyping

Target	Sequence 5'→3'
Rosa26SpliAcB	CAT CAA GGA AAC CCT GGA CTA CTG
RosaFA	AAA GTC GCT CTG AGT TGT TAT
RosaRA	GGA GCG GGA GAA ATG GAT ATG

Target	Sequence 5'→3'
CX3Cr1 common	GCA GGG AAA TCT GAT GCA AG
CX3Cr1 Mutant Forward	GAC ATT TGC CTT GCT GGA C
CX3Cr1 WT Forward	CCT CAG TGT GAC GGA GAC AG

2.1.7b Assays used for RT-qPCR

Table 2.11 | Primers used for RT-qPCR

Target	Assay ID
Cx3cr1	4331182 Mm00438354_m1
P2ry12	4331182 Mm00446026_m1
Rbfox	4331182 Mm01248771_m1
MBP	4331182 Mm01266402_m1
CD31	4331182 Mm01242576_m1
GFAP	4331182 Mm01253033_m1
Ccr2	4331182 Mm00438270_m1
Vegfa	4331182 Mm00437306_m1
TBP	4331182 Mm01277042_m1
Sdha	4331182 Mm01352366_m1
Tmem119	4331182 Mm00525305_m1
CD86	4331182 Mm00444540_m1
Tnf-a	4331182 Mm00443258_m1
Arg1	4331182 Mm00475988_m1
Fizz1	4331182 Mm00445109_m1

2.1.8 Software

Table 2.12 | Analysis and visualisation software

Software	Company
GraphPad Prism V9.4.0	GraphPad Software
ImageJ (Version 2.0.0)	Fiji
NDP.view Ver 2.9.29	Hamamatsu
FlowJo v10.8	BD Bioscience
NanoDrop ND2000 V3.5.2	ThermoScientific

Software	Company
R 4.0.5	Open source
FastQC 0.11.9	Babraham Bioinformatics
Cytoscape 3.9.1	Open source
Displayr	Online tool
Enrichr	Ma'ayan Laboratory
FACSDiva (V 8.0)	BD Bioscience
BioRender	Online tool

2.2 Methods

2.2.1 Molecular methods

2.2.1.1 Genotyping

2.2.1.1a DNA extraction

DNA was extracted from murine tail or ear samples using QuickExtract® according to manufacturer's protocol. Briefly, the respective tissue was cut into small pieces to facilitate lysis before adding 20 µl QuickExtract® solution. The mixture was vortexed thoroughly and incubated for 45 min at 65°C and 700 rpm in a thermomixer (Eppendorf). Next, samples were again vortexed briefly and incubated at 98°C for 10 min, 700 rpm in a thermomixer (Eppendorf). After extraction, the samples were either further analysed directly or stored at -20°C until use.

2.2.1.1b Polymerase chain reaction (PCR) amplification

PCR was performed to amplify relevant DNA products for subsequent detection by gel electrophoresis. To this end, the Emerald Amp® GT PCR Master Mix kit (Takara) was used. 10 µl of the provided PCR Master Mix (2x) was mixed with 1 µl of each primer (section 2.1.7), 1 µl of template DNA, and an adequate volume of dH_2O to add up to a final volume of 20 µl per sample. After briefly spinning down the PCR well plate, a PCR was run on a thermocycler (Analytik Jena) with the following conditions: 98°C for 10 s, then 30 cycles of 60°C for 30 s and 72°C for 1 min. After amplification, samples were held at 4°C.

2.2.1.1c Gel electrophoresis

Gel electrophoresis is used for separating DNA by their length in base pairs (i.e. size) for subsequent visualization. By application of an electrical current, the negatively charged DNA is moved through a gel

matrix toward a positive electrode. The following protocol was applied: First, a 1% agarose gel was prepared by mixing 1 g agarose powder with 100 mL 1x TAE buffer. Mixture was microwaved for 1-3 min until the agarose was completely dissolved. After an intermittent 5 min, where the agarose solution was left to cool down, 10 µl of Roti®GelStain was added. Next, the solution was poured into a gel tray with sufficient amount of combs in place. Once the agarose gel solidified, the gel tray was placed into the electrophoresis unit and submerged in 1x TAE buffer. After adding 10 µl of 1 kb Plus molecular weight ladder (invitrogen), the gel was loaded with 20 µl of sample per well. Next, the electrophoresis unit was closed and the gel was run at 120 V for ~1 h. Finally, DNA fragments on the gel were visualized under UV light.

2.2.1.2 Transcriptomic analyses

2.2.1.2a RNA purification

RNA was isolated and purified from isolated either murine Microglia cells or whole CNS tissue using the RNeasy Micro Kit (Qiagen) according to manufacturer's protocol. Briefly, cells or ~15 mg of CNS tissue were lysed in 600 µl RTL lysis buffer supplemented with 1% beta-mercapto-ethanol. Cell samples were homogenized by vortexing thoroughly for 1 min, tissue samples were homogenized using a PTFE pestle and glass tube. All samples were subsequently centrifuged at full speed at RT for 3 min. The supernatant and an equal volume of 70% EtOH were mixed and thoroughly blended by pipetting, transferred to a RNeasy MinElute spin column and subsequently centrifuged for 15 s at RT and ≥ 8,000 g. Now, successively add 350 µl RW1 buffer twice, and 500 µl RPE buffer to the column with intermediate centrifugation at > 8,000 g and RT for 15 s. Flow-through was discarded after each centrifugation. Next, 500 µl of 80 % EtOH was added and samples were centrifuged for 2 min at ≥ 8,000 g. Flow-through was again discarded. For RNA suspension, RNeasy MinElute spin columns were transferred to new 1.5 ml tubes (Eppendorf). 17.5 µl RNase-free water was added to each column, which were then incubated for 1 min at RT. Columns were then centrifuged for 1 min at RT and full speed. This final elution step was repeated once to maximize RNA yield. The purified RNA was immediately put on ice. 1.5 µl of the final eluate was transferred to a separate 0.6 ml microcentrifuge tube (Sigma) for further RNA bioanalysis (see 2.2.1.2b). All samples were stored at -80°C until further use.

2.2.1.2b RNA bioanalysis

To determine the average concentration and integrity of RNA (RNA integrity number, RIN) in each sample, electrophoretic measurements were conducted using the Agilent Bioanalyzer 2100 system (Agilent Technologies). Measurements were performed according to manufacturer's protocol. Briefly, kit

reagents were equilibrated to RT for 30 min before use. Next, the fluorescent dye concentrate RNA 6000 Nano was vortexed and spun down. 1 µl of dye concentrate was then added to a 65 µl aliquot of filtered gel. The gel-dye mixture was thoroughly vortexed for 1 min and spun down for 10 min at RT at 13,000 g. In the meantime, a chip was placed on the chip priming station. RNA samples were heat denatured at 70°C for 2 min to minimize secondary structure. Next, 9 µl of the gel-dye mix was transferred onto the gel. After pressurizing, the chip was loaded with the remaining gel-dye mix. Next, 5 µl of the RNA 6000 Nano marker was added to all sample and ladder wells on the chip. Finally, 1 µl of the RNA ladder and 1 µl of each sample was pipetted into the respective wells. The loaded chip was vortexed for 1 min at 2400 rpm and inserted into the Agilent 2100 bioanalyzer for analysis. Successful preparation was determined by assessment of ladder (1 marker peak, 6 RNA peaks, all well resolved) and sample run (1 marker peak, 2 ribosomal peaks) of the respective electropherogram. For RNA-Seq analyses, only samples with a RIN ≥ 8 were selected.
Fluorescent dye concentrate as well as gel-dye mixture were protected from light throughout chip preparation. Samples were kept on ice at all times.

2.2.1.2c Synthesis of complementary DNA (cDNA)

Reverse transcription (RT) was conducted to generate cDNA from an RNA template using the RevertAid H Minus First Strand cDNA Synthesis Kit (Thermo Fisher Scientific). Briefly, for each sample total RNA was mixed with 1 µl random hexamer primer and nuclease-free H_2O to a final volume of 12 µl. The mixture was incubated at 65 °C for 5 min in a thermocycler (Analytik Jena). As random hexamer primers contain all 6 base single strands of DNA, they can hybridize anywhere on the RNA. A double-stranded RNA segment acts as a primer for the reverse transcriptase, which is subsequently introduced. More specifically, 4 µl 5X Reaction Buffer, 1 µl RiboLock RNase Inhibitor, 2 µl 10 mM dNTP Mix, and 1 µl RevertAid H Minus M-MuLV Reverse Transcriptase were added to each sample. The mixtures were vortexed shortly and centrifuged. The mixtures were then incubated in a thermocycler (Analytik Jena) at 25 °C for 5 min, followed by 60 min at 42 °C, and ultimate heating at 70 °C for 5 min to terminate the reaction. The generated cDNA was stored at -20 °C until further use.

2.2.1.2d Quantitative polymerase chain reaction (qPCR)

qPCR was conducted to asses starting amounts of cDNA targets. PCR products were detected using fluorescence labeled TaqMan™ probes. These probes are sequence-specific and carry a fluorophore, located at the 5’ end, and a quencher moiety at the 3’ end. The probe is then cleaved by 5’-3’ exonuclease activity of Taq DNA polymerase during the annealing/extension phase of the PCR,

resulting in the separation of the fluorophore and quencher moiety. The thereby emitted fluorescence signal is detected and correlated with the amount of accumulated PCR product.

Samples for qPCR analysis were prepared in 96 well microplates using 1X of the respective TaqMan™ probe, 1X TaqMan™ gene expression master mix (Applied Biosystems), 2 µl of 5-fold diluted cDNA sample, and RNase-free water in a final volume of 20 µl per well. Microplates were then centrifuged shortly to prevent air bubbles in the mixture before the plates were sealed using adhesive film. Samples were then analyzed using a 7900HT Fast Real-Time PCR System (Applied Biosystems). The following thermal profile was run for 40 cycles: 50 °C for 2 min, 95 °C for 10 min, 95 °C for 15 s, 60 °C for 1 min. Results show average of sample triplicates normalized to *Tbp* (TATA sequence binding protein) and *Sdha* (Succinate Dehydrogenase Complex Flavoprotein Subunit A). Data was assessed by $\Delta\Delta C_t$ method for relative quantification.

2.2.1.2e RNA-Sequencing (RNA-seq): library preparation and transcriptome analysis

RNA-seq libraries and differential gene expression (DEG) analysis was done conducted by the NIG core facility of Göttingen University. Briefly, libraries were prepared with the NEBNext Ultra RNA Library Preparation Kit (New England Biolabs), pooled and sequenced on a HiSeq2000 sequencer (Illumina) to generate 50 base pair single-end reads. After verifying sequencing quality by FastQC (v.0.11.9), reads were aligned to the Ensembl mouse reference genome (mm10) using STAR v.2.4 (Dobin, 2013) with default parameters. The following analyses were conducted in an R environment (v.4.1.2) with publicly available packages. DEG analysis was done using DESeq2 (v.1.34.0; Love, 2014) defining genes with a minimal twofold change and false discovery rate (FDR)-adjusted $P < 0.05$ as differentially expressed (DE). To assess sample similarity, principal component analysis (PCA) and dendrogram analyses were performed on normalized expression values using the topmost variable genes. Plots were compiled with ggplot2 (v.2.2.1).

2.2.1.2f Downstream functional assessment of RNA-Seq data

First, for direct comparison between experimental groups, gene expression was normalised for all conditions by comparing all expressed genes by the DESeq2-derived *t* statistics against complementary sham control, i.e. baseline gene expression. Consecutive analyses were performed using the online software tool enrichr (Chen, 2013; Kuleshov, 2016; Xie, 2021) with default parameters. Results were visualised as enrichment plots (Merico, 2010) by summarising functionally associated gene sets into nodes; each node thus represents a regulated biological function.

2.2.2 Flow cytometry

2.2.2a Tissue preparation

Animals were sacrificed and perfused as described (see 2.2.4.2b). In case blood was analysed, blood samples were drawn directly from the heart prior to perfusion; for collecting immune cells from the peritoneal cavity, a lavage was performed prior to perfusion; in all other cases, tissue samples were taken post perfusion.

For blood collection, after thoracotomy, a 25 gauge needle was inserted into the left ventricle of the heart. At least 1 mL blood was collected by slowly pulling the syringe's plunger. After collection, blood was transferred to a heparin blood collection tube.

For an intra-peritoneal lavage, a small incision was made in the abdominal skin of the mouse. Skin was gently removed to each side of the mouse. The needle of a 10 mL syringe was inserted into the lower abdominal area of the mouse. Special care was taken to not perforate any internal organs. Immediately after insertion, 5 mL lavage buffer was injected into the intra-peritoneal cavity. The needle was removed slowly before the mouse was gently rotated to distribute the injected buffer. Finally, the buffer was removed by inserting the syringe again, this time in the upper part of the abdomen, and slowly extracting the intra-peritoneal fluid. At least 3 mL of buffer were collected and placed on ice.

The CNS was collected by, firstly, decapitating the mouse and removing the skin. Next, occipital and interparietal bones were cut. The calvaria was cracked open by inserting the tip of a scissor into the skull at the junction of frontal and parietal bones, thus exposing the brain. The CNS was removed carefully with forceps and transferred into petri dishes filled with 1x PBS on ice.

The spleen was removed from the abdomen by gently removing it from the surrounding connective tissue using forceps. It was then placed into a 15 mL falcon tube filled with 1x PBS on ice.

For CNS preparation, the cerebellum and olfactory bulb was removed and hemispheres were separated. For downstream microglia RNA collection, only the infarcted hemisphere was further processed, in all other cases, both hemispheres were further processed separately. The tissue was dissociated manually using a scalpel before enzymatic digestion by incubation in 4 ml digestion buffer at 37°C for 30 min.

CNS and spleen were further minced by passing the respective tissue through a 40 µm strainer. Next, all samples were centrifuged at 310 g for 10 min at 4°C. Supernatant was discarded.

To remove the myelin from the CNS samples, a Percoll gradient separation was performed: Samples were resuspended in 33% Percoll solution carefully layered on top of a 70% Percoll solution. Gradient was centrifuged for 40 min at 300 g at 4 °C without brakes. Next, the interphase between the 70% and 33% Percoll was carefully removed and transferred to a separate collection tube. Isolated cells were washed twice by adding 10 ml of 1x PBS and centrifuging at 310 g and 4°C for 10 min each. Supernatant was discarded after each centrifugation.

Lastly, samples were erylysed by incubating the samples in 5 ml erylysis buffer at 4°C for 7 min. Reaction was stopped by adding 1x PBS to the samples and centrifuging them at 310 g at 4°C for 10 min. Supernatant was carefully removed.
Before proceeding to staining, samples were washed again by adding 1x PBS and centrifuging at 310 g at 4°C for 10 min. Supernatant was discarded.

2.2.2b Staining

For surface staining of cells, an antibody cocktail with all necessary antibodies was prepared. To prevent unspecific binding of antibodies to the Fc domain on certain cell types, an Fc blocking agent was added to the antibody cocktail. The final volume of the antibody cocktail was adjusted with FACS buffer.
Samples were incubated in 100 µl of antibody cocktail for 30 min in the dark at 4°C. Next, cells were washed by adding 2 mL FACS buffer to each sample and centrifuging for 10 min at 350 g and 4°C. Supernatant was removed and before repeating the last washing step. Finally, after discarding the supernatant, cells were resuspended in either 200 µl FACS buffer (for quantitative analyses) or 100 µl sorting buffer (for cell sorting).
Samples were kept on ice at all times.

2.2.2c Fluorescence-activated cell sorting (FACS) measurements

Measurements were conducted at either a LSR Fortessa system for quantitative analysis of immune cell populations within a sample, or using an AriaIIIu system for cell sorting.
All measurements were done at the Cytometry and Cell Sorting Core Unit of the UKE using FACSDiva.

2.2.3 Animal Experiments

All animals of this study had a C57BL/6 background and were kept at the Central Animal Facility and at the Animal Housing Facility of Campus Forschung of the University Medical Center Hamburg-Eppendorf. They were housed in individually ventilated cages under specific pathogen-free housing conditions, had continuous access to food and water and were kept under a 12h day/night cycle. Mice were between 12-16 weeks old when they underwent transient middle cerebral artery occlusion (tMCAO) surgery.
All animal experiments were approved by the local ethics committee (Behörde für Soziales, Familie, Gesundheit und Verbraucherschutz in Hamburg) under Tierversuchsantrag 059/2017 and 099/2020.

2.2.3.1 Mouse strains

C57BL/6: Wild-type (WT) i.e. genetically not modified; background strain. Obtained from Charles River Laboratories, Germany.

$CX3CR1^{creERT2}$ x $iDTR^{+/-}$ x $eYFP^{+/-}$ (Microglia depleted mice, MG-) resp. $CX3CR1^{creERT2}$ x $iDTR^{-/-}$ x $eYFP^{+/-}$ (Microglia non-depleted littermate control mice, MG+; Bruttger et al., 2015): This mouse line was used to selectively ablate and thereby study Microglia cells of the CNS.

In these mice, a tamoxifen-inducible CreERT2 recombinase is expressed under the control of the endogenous *Cx3cr1* promoter of the mononuclear phagocyte system. Additionally, these mice express an enhanced yellow fluorescence protein (eYFP) as well as an exogenous Diphtheria toxin receptor (DTR) at the Rosa26 locus, a locus known for its constitutive, generalised gene expression (Soriano et al., 1991; Casola, 2010). Initially, the expression of both eYFP and DTR are suppressed by *loxP*-flanked stop codon sites.

Mice were kindly provided by Ari Waisman, Institute for Molecular Medicine, Johannes Gutenberg-University Mainz.

2.2.3.1a Microglia cell depletion

Microglia cell depletion was initialised by firstly treating $CX3CR1^{creERT2}$ x iDTR x eYFP mice with 2 mg tamoxifen by subcutaneous injection of 200 µl on postnatal days 12 and 14. To this end, tamoxifen (TAM; Sigma) was suspended in corn oil on a shaker at 37°C overnight and sterile filtered before use. Once solved, TAM was stored at either -80°C for long-term storage or at 4°C for the duration of injections.

Upon TAM treatment, the Cre recombinase, which is normally present in the cytoplasm bound to heat shock protein 90 (HSP90) and thus unable to enter the nucleus, is enabled to translocate to the nucleus by TAM disrupting the interaction between HSP90 and Cre. Once translocated, Cre excises the *loxP* flanked stop condon sites in front of both, the DTR and the eYFP, thus effectively enabling their expression. In $CX3CR1^{creERT2}$ x $iDTR^{-/-}$ x $eYFP^{+/-}$ mice TAM treatment only led to the expression of eYFP, whereas in $CX3CR1^{creERT2}$ x $iDTR^{+/-}$ x $eYFP^{+/-}$ mice TAM treatment induced eYFP and DTR expression.

Importantly, since the Cre recombinase is expressed under the *Cx3cr1* promoter and thus widely present in the phagocyte system, inducing DTR and eYFP expression is initially not restricted to Microglia cells of the CNS but widespread in both circulating and other tissue-resident monocyte populations. To circumvent this issue and ensure Microglia cell-specific DTR and eYFP expression, an interim period of 10 weeks was introduced before further experiments were initiated. As a result, short-lived circulating and other tissue-resident macrophages lost their DTR and eYFP labeling, whereas Microglia retained the induced DTR and eYFP expression due to their slow turnover rates.

Lastly, Microglia cell depletion was induced by intraperitoneal (i.p.) administration of 500 ng Diphtheria toxin (DTx; Merck Millipore) on three consecutive days. DT was suspended in 0.9% NaCl and sterile filtered before administration.

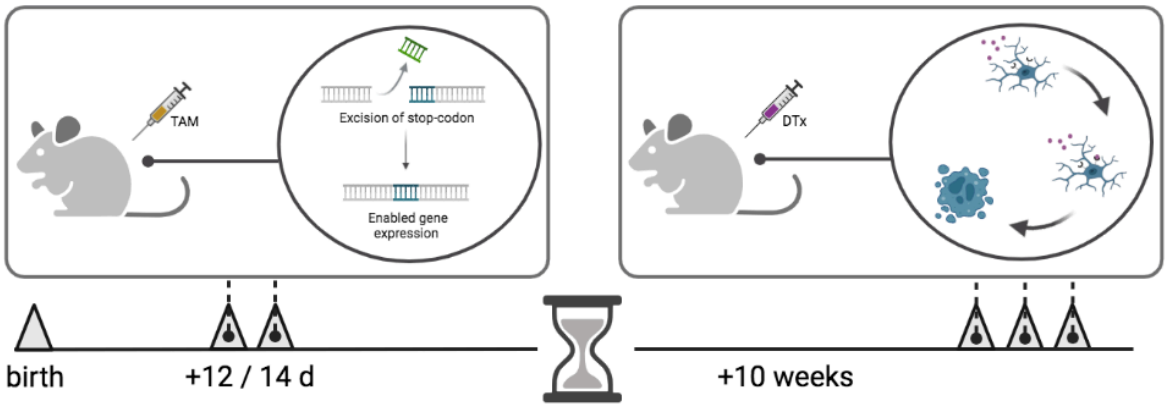

Figure 2.1 | **Schematic representation of microglia cell depletion**

2.2.3.2 Surgical procedures

All procedures were carried out in accordance with ARRIVE guidelines and only performed by trained and approved personnel.

2.2.3.2a Induction of ischemic stroke: tMCAO

Sham and tMCAO surgeries were based on previously established protocols (Arumugam et al., 2006). 24 h prior to surgery, mice were analgetically treated by introducing 0.5 mg/ml Tramadol (Tramadol AL, ALIUD Pharma) in their drinking water. Additionally, mice were treated with 0.05 mg/kg BW Buprenorphine (Arevipharma) by i.p. injection 30 min prior to surgery. Anaesthesia was initiated at 5 % isoflurane in oxygen and maintained at 1.5% isoflurane in oxygen. Throughout anaesthesia, mice were monitored for their breathing frequency and heart rate. Moreover, to ensure a stable body temperature during the procedure, mice were kept on a heating mat at 37°C.

Surgery is then begun by shaving the animal's neck and disinfecting the skin. To temporarily occlude the middle cerebral artery, essentially, a filament is introduced from the periphery into the CNS. To this end, a small incision is made in the neck to expose the common carotid artery (ACC), internal carotid artery (ACI) and external carotid artery (ACE). Next, the ACC and ACI are temporarily proximally ligated to circumvent blood flow to the surgically affected areas. Then the ACE is sealed distally, opened, and a thin silicone-coated filament (Doccol) is inserted. As all ACE-supplied areas are also supplied by the pterygopalatine artery, permanently sealing the ACE does not negatively affect the mouse. Next, in order to advance the introduced filament cerebrally, the originally cranially directed ACE is carefully folded caudally, thus enabling the filament to be moved from the ACE to the CNS, where it occludes the

middle cerebral artery (MCA). After an occlusion time of 40 min, the filament is removed, thus initiating reperfusion of the MCA. The severed end of the ACE is ligated and finally, the ACC is reopened. The neck incision is closed and treated antiseptically (Betaisodona, MUNDIPHARMA).
For sham surgery, the procedure remains largely identical except for not introducing the filament, thus not occluding the MCA.
Surgeries were done by O. Schnappauf, I. S. Schädlich, and V. Roth.

2.2.3.2b Perfusion

Mice were euthanized by i.p. injection of 10 ml kg^{-1} of 12 mg ketamine (Ketanest® S, Pfizer Pharma) and 1.6 mg xylazine (Rompun™, Bayer) in 0.9% sodium chloride (NaCl; Braun) solution. Once reflexes could no longer be detected, animals were fixed in supine position and their thoraxes were opened. The heart's left ventricle was punctured with a needle and a small incision was made in the right atrium. To clean the vessels from blood, animals were perfused with ice-cold PBS before 4% PFA was circulated for 6 min for tissue fixation. After perfusion, brains and spinal cords were extracted and post-fixed in ~10 ml of 4% ice-cold PFA for 1 h. Subsequently, tissues were placed in 30% sucrose solution until the respective tissue sank down. Tissue was eventually further processed for histological analyses as described in 2.2.5.

2.2.3.3 Assessing clinical presentation

Prior to any treatment, the bodyweight (BW) of each animal was assessed as a reference for following weight changes during the course of the respective experiment.
After TAM treatment, mice were monitored and their physiological development was assessed on a daily basis. Upon treatment with DT, mice were also assessed for behavioural alterations.
Following tMCAO induction, animals were weighed twice daily and clinical disease scores were determined according to the following scale: 0 = no clinical deficits, i.e. healthy; 1 = moderate motoric deficits present contra-lesionally and moderate circling behaviour; 2 = clear motor disturbances and circling behaviour in ipsi-lesional orientation, overall motile; 3 = severe motor disturbances and strong circling behaviour in ipsi-lesional orientation while motility overall reduced; 4 = severe motor disturbances and strong circling behaviour in ipsi-lesional orientation, presented motility only upon incentive while otherwise stationary; 5 = premorbid or dead. Animals were euthanized at a score ≥4 and once overall wellbeing deteriorated considerably (indicated by excessive weight loss, behavioural alterations, physical abnormalities). Due to ethical considerations, mice were provided with heating pads and wet food.

2.2.4 Histology

2.2.4a TTC staining

2,3,5-Triphenyltetrazolium chloride (TTC) is a marker for metabolic function and can thus be used to assess infarct sizes after tMCAO. The mitochondrial enzyme succinate dehydrogenase reduces TTC into formazan, which is tinted deep red. Thus, upon TTC exposure, tissue with functional mitochondria, i.e.: healthy tissue, will turn red, whereas necrotic tissue remains colourless (Bederson et al., 1986).

For TTC staining, mice were euthanized and perfused as described (see 2.2.3.2b). Brains were collected, dissected and sliced in a matrix device (Braintree Scientific) into 1 mm coronal sections. Olfactory bulb and cerebellum were discarded. All other slices were incubated in 2% TTC (Sigma-Aldrich #T8877) in 1x PBS at RT for 15 min. Slices were covered with aluminium foil. Next, TTC buffer was removed and brain slices were scanned (Sony Printer PJ790) for infarct volume analyses. Tissue was either further worked with directly or discarded.

2.2.4b Microglia staining

To assess microglia quantity and morphology after ischemia, avidin-biotin complex (ABC) immunoperoxidase staining for ionized calcium binding adaptor molecule 1 (Iba1) was done using both the Vectastain Elite ABC Kit Peroxidase (HRP) and the Vector SG Peroxidase Substrate Kit (Vector Laboratories) on CNS tissue of mice. Briefly, the staining was done as follows: After washing the tissue sections thrice in 1x PBS for 10 min each, endogenous peroxidase was quenched by incubating the tissue with 0.3% H_2O_2 in 1x PBS for 30 min at RT on a shaker. Next, after washing three times in 1x PBS for 10 min each, unspecific binding was blocked by incubating the tissue sections with blocking buffer (0.3% Triton X-100 and 5 % normal horse serum in 1x PBS) for 1 h on a shaker at RT. Subsequently, the tissue was incubated with the primary antibody mixture (0.3% Triton X-100, 2% normal horse serum, and 0.1% anti-Iba1 (see 2.1.6a) in 1x PBS) over night at 4°C. Tissue sections were washed again three times in 1x PBS for 10 min before being incubated for 30 min with blocking buffer (1% normal horse serum in 1x PBS) and 1:200 diluted biotinylated secondary antibody (Kit). Tissue was washed once for 10 min in 1x PBS before being incubated again for 30 min at RT with Vectastain Elite ABC Reagent (Kit). Lastly, after another washing step for 10 min in 1x PBS at RT, the tissue was incubated with 3% SG Blue (Kit) and 3 % H_2O_2 in 1x PBS for 15 min. After rinsing briefly, the tissue sections were cleared and mounted.

Stainings were recorded by the Neuropathology Department of the University Medical Center Hamburg-Eppendorf.

2.2.5 Quantitative analyses and statistics

FACS data were quantified using the BD FACSDiva and FlowJo software. Histological assessments were done with the Fiji Image J software and NDP.view. Statistical analyses were conducted with GraphPad Prism, R, and R addins displayr and enrichr. Visualisation was done using GraphPad Prism, R, Displayr, BioRender, and Cytoscape. Statistical significance was assessed by Student's *t*-test (parametric data, two groups), ANOVA (parametric data, more than two groups) or Mann-Whitney Rank Sum Test (non-parametric data, two groups) with appropriate *post hoc* analysis as specified in the following. Statistical significance was accepted when $p < 0.05$. All values are presented as means ± s.e.m.

Sham and tMCAO surgeries were done blinded, other experimental procedures were conducted without blinding. In the case of the CX3CR1^{creERT2} x iDTR x eYFP mouse strain, experimental groups were assigned based on genotype. In the case of WT C57BL6/J mice, experimental groups were quasi-randomized based on order of trail completion.

3. Results

3.1 Depletion of microglia results in increased post-ischemic lesions in female mice. To assess the influence of microglia cells in acute stroke, we selectively depleted microglia from CX3CR1^{creERT2} x iDTR$^{+/-}$ x eYFP$^{+/-}$ transgenic female (F MG-) and male (M MG-) mice and induced tMCAO, the animal model of ischemic stroke. CX3CR1^{creERT2} x iDTR$^{-/-}$ x eYFP$^{+/-}$ littermates (F/M MG+) served as controls, as their microglia population remains non-depleted. Of note, steady-state microglia depletion and repopulation dynamics were comparable between female and male mice (Supplementary Fig. 1a). We chose to perform tMCAO on the consecutive day of a three-day DTx treatment regimen to ensure a microglia depletion of approx. 80% at the time of stroke induction (Fig. 3.1a, c); thus, this model can reveal how microglia affect the CNS milieu of female and male mice during acute ischemia. To assess the amount of tissue damage sustained by tMCAO, we TTC-stained the CNS of MG- and MG+ female and male mice and quantified the infarcted area. This revealed significantly enlarged infarcts in female MG- mice compared to their MG+ littermates, whereas infarct sizes in male mice appeared to be unaffected by microglia depletion (Fig. 3.1b). Interestingly, microglia cells showed rapid repopulation dynamics upon cessation of DTx treatment (Fig. 3.1c); this appeared to be additionally bolstered upon CNS injury as three days after tMCAO we observed prominent abundance of Iba1+ cells in the ischemic area of the MG+ and MG- CNS alike (Fig. 3.1c, d) which strongly suggests a pathophysiological importance of these cells. This is further corroborated by region-specific morphological phenotypes that we observed in these Iba1+ cells with a ramified appearance of resting microglia in the contralateral hemisphere, and a predominance of amoeboid shapes of activated microglia in the ischemic region (Fig. 3.1d). We ensured that there was no pre-existing activated microglial phenotype due to DTx treatment (Supplementary Fig. 1b). Accordingly, the observed morphological alterations and concomitant functional activation of microglia cells appeared to be a genuine response to ischemia.

In addition to infarct sizes, we also assessed clinical scores and bodyweight reduction as correlates of disability and disease severity, respectively. Interestingly, while infarct sizes differed significantly, neither scores nor bodyweight changes reflected a correspondingly aggravated state of disability in female MG- compared to MG+ mice (Fig. 3.1e). On the other hand, unaltered infarct sizes between male MG+ and MG- mice were accompanied by a similar reduction in bodyweight in both conditions, whereas clinical scores hinted at an ameliorated disease course in MG- compared to MG+ mice (Fig. 3.1e).

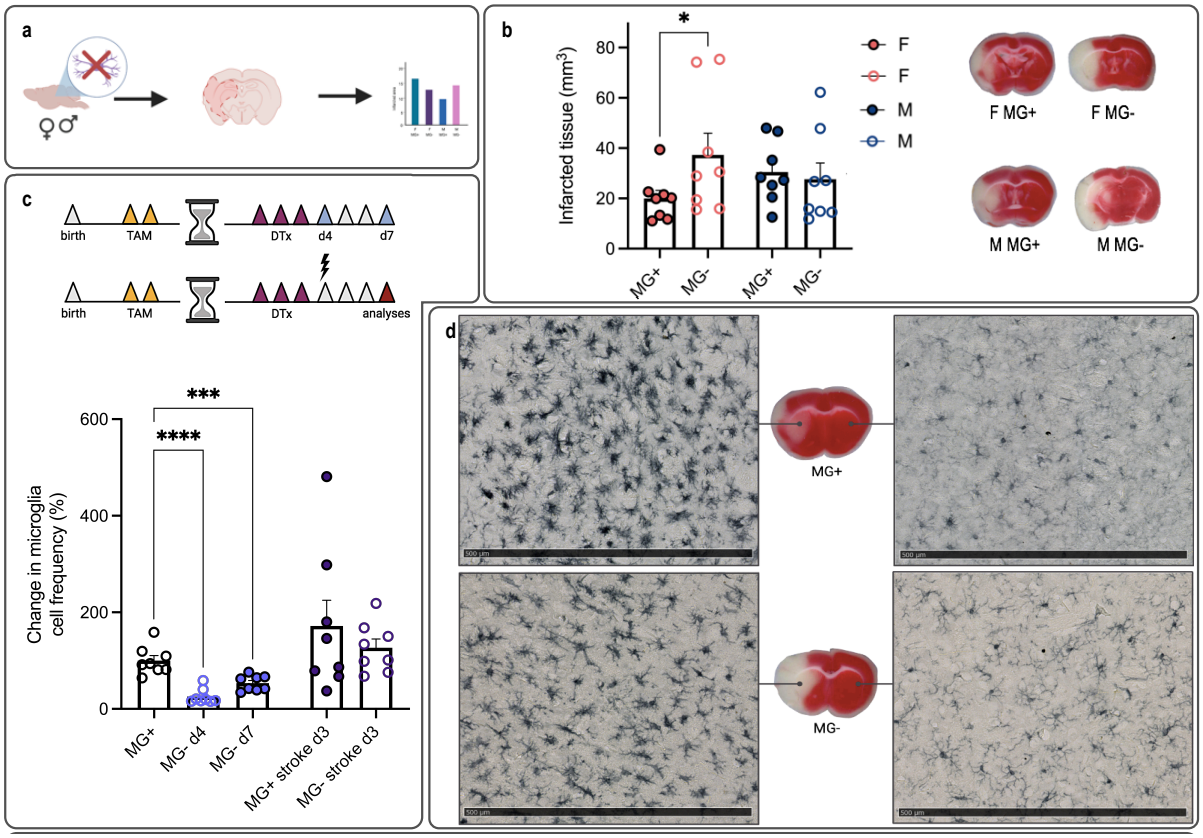

Figure 3.1 | Microglia-mediated differences in stroke between female and male mice. a, Schematic experimental overview. **b,** Changes in infarct size between female and male MG-depleted and non-depleted mice 3 d post-ischemia. One-tailed, two-sample *t*-test for females ($t(14) = 1.883$, $p = 0.0404$) and males ($t(14) = 0.3680$, $p = 0.3592$) respectively; $n = 8$ MG-depleted versus $n = 8$ wild-type littermate controls for each female and male mice. The bars show mean values ± s.e.m. **c,** Microglia cell dynamics after depletion, upon repopulation, and three days post-ischemia. Ordinary one-way ANOVA against controls normalized to 100: $n = 8$ per group; $F(2, 21) = 25.19$, $p < 0.0001$. Sidák's post hoc test: MG+ versus MG- d4, $p < 0.0001$; MG+ versus MG- d7, $p = 0.0005$; MG+ versus MG+ stroke d 3, $p = 0.3565$; MG+ versus MG- stroke d 3, $p = 0.5721$. The bars show mean values ± s.e.m. **d,** Histological staining of microglia cells repopulating the ischemic CNS of depleted and non-depleted mice 3 d after stroke. No quantification. Scale bar, 500 µm. *Figure continued on p. 41.*

3.2 Microglia profiling after ischemic stroke. Next, for a better understanding of the underlying mechanisms of the different sex-specific MG phenotypes, we decided to investigate the transcriptome of microglia from female and male mice in the wake of ischemic stroke. To this end, we isolated $CD45^{int}CD11b^{high}$ microglia cells from C57Bl6/J wild-type mice at different time points after tMCAO via FACS and extracted RNA from these cells (Fig. 3.2a, b); sham surgery served as control. As our main aim was to understand the observed protective phenotype of female microglia in acute stroke, we focussed further analyses on day one and three post-ischemia. Per time point, we sampled three biological replicates of microglia extracted after tMCAO from male and four replicates from female mice, and three biological replicates from microglia of male and female mice after sham surgery (Supplementary Fig. 2a). Consistency of the acquired dataset was verified by principal component analysis (PCA) and unsupervised clustering (Supplementary Fig. 2b-d). Additionally, we assessed the

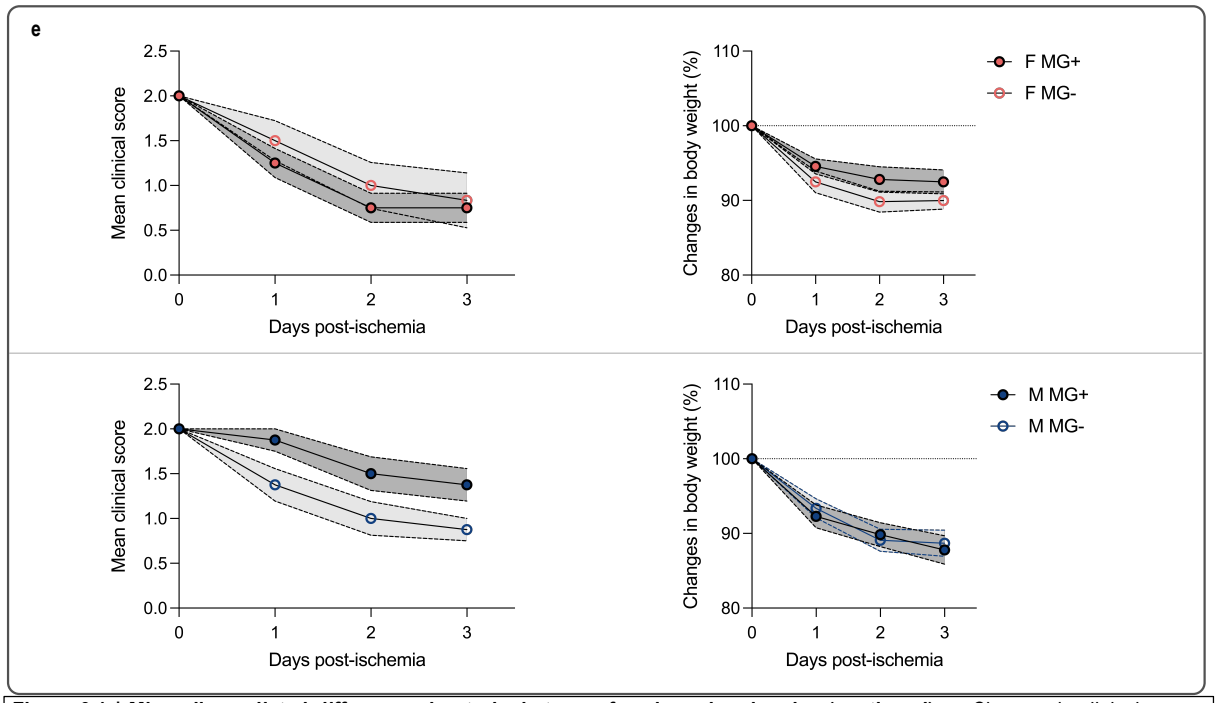

Figure 3.1 | Microglia-mediated differences in stroke between female and male mice (continued). e, Changes in clinical scores (two-tailed Mann-Whitney *U*-test; n = 8 MG+ versus n = 8 MG- mice for females, p = 0.5143, and males, p = 0.1061) and bodyweight (repeated measurement two-way ANOVA (females: $F(3, 36) = 1.050$, p = 0.3852, males: $F(3, 51) = 0.3101$, p = 0.8180) and Sídak's post hoc test (females: mean adjusted p = 0.6518, males: mean adjusted p = 0.9881)) as parameters of disease severity after ischemic stroke. Data are pooled from two independent experiments. Mean values ± s.e.m. are shown. *p < 0.05, ***p < 0.001, ****p < 0.0001

cellular homogeneity of our microglia samples by checking for transcripts from other CNS-resident and CNS-infiltrating cells. To this end, we compiled core marker genes for microglia (*Cx3cr1, P2ry12*), neurons (*Rbfox*), oligodendrocytes (*Mbp*), endothelial cells (*Cd31*), astrocytes (*Gfap*) and macrophages (*Ccr2*) and checked for their expression in our FACS-isolated microglia samples via qPCR. As expected, microglial markers were upregulated in our samples, whereas other cellular markers were de-enriched with the notable exception of *Ccr2* (Fig. 3.2c). Since *Ccr2* expression has been described for both infiltrating macrophages and activated microglia, we introduced an additional marker to accurately differentiate and pinpoint the origin of the observed *Ccr2* expression. Indeed, upon including the macrophage-specific marker *Vegfa* we were able to rule out infiltrating macrophages as a source of the *Ccr2* signal and thus concluded that our microglia samples were pure.

To understand the biological meaning of the changes in gene expression in post-ischemic microglia of female and male mice, we performed an overrepresentation analysis (ORA) by enrichr on all differentially expressed genes with an average logFC ≥ ±2 (Supplementary Fig. 2e-h) and visualised the results as KEGG pathway enrichment clusters (Fig. 3.2d). This analysis revealed an overall stronger activation in female compared to male microglia based on number of DE genes, especially on day one which is then roughly attenuated by day three post-ischemia. Apparently, activation of male microglia was governed by a longer latency compared to female microglia, where we could observe a more differentiated activation profile during early stroke already. A more in-depth analysis of the

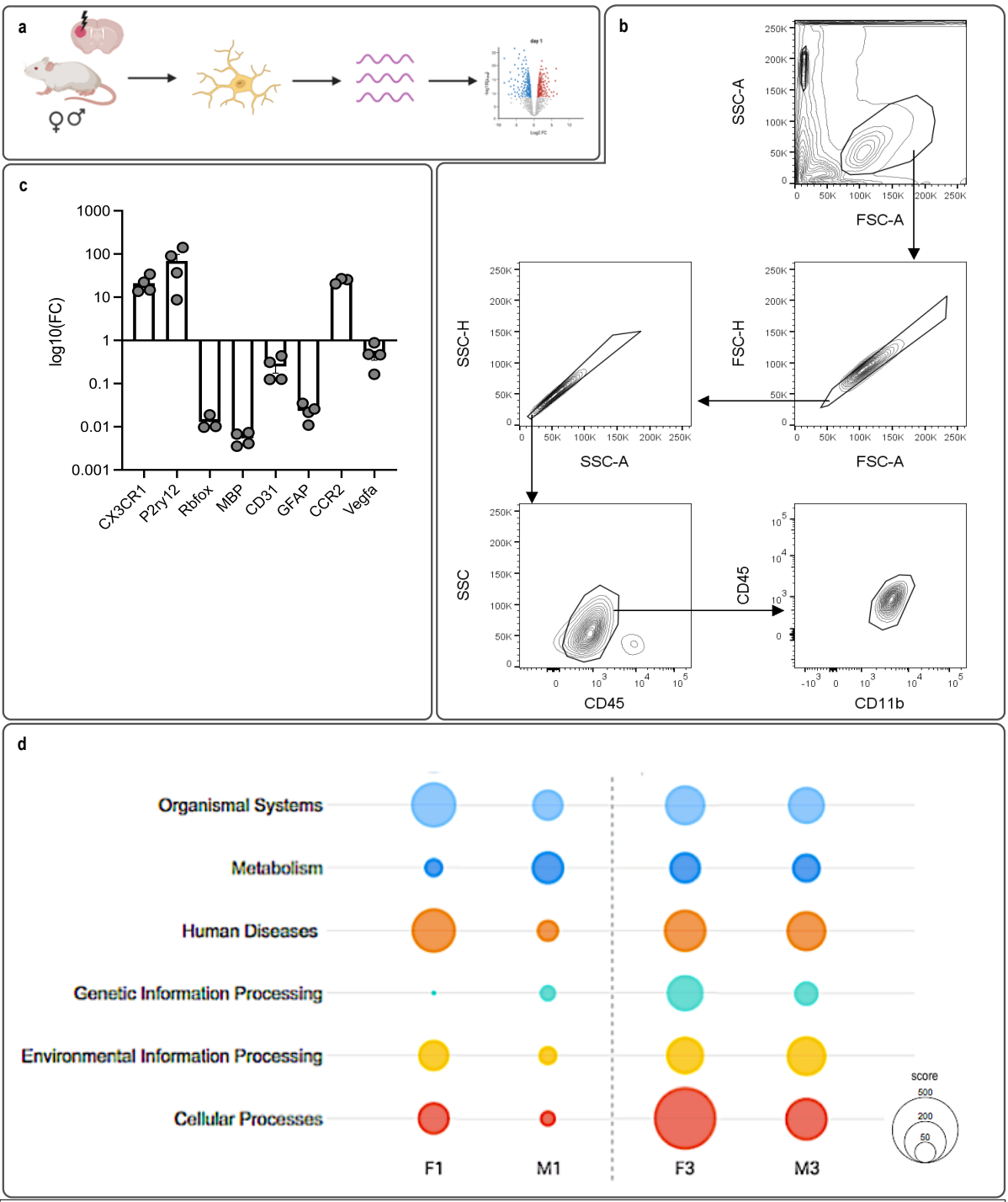

Figure 3.2 | Expression profiling of microglia cells after ischemic stroke. a, Experimental overview. **b,** FACS gating strategy for microglia cell isolation as CD45^{int}CD11b^{high}. **c,** Quantification of core CNS cell marker genes in microglia samples via qPCR. **d,** Enrichment plot of regulated KEGG terms in RNA-Seq of female and male microglia cells one and three days post-stroke. Node size, Enrichr computated combined score ranking. *Figure continued on p. 43.*

topmost regulated KEGG pathways helped us to further elaborate and corroborate this assessment (Fig. 3.2e): On day one post-ischemia, we found in male microglia an overrepresentation of genes involved in metabolic processes suggesting a response primarily aimed at counteracting hypoxia-induced stress and energy shortage. Specifically, we observed a pronounced increase in genes

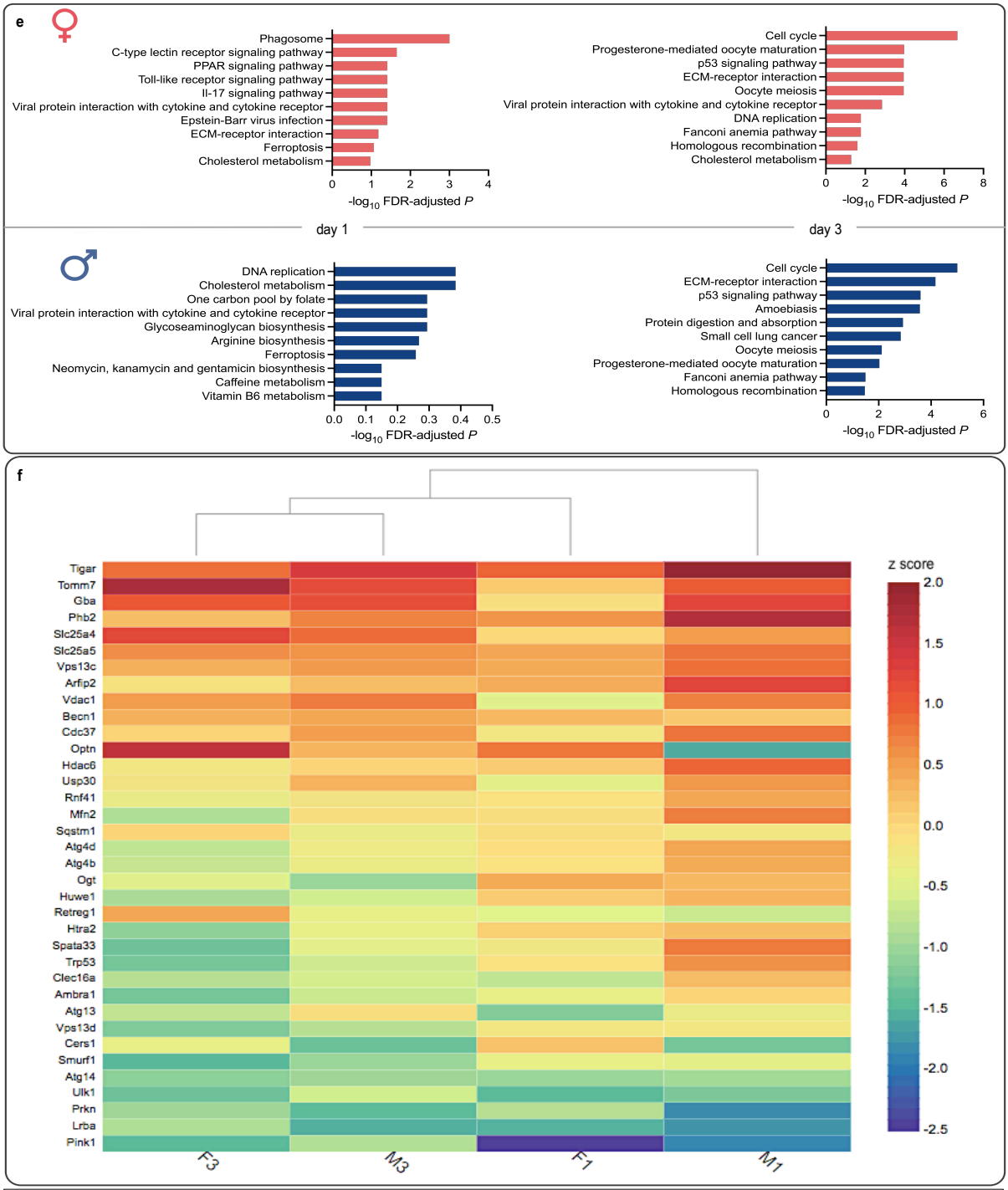

Figure 3.2 | Expression profiling of microglia cells after ischemic stroke (continued). e, Top ten significant KEGG pathways in female (red) and male (blue) microglia one day (left) or three days (right) after stroke with their respective FDR-adjusted *p* values. Enrichr adjusted for multiple comparisons by FDR; *n* = 4 independent samples per condition. **f**, Heatmap of genes related to mitophagy in female and male microglia at day one (F1, M1) and day three (F3, M3) after stroke. Dendrogram for similarity assessment in expression of selected genes across all investigated conditions. Red, upregulated; blue, downregulated. *Figure continued on p. 44.*

involved in the One-Carbon metabolism. In cancer cells, it was shown that One-Carbon metabolism maintains mitochondrial redox balance under hypoxic conditions (Martinez-Reyes and Chandel, 2014), hinting at an adaptive mechanism aimed at maintaining energy metabolism post-stroke in male microglia. In light of this, we decided to check for mitochondrial vitality by assessing gene expression

related to mitophagy (GO:0000423; Fig. 3.2f). Indeed, we found the most pronounced upregulation of mitophagy-associated genes in male microglia on day one post-stroke substantiating our assumption of greater impairment in energy metabolism in male microglia during early phases after stroke. A direct comparison of metabolic activity between male and female microglia further revealed a more pronounced reliance on lipid and amino acid metabolism in female microglia (Fig. 3.2f, Supplementary Fig. 3.2j-k), thus suggesting sex-specific metabolic coping mechanisms of microglia cells in the face of corrupted glucose and oxygen supply. However, these results yet require further functional validation.

By contrast, in female microglia we predominantly saw an overrepresentation of genes involved in phagocytosis and immune-related pathways (Fig. 3.2e), which indicated a response geared toward clearance and resolution of tissue damage in the early post-stroke phase.

By day three, we observed a more similar pattern of pathway activation between female and male mice (Fig. 3.2e), suggesting a functional alignment in the later phases after stroke. Notably, we found an overrepresentation of genes involved in cell cycle processes, which could reflect a regenerative effort of the injured CNS of female and male mice alike.

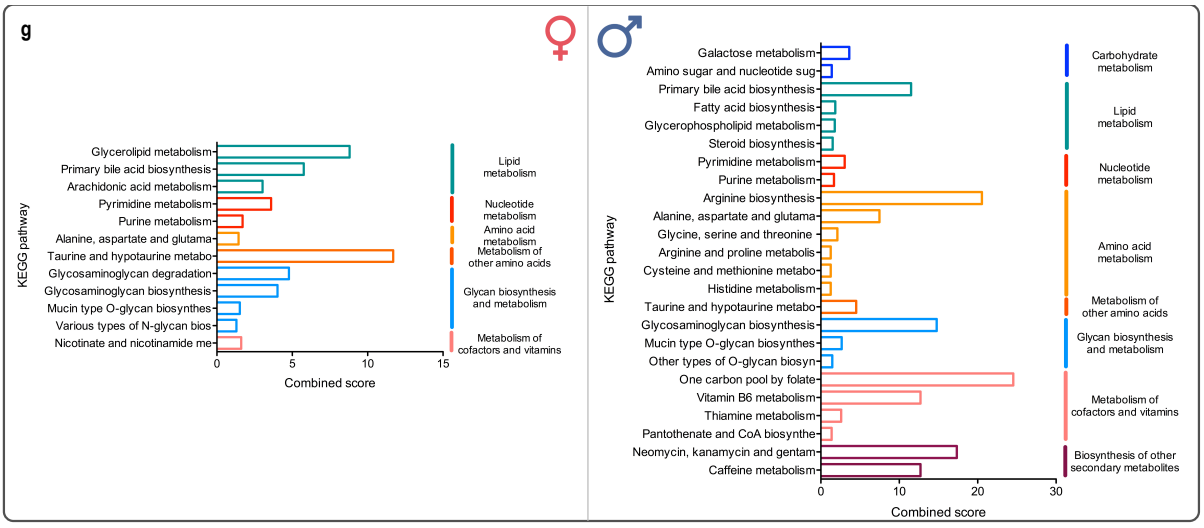

Figure 3.2 | Expression profiling of microglia cells after ischemic stroke (continued). g, Overrepresented KEGG metabolic pathways in female (left) and male (right) microglia 1 d after tMCAO. Enrichr computed combined score.

3.3 Less infiltrating neutrophils in the presence of female microglia. Next, for a deeper understanding of how female and male microglia affect the ensuing post-ischemic inflammation, we decided to analyse and contrast changes in the CNS immune compartment in the presence and absence of microglia cells, respectively (Fig. 3.3a). To this end, we characterised infiltrating immune cells in the CNS of CX3CR1^{creERT2} x iDTR$^{+/-}$ x eYFP$^{+/-}$ microglia-depleted female and male mice, and their CX3CR1^{creERT2} x iDTR$^{-/-}$ x eYFP$^{+/-}$ non-depleted littermates. Again, we decided to focus our analyses on day three after tMCAO, on the one hand to complement our findings on differing lesion

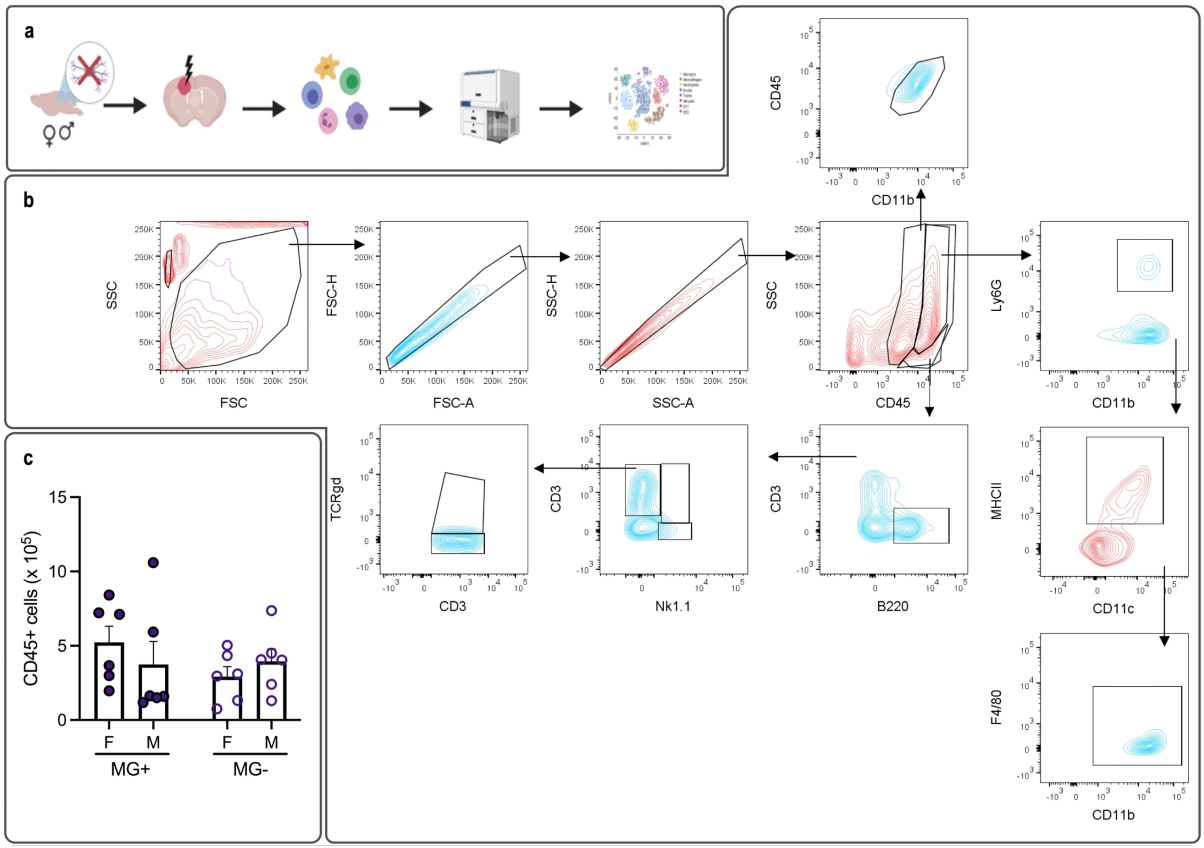

Figure 3.3 | Female and male microglia differentially regulate inflammation post-stroke. a, Experimental overview. **b,** FACS gating strategy to identify different resident and infiltrating immune cell populations. **c,** Quantification of immune cells present in the CNS of MG-depleted or non-depleted female and male mice 3 d after stroke. Ordinary two-way ANOVA (n = 6 per group; $F(1, 20)$ = 1.292, p = 0.2689) with Sidák's post hoc test: F MG+ versus M MG+, p = 0.9827; F MG- versus M MG-, p = 0.9983; F MG+ versus F MG-, p = 0.7005; M MG+ versus M MG-, p > 0.9999; F MG+ versus M MG-, p = 0.9347; M MG+ versus F MG-, p = 0.9850. The bars show mean values ± s.e.m. *Figure continued on p. 46.*

sizes (Fig. 3.1b), and on the other hand to account for the temporal dynamics of post-ischemic infiltration with most peripheral infiltrates peaking at day three after stroke (Gelderblom et al., 2009). We identified the following cell types via FACS (Fig. 3.3b): First, after excluding doublets and debris, immune cells were selected for on the basis of CD45 expression, a pan-hematopoietic immune marker. We distinguished between microglia ($CD45^{int}$), myeloid ($CD45^{high}$, SSC^{high}) and lymphoid ($CD45^{high}$, SSC^{low}) populations. Myeloid cells were further subdivided into neutrophils ($Ly6G^{+}CD11b^{+}$), dendritic cells (DCs; $CD11c^{high}MHCII^{+}$), and monocytes (after DC exclusion: $CD11b^{+}F4/80^{low}$). Lymphoid cells were distinguished into B cells ($B220^{+}CD3^{low}$), NK cells ($Nk1.1^{+}CD3^{low}$), NK T cells ($Nk1.1^{+}CD3^{high}$), ab T cells ($CD3^{+}TCRDgd^{-}$), and gd T cells ($CD3^{+}TCRDgd^{+}$). First and foremost, we broadly checked for quantitative changes in overall infiltration to see if the absence of female and male microglia leads to a more or less pronounced infiltration from peripheral immune cells; however, no such changes were observed (Fig. 3.3c). Thus, we concluded that recruitment and infiltration of peripheral immune cells into the CNS happened independent from microglial activity in both female and male mice. Next, we considered a potential heterogeneity of the cellular composition in the myeloid and lymphoid

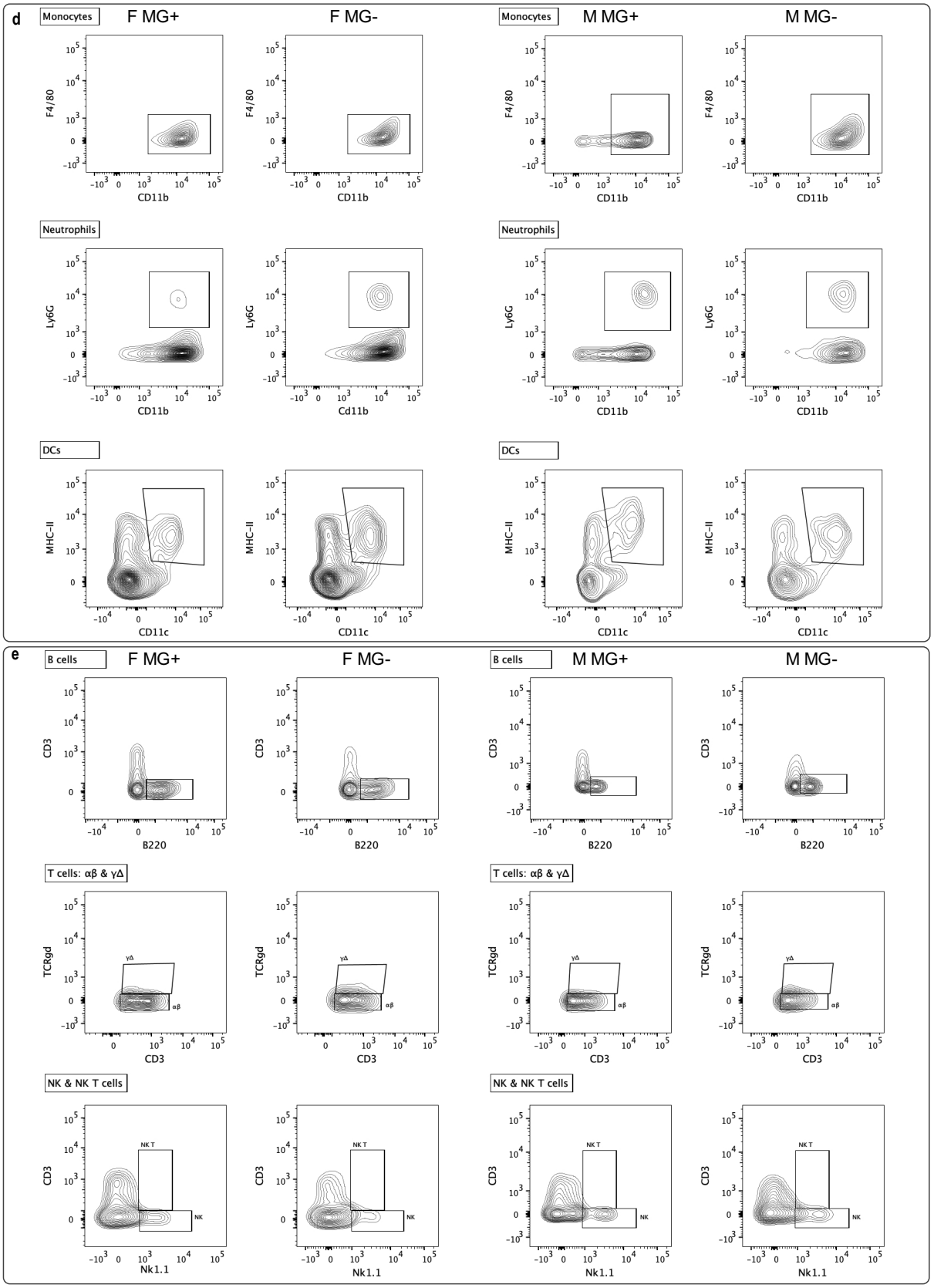

Figure 3.3 | Female and male microglia differentially regulate inflammation post-stroke (continued). d-e, FACS overview of identified myeloid (d) and lymphoid (f) populations in female (left) and male (right) non-depleted (MG+) or MG-depleted (MG-) CNS 3 d after stroke. *Figure continued on p. 47.*

compartment, respectively, depending on whether or not microglia are present at the time point of ischemia. Indeed, at least in females, we observed a significant shift toward neutrophil enrichment and

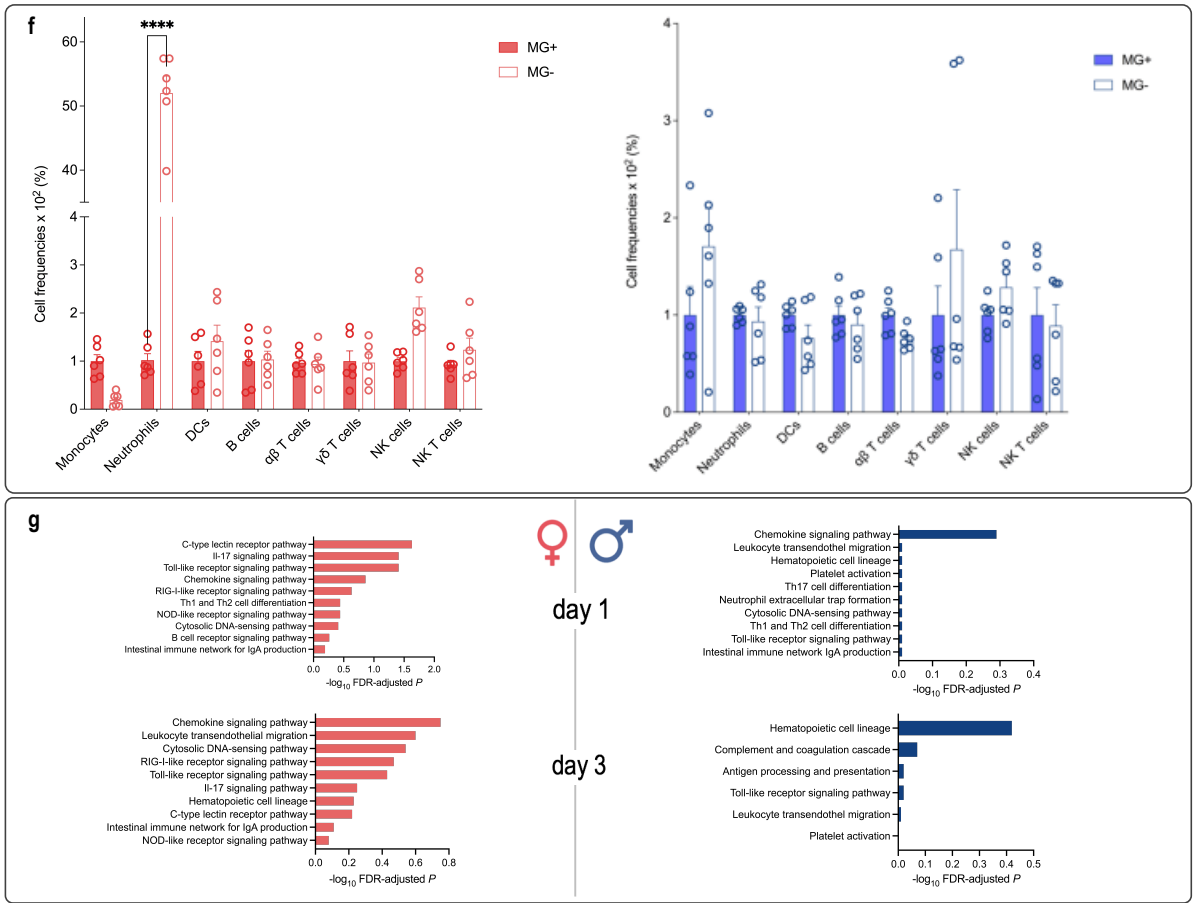

Figure 3.3 | Female and male microglia differentially regulate inflammation post-stroke (continued). f, Microglia-mediated changes in CNS infiltration of different peripheral immune cell populations in female (red) and male (blue) mice 3 d after stroke. Respectively, ordinary two-way ANOVA against MG+ control normalized to 1: n = 6 per group; females: $F(1, 80) = 355.5$, $p < 0.0001$; Sidák's post hoc test: MG+ neutrophils versus MG- neutrophils, $p < 0.0001$; males: $F(1, 80) = 0.9041$, $p = 0.3446$. The bars show mean values ± s.e.m. **g,** Most significant immune-related KEGG pathways in female (red) and male (blue) microglia 1 d (top) or 3 d (bottom) after stroke with their respective FDR-adjusted P values. Enrichr adjusted for multiple comparisons by FDR; n = 4 independent samples per condition. **h**, Gene expression heatmap of cytokine genes involved in neutrophil recruitment in female and male microglia on day one (F1, M1) and day three (F3, M3) after tMCAO. Yellow, upregulated; blue, downregulated. ****$p < 0.0001$

concomitant monocyte reduction in the myeloid compartment in microglia-depleted mice (Fig. 3.3d, f, Supplementary Fig. 3a); we found no alterations in the lymphoid compartment (Fig. 3.3e, f, Supplementary Fig. 3b). In male mice, on the other hand, the absence of microglia at the time of stroke induction did not exert any observable changes in cell composition in both, myeloid and lymphoid populations (Fig. 3.3d-f, Supplementary Fig. 3a, b). Notably, neutrophils have been ascribed a plethora

of adverse effects in ischemic stroke, negatively impacting prognosis (Jickling et al., 2019), severity and infarct volume (Perez-de-Puig, 2015; Chen et al., 2021); their accumulation in the post-ischemic CNS is thus considered harmful. In light of this, our findings of less neutrophils in the presence of female microglia provided a tangible explanation for smaller infarct sizes in female MG+ mice.

Lastly, to better understand the biological processes underlying our observations, we had a deeper look at the respective topmost regulated immune-associated KEGG pathway in female and male microglia (Fig. 3.3g). Again, observing only minimal pathway activity in male mice corroborated our assessment of comparatively little microglia involvement in immune regulation during early stages after stroke and complemented our findings of unaltered infiltration dynamics and lesion sizes in the absence of male microglia. As for female microglia, our main aim was discerning the mechanisms behind the significant increase of infiltrating neutrophils in their absence during tMCAO. We considered two possible explanations: Either, infiltration cascades are altered by microglia depletion because of e.g. absent microglial signals inhibiting neutrophil invasion; or neutrophils accumulate in the absence of microglia because they are no longer readily and quickly cleared from the CNS upon entry. We found that most microglial pathway activity on day one post-stroke was geared toward pattern recognition receptor (PRR) activation, and thus, effective shaping of the immune response: We observed strong association of DE genes with the archetypical Toll-like receptor (TLR) signalling, as well as C-type lectin receptor, nucleotide-binding and oligomerization domain (NOD)-like receptor and retinoic acid-inducible gene (RIG-I)-like receptor signalling. Concomitantly, an overrepresentation of genes involved in the activation of IL-17 receptor signalling pathway and the known involvement of IL-17 in neutrophil recruitment (Weaver, 2013; Flannigan, 2017) suggested that female microglia also participate in the orchestration of neutrophil invasion. This notion was further corroborated by an additional in depth analysis of expression levels of neutrophil attracting chemokines and cytokines (Cai et al., 2020; Metzemaekers et al., 2020) that revealed a pronounced upregulation in female microglia and no or downregulation in male microglia (Fig. 3.3h). Taken together, our analyses suggested that female microglia actively attract and recruit neutrophils to the CNS. However, in spite of this, we had observed an accumulation of neutrophils upon female microglia cell depletion (Fig. 3.3f). Consequently, we hypothesised that the shift toward neutrophil accumulation in the female MG- CNS might have resulted from a lack of microglial clearance activity that decimate neutrophils upon their CNS entry.

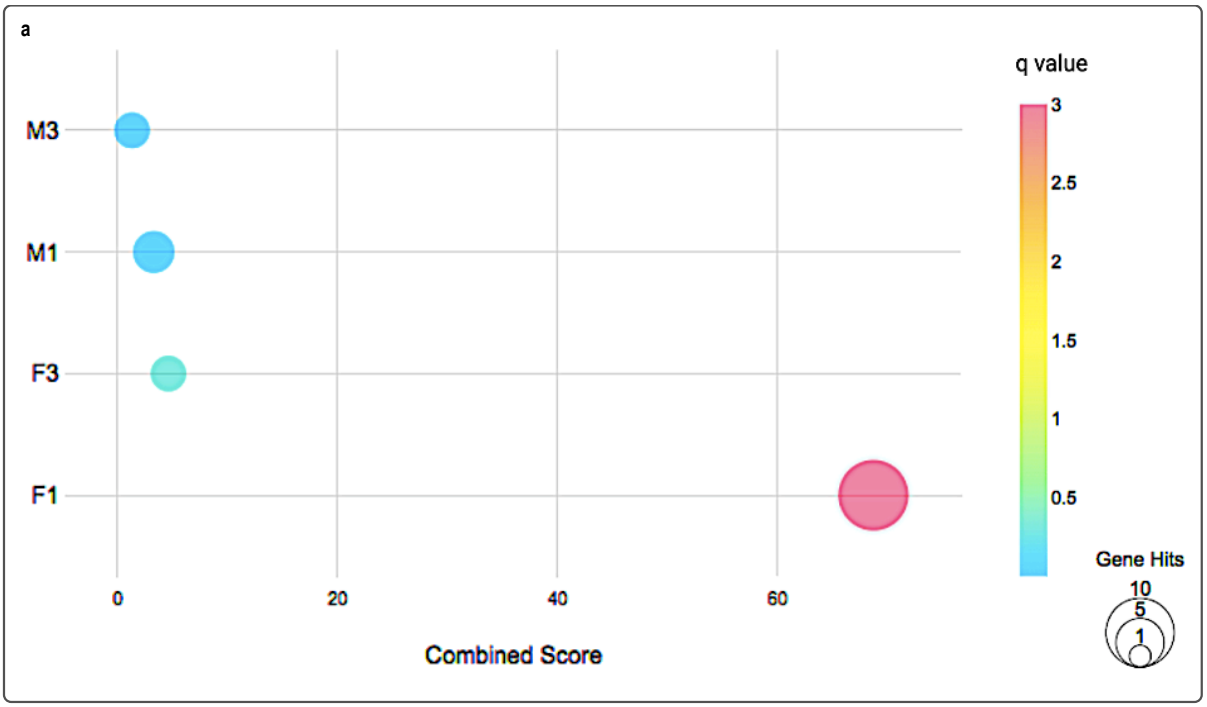

Figure 3.4 | Phagocytosis is a key activity of female microglia in acute stroke. a, Bubble plot of phagocytosis-related gene enrichment in female and male microglia at day one and three after stroke. Red, upregulated; blue, unaffected; node size, gene set size. *Figure continued on p. 51.*

3.4 Phagocytosis as a key function of female microglia in early stages after stroke. Finally, following the notion that female microglia might exert their ameliorative influence by expunging neutrophils from the post-ischemic CNS, we decided to assess microglial phagocytic functioning. To this end, we analysed our RNA-Seq data for phagocytosis-associated gene sets (Fig. 3.4a). Our results were striking: We found a strong overrepresentation of genes involved in phagocytosis in female microglia on day one post-ischemia, thus substantiating our assumption of neutrophil clearance by female microglia. Interestingly, by day three after stroke, phagocytosis-associated genes were considerably less regulated, implying a temporally sensitive dynamic underlying the phagocytic activity of female microglia. In male microglia, on the other hand, we overall did not observe a pronounced overrepresentation of genes involved in phagocytosis, thus highlighting and corroborating a sex-specific dimension of differential microglial functioning in stroke (Villa, 2018).

Additionally, we checked the biological significance of the phagocytosis-associated DE genes in female and male microglia on day one after stroke (Fig. 3.4b). As expected, not only did we find more relevant phagocytosis-associated genes in female microglia but they were also constitutively stronger upregulated.

Next, we assessed how phagocytosis might interact and affect other relevant microglial functions at one day after stroke. To this end, we evaluated shared DE gene activation between different identified

KEGG pathways in female and male mice (Fig. 3.4c). We found a more pronounced interconnectedness between different functions in female microglia with the most prominent associations between phagocytosis, immune system activation, and molecular signalling hinting at an interplay of these processes. In male microglia, interconnectedness between functions was found to be a lot less tangible with only hints of shared gene activity between phagocytosis, immune system and metabolic processes. Taken together, female microglia functioning appeared to be a lot more intricately attuned and interwoven compared to their male counterpart.

Lastly, since our research ambitions are ultimately directed at translating our findings to human patients, we sought to substantiate our findings by comparing murine and human DE genes. As obtaining CNS samples of a critical, early time frame from human stroke patients proved difficult, we instead opted for an analysis of blood. We used a published dataset from human blood samples of stroke patients 3 h after stroke (Theofilatos, 2019) and assessed the similarity in gene expression between human and murine samples (Fig. 3.4d). Since the majority of detected transcripts were of monocytic origin (Theofilatos, 2019) and blood-derived monocytes are known to adopt a microglia-like phenotype in the post-ischemic CNS (Miro-Mur et al., 2016; Pedragosa et al., 2020; Ju et al., 2022) we believed valuable insight to be gained nonetheless. Of our 310 DE genes in female microglia, 168 (approximately 54%) were also found in human blood; in the case of male microglia, of 565 DE genes 325 (approximately 58%) were detected. We then performed GSEA by Enrichr on the gene set implicated in female and male mice as well as human patients and found an overrepresentation of genes involved in phagocytosis. Taken together, we believe this provides strong evidence for the translational applicability of our findings from mouse to man. Ultimately, our data establish phagocytosis as a key function of female microglia during early post-stroke phases and implicate it in neutrophil clearance and lesion size reduction. In light of this, we propose the targeted modulation of microglial phagocytic activity as a viable therapeutic avenue for human stroke patients.

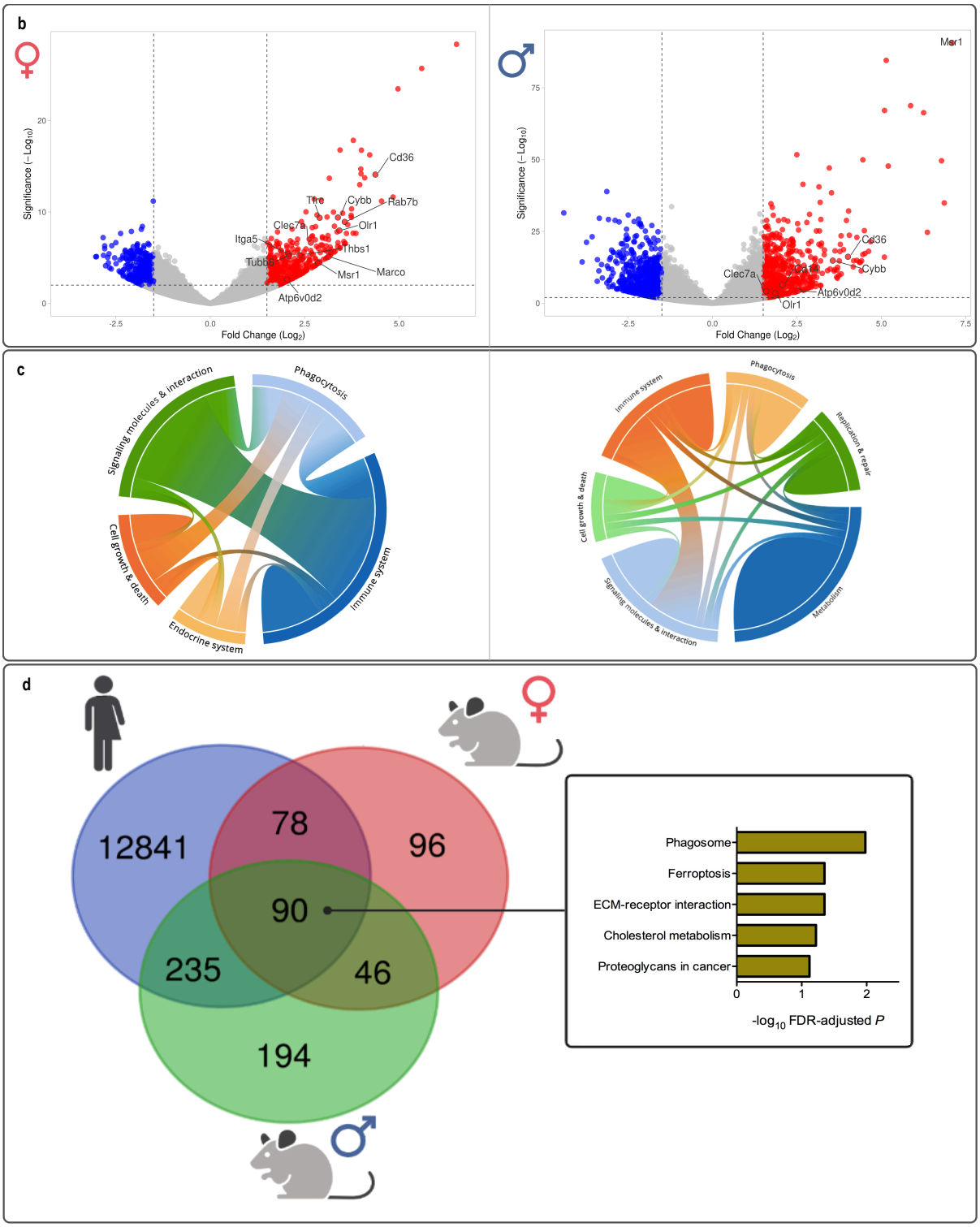

Figure 3.4 | Phagocytosis is a key activity of female microglia in acute stroke (continued). b, Volcano plot showing DE genes associated with phagocytosis in female (left) and male (right) microglia 1 d post-ischemia. **c,** Chord plot of shared gene expression between relevant activated KEGG pathways in female (left) and male (right) microglia of mice 1 d post-ischemia. Strength of connecting lines, similarity in gene expression; arc, gene set size. **d,** Venn diagram showing the overlap between genes upregulated in human stroke patients and DE candidates from either female or male mice 1 d post stroke. Top five most significantly regulated KEGG pathways in the overlapping gene set were identified by Enrichr and are shown with their respective FDR-adjusted *P* values.

4. Discussion

Despite sex being a well-known influencing factor on stroke risk and recovery, there is currently little mechanistic insight into how these sex-specific phenomena occur. One reason for this is the multifaceted nature of sexual dimorphisms which affects and manifests in area-specific (Schwarz et al., 2012), cellular (Klein et al., 2012) and hormonal differences (Cheng et al., 2007; Kavanagh et al., 2009). Nonetheless, considering the immense therapeutic potential to be reaped from understanding physiological sex-specific phenotypes in stroke, unravelling differential changes between females and males appears crucial. In this study, we dismantled sex-specific functional responses in microglia cells in tMCAO and identified female microglia as a key mediator of the post-stroke protective phenotype we see in females (Fig. 3.1). Our RNA-Seq data revealed a stronger divergence in the sex-specific post-stroke response of microglia cells in the early phase after stroke and a lessening in functional divergence over time (Fig. 3.2). During the early phase, metabolic activity dominated in male microglia, whereas female microglia showed a strong increase in phagocytosis. Concomitantly, we found a strong decrease of infiltrating neutrophils in the presence of female microglia (Fig. 3.3). Comparison between DE genes in human stroke patients and tMCAO mice corroborated phagocytic activity as a viable target for therapeutic intervention (Fig. 3.4). Our data thus provides a valuable breach from identifying sex-specific cell type-mediated protective mechanisms to devising promising therapeutic strategies in translational stroke research.

In the following, we will discuss 1. the role of microglia in mediating sex bias in stroke, 2. the functional phenotypes of female and male microglia during the early post-ischemic phase, and 3. the modulation of microglia cell activation as a potential treatment approach in translational stroke research.

4.1 Microglia mediating sex bias in stroke

This study was fundamentally based on the well-known phenomenon that women show, at least pre-climacteric, a protective phenotype in stroke (Golomb et al., 2009; Go et al., 2013). This observation was generally found to be reproducible in the tMCAO animal model of ischemic stroke (Alkayed et al., 1998; Hawk et al., 1998; Turn et al., 2000; Park et al., 2006) where female compared to male mice exhibit smaller infarct sizes. However, it should be noted that the literature on this topic is not entirely consistent with some studies also reporting larger infarcts in female specimen or no sex bias in infarct sizes at all (Kleinbongard et al., 2022; Leppert et al., 2022). In our study, we found a tendency toward smaller infarct sizes in wild-type female (F MG+) compared to male (M MG+) mice, albeit nonsignificant (Fig. 3.1b). One reason for this might be the animals' age at the time point of stroke: In our study, mice underwent tMCAO at an early adult age of 12-14 weeks, whereas some studies extend the treatment window to up to 20 months (Ritzel et al., 2018). As increasing age correlates with increased risk of

stroke and worsened outcome (Kharlamov et al., 2000), it seems possible that using younger animals might preclude and thus obscure some of the more debilitating outcomes in either or both sexes. Another potentially influencing factor might be the microglia-depletion induction regime of TAM- and DTx-treatment. Even within animals where microglia would not be affected by DTx-treatment, i.e. wild-type controls (F/M MG+), exposure to TAM and DTx might affect the CNS more broadly or even microglia cell more specifically. Correspondingly, some studies observed a cytokine storm upon DTx treatment (Bruttger et al., 2015) or behavioural aberrations (Parkhurst et al., 2013). Another study recently demonstrated that microglia are susceptible to pre-conditioning, where exposure to an initial stimulus shapes their response to a later one (Wendeln et al., 2018). In light of this, we decided to check non-depleted (MG+) and repopulating (MG-) microglia cells for an activated phenotype after DTx treatment (Supplementary Fig. 1b). We found a high variability and sporadic downregulation of the homeostatic marker genes *P2ry12* and, to a lesser degree, *Tmem119* in non-depleted but not repopulating microglia, suggesting a reactive state of microglia in MG+ mice. However, since we simultaneously detected a consistent downregulation of microglia activation and pro-inflammatory marker genes (*CD86*, *Tnfa*) and were unable to detect anti-inflammatory marker genes (*Arg1*, *Fizz1*), the explicit nature of DTx-induced microglia activation remains unclear. Most likely, DTx-treatment did indeed perturb the CNS environment but not sufficiently to warrant a decided phenotypic shift toward activation in microglia. We cannot rule out, however, that other CNS cell types displayed a stronger and lasting phenotypic change due to DTx exposure, thus also differentially affecting infarct sizes. Lastly, it has become increasingly recognized that the female's estrous cycle also impacts stroke lesion size with smaller infarcts occurring during proestrus and larger during metestrus (Carswell et al., 2000). As estrous cycles of murine females synchronize when housed together, we can assume that same-litter experimental and control animals underwent the experiments at the same estrous stage. However, there might be differences between litters that we cannot account for as we did not time our experiments in accordance with the animals' estrous cycles. Hence, it is possible that a clearer sex bias in lesion size between female and male mice was partially obfuscated by not adequately controlling for estrous stage as a confounding factor.

Nonetheless, upon introducing microglia cell depletion, we found striking changes in infarct sizes in female mice (Fig. 3.1b). Our observation of enlarged lesion sizes in microglia-depleted females is in line with a recent study which also reported a protective phenotype of female microglia in a different animal model of stroke (Villa et al., 2018). Interestingly, this study additionally described a detrimental phenotype of male microglia, a finding which we were not able to replicate in our tMCAO model. Instead, our data suggests that in male mice, the stroke-induced tissue damage remains largely unaffected by the presence or absence of microglia cells at the time point of ischemia. It should be noted, however,

that we found the stroke-sustained motor deficits in male mice to be ameliorated upon microglia-depletion (Fig. 3.1e), albeit not significantly. Nonetheless, this potentially hints toward a latent detrimental male microglia phenotype also present in our stroke model. Interestingly, despite the stark increase in infarct sizes in female MG- mice, motor deficits did not worsen correspondingly but retained a similar severity as observed in MG+ mice (Fig. 3.1e). As we employed the Bederson scoring scale, the standard albeit large-scale grading tool for assessment of clinical presentation and motor functions, it is possible that a more elaborate and fine-tuned evaluation of afflicted motor skills would reveal a more complex picture.

Nonetheless, in sum, our study substantiated a sex bias in stroke favouring females over males. Moreover, we were able to confirm microglia as crucial mediators of sex-specific phenotypes in stroke. Since sex bias are increasingly recognised in a variety of different pathologies (Zhu et al., 2016; Gold et al., 2019; Crawford et al., 2022), uncovering their biological underpinnings becomes paramount to ensure and maximize treatment efficacy in both women and men. Accordingly, by establishing female microglia as a key regulator of sex bias in stroke, our study prompts these cells as strong contenders for utilizing and regulating sexual dimorphisms for therapeutic intervention.

4.2 Female and male microglia phenotypes in the early post-stroke phase

In recent years, it has become increasingly clear that microglia are the centre of convergence of many CNS processes and functions: Their differentiation is mediated by sex-specific influences (Schwarz et al., 2012; Nelson et al., 2017) and they, in turn, mediate the sexual differentiation of the CNS (Lenz et al., 2013, 2018; VanRyzin et al., 2018; Kopec et al., 2018). They have been shown to not only be engaged in crosstalk with other resident cells within the CNS (Marinelli et al., 2019; Jha et al., 2019) but were also found to be among the first communicators with peripheral immune cells upon CNS injury (Gelderblom et al., 2009). They have been shown to be crucial for proper CNS development (Paolicelli et al., 2011; Schafer et al., 2012; Paolicelli & Ferretti, 2017; Scott-Hewitt et al., 2020), and also crucially involved in many CNS-pathologies (Duffy et al., 2018; Hammond et al., 2019; van der Poel et al., 2019). In short, microglia are a kaleidoscope of diverse functionality, which on the one hand explains why their specific role in a given context can be difficult to pin down, and at the same time showcases their oftentimes integral versatility in establishing and maintaining CNS functions. In our study, we found the following major facets of functional divergence between male and female microglia: a. cell metabolism (Fig. 3.2e, f), b. orchestration of peripheral immune cell infiltration (Fig. 3.3c - h), and c. phagocytic activity (Fig. 3.4a).

Physiologically, as the BBB prevents influx from alternate substrates, the CNS crucially depends on glucose as its energy source. Interestingly, it was found that the developing CNS is not limited to

glucose to power its metabolism, but can instead utilise a variety of alternate fuel sources including ketone bodies, glycerol, lactate, amino acids, and fatty acids for energy and for the biosynthesis of lipids and proteins required for brain development (Nehlig, 2004; Brekke et al., 2015; McKenna et al., 2018). Moreover, a bioenergetic shift was also found in the aged CNS, where microglia switched from glucose to fatty acid utilisation as metabolic fuel (Flowers et al., 2017).

Changes in energy metabolism have been observed in a variety of CNS disorders (Ghosh et al., 2018). At the same time, surprisingly little is known about the bioenergetics in microglia. It has become increasingly recognised, however, that microglia metabolic function displays high adaptive flexibility: *In vitro* studies showed that microglia activation is accompanied by metabolic changes in these cells (Moss et al., 2001; Chenais et al., 2002; Gimeno-Bayon et al., 2014). Concomitantly, transcriptional profiling revealed that microglia express genes related to both, oxidative phosphorylation and glycolysis (Zhang et al., 2014); homeostatic microglia are believed to predominantly rely on OXPHOS for ATP production, whereas activated microglia are thought to rely more heavily on glycolysis to meet energy demands (Van den Bossche et al., 2016; Holland et al., 2018). Indeed, a microglial switch to glycolysis has recently been reported in both, animal models and human patients of neurodegenerative disease, where glycolysis was linked to the extent of present neuroinflammation (Xiang et al., 2021). A switch to glycolysis is known to occur at times when energy is required in the absence of oxygen by routing OXPHOS to produce ATP and lactate. However, it was found that sustained glycolytic metabolism activation leads to low efficiency of ATP production and thus compromised microglial function (Baik et al., 2019).

Interestingly, sex-specific features in metabolic activity have recently been described in a mouse model of Alzheimer's disease suggesting that sex-related differences in microglia metabolism might, at least in part, explain the sexual dimorphism observable in different neuropathological contexts (Guillot-Sestier et al., 2021).

Our data show a higher degree of mitochondrial dysfunction in male compared to female microglia at early time points after stroke (Fig. 3.2f). At the same time, we found overall activity levels in male microglia are considerably less prominently featured than in their female counterparts (Fig. 3.2e, 2.3e). Taken together, this hints at an aggravated difficulty of male microglia to meet their cellular energy demands in ischemic and early post-ischemic CNS conditions and consequently, compromised microglial function. On the other hand, as an effective energy metabolism is required for phagocytosis and tissue clearance, female microglia seem metabolically capable to sustain energy production throughout the early post-ischemic phase.

Concomitantly, we observed a more pronounced effect of female microglia cells on orchestrating the post-stroke infiltration of peripheral immune cells. Interestingly, we did not find a microglia-dependent

modulation of total infiltrating cells in both, female and male mice (Fig. 3.3c), suggesting that microglia rather modulate instead of instigate the post-stroke recruitment of peripheral immune cells to the CNS. In line with previous observations, we did not find strong effects of microglia removal from the male CNS during stroke, whereas in females, we observed a striking shift in infiltrating immune cell composition (Fig. 3.3d). Neutrophils were by far the most strongly affected cell type with their accumulation dramatically increasing in the MG- female CNS. As neutrophils are the first blood-derived immune cell population to enter the CNS upon injury (Gelderblom et al., 2009; Ruhnau et al., 2017), the observed effect of a strong microglia-mediated modulation might be due to the temporal overlap between microglia cell depletion and post-stroke inflammation, not necessarily hinting at a stronger intrinsic link between these cells. Conversely, observing little alterations in the lymphoid cell compartment might be explained by the longer latency in recruitment of these populations to the CNS (Schulze et al., 2021), thus not being influenced by a prior microglia cell depletion.

Recently, it has become increasingly recognized that neutrophil are able to adopt different phenotypes, some of which have been described as beneficial (Cuartero et al., 2006) but mostly detrimental (Adrover et al., 2020; Blanko et al., 2021). Thus, the reduction in neutrophils we observed in the presence of female microglia will most likely exert ameliorative effects on the post-ischemic CNS. As our study does not allow for an in-depth assessment of neutrophil phenotypes, it remains unclear whether their expulsion from the CNS happens in response to a specific phenotypic shift. However, what has long been established is the neuroprotective potential of microglia cells to phagocytose infiltrating neutrophils in stroke (Neumann et al., 2008). More recently, crosstalk between neutrophils and microglia was shown to induce a revered trans-endothelial migration of neutrophils back to the bloodstream (Kim et al., 2020). In light of this, our study substantiates an ongoing interaction between microglia and neutrophils in the post-stroke CNS and, in the context of recent advances, highlights a viable microglia-mediated therapeutic opportunity by modulating neutrophil accumulation in the post-ischemic CNS.

Lastly, our study found a stark contrast in phagocytic activity between female and male microglia in the early post-stroke phase (Fig. 3.2e, Fig. 3.4a, b). Phagocytosis is known as an integral process in the necessary removal of dead cells and tissue debris in stroke (Neumann et al., 2008; Jolivel et al., 2015; Otxoa-de-Amezaga et al., 2019) as well as other neuropathological diseases (Koenigsknecht et al., 2004; Boekhoff et al., 2012; Redondo-Castro et al., 2013). Consequently, dysfunction in microglial phagocytosis was shown to contribute to various CNS disorders (Fu et al., 2014). Moreover, microglia-mediated sex differences in resolution of inflammation have been described (Yanguas-Casas et al., 2018). In line with this, an increase in phagocytic gene expression was found in female microglia from early postnatal rat brains (Nelson et al., 2017), and cultured female microglia have been found to exhibit increased phagocytic activity (Yanguas-Casas et al., 2018). Conversely, a recent study found similar

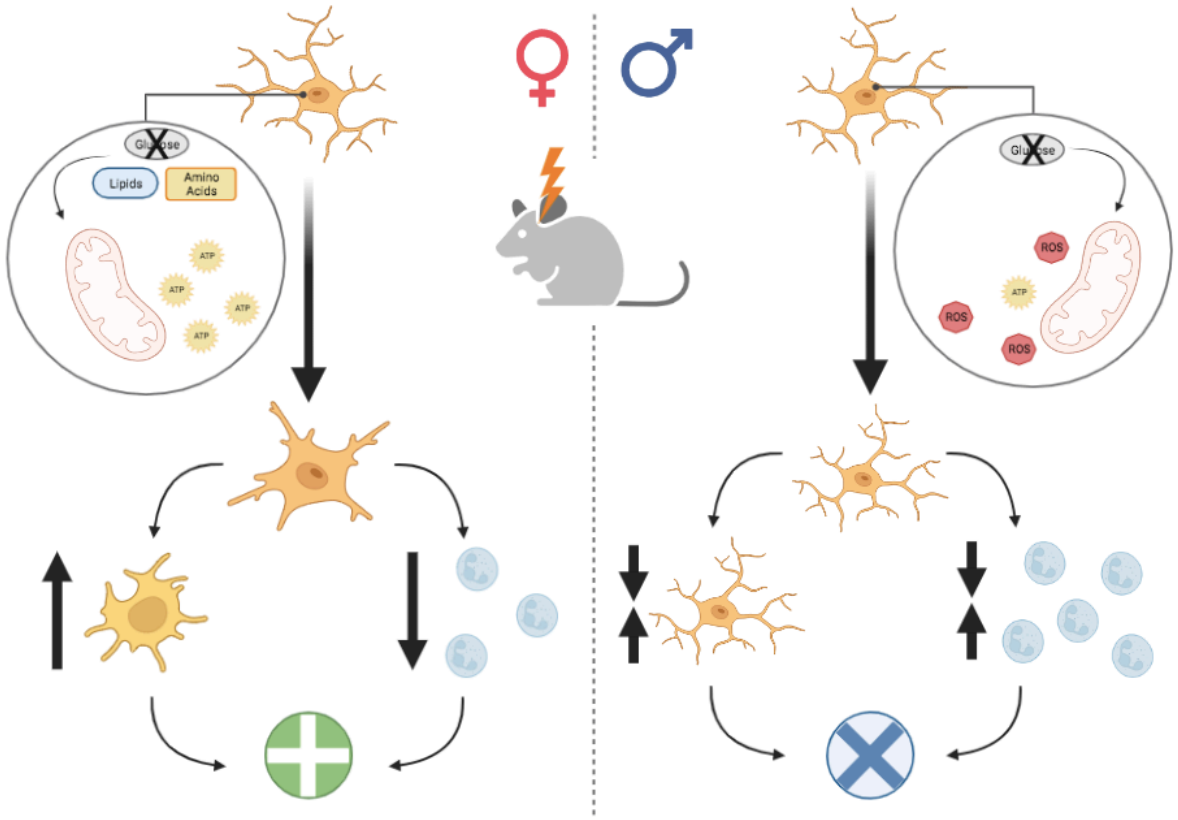

Figure 4.1 | Graphic summary. Sex-specific microglia response during the early post-stroke phase. Left: In female mice, microglia are able to maintain energy metabolism, possibly by supplementing glycolysis with lipids and amino acids under hypoglycemic conditions. Thus, female microglia are able to differentiate into an activated phenotype, increase phagocytosis and reduce infiltrating neutrophil presence. Taken together, female microglia exert an ameliorative effect on the post-ischemic CNS. Right: In male mice, microglia presumably accumulate mitochondrial dysfunction reflected in increased mitophagy. Hence, their energy metabolism appears more strongly impaired by stroke-induced glucose deprivation. As a result, male microglia show overall less functional activation and no strong modulation of peripheral immune cell infiltration, resulting in a neutral phenotype in the early post-stroke phase.

phagocytic activity levels between male and female microglia (Gunekaya et al., 2018). Hence, instead of a pre-existing sex-based feature, enhanced phagocytic activity in female microglia might rather be a latent attribute pre-disposing female microglia to more readily respond to specific circumstances by increased phagocytosis. Interestingly, phagocytic activity has also been described as a core function of a recently identified microglia subtype which emerged in the context of neurodegenerative disease (Krasemann et al., 2017; Keren-Shaul et al., 2017). Overall, phagocytic function seems to be associated with an ameliorative microglia phenotype in various neuropathological diseases (Spiller et al., 2018; Li et al., 2020; Grubman et al., 2021). Fittingly, we also observed aggravated lesion sizes in stroke upon female microglia removal, thereby effectively eliminating their beneficial phagocytic function from the early post-ischemic CNS.

Taken together, our study suggests a sex-based microglia phenotype in bioenergetics resulting in a diminished capacity of male microglia to meet their cellular energy demands and, consequently, reduced overall function. On a more general note, however, it should be appreciated that we conducted bulk RNA-seq. As such, our analyses present an assessment of broad, overarching changes at the

expense of an in-depth study of cellular responses on a single cell level. Naturally, our findings would profit from a substantiation on a single cell level. On the other hand, however, we belive that identifying a general response pattern across celltype heterogeneity presents a valuable pointer for globally acting therapeutics. Accordingly, bolstering energy metabolism in males might present a viable treatment option in stroke. One possible approach is the identification of alternate substrates utilizable for male microglia to power their cell metabolism in hypoxic and hypoglycemic conditions. Alternatively, or concomitantly, stimulating male microglia into increasing their phagocytic activity might prove additionally beneficial in alleviating stroke-induced CNS injury.

4.3 Microglia as a therapeutic target in translational stroke research

Microglia are increasingly recognized as central players and, accordingly, promising targets in neuropathological diseases (Salters et al., 2017; Du et al., 2017; Fumagalli et al., 2018). To utilize and harness their therapeutic potential, however, it is necessary to understand human post-stroke microglial phenotypes in order to adequately match them to observations from animal studies. Our study found of a higher similarity between gene signatures of human stroke patients and male mice (Fig. 3.4d) which can be seen as a tentative hint toward human microglia displaying a phenotype more closely resembling the one we also observed in male mice. Hence, therapeutic strategies should be tailored according to the idiosyncratic nature of male microglia and focus on favourably modulating their post-stroke behaviour.

One such approach might present the „feminization" of male microglia to promote a protective phenotype in stroke. To this end, understanding biological processes underlying sexual differentiation of microglia cells is paramount. Interestingly, while a sex-specific CNS dimorphism was classically believed to be the result of pubescent hormonal surges and accordingly, a sexually differentiated CNS only fully established after adolescence (MacLusky & Naftolin, 1981), this notion has lately been increasingly challenged. On the one hand, substantiating the idea of the hormonal milieu as the basis of sex bias lies the fact that women lose their protective phenotype in stroke once they reach menopause, i.e. once their bodies' estrogen levels drop (Wenger et al., 1993). On the other hand, however, sex differences in stroke were also found in neonatal animals (Nunez et al., 2012) and increasing incidence of stroke in children reflects a similar sex bias of protection in girls (Ferriero et al., 2019) hinting at sex hormones not being the sole or key factor behind sex bias in neuronal injury. In line with this, a recent study found that microglia from adult mice retained their sex-specific signature even in culture (Villa et al., 2018). Moreover, it was previously found that incomplete X chromosome inactivation could cause some genes to be doubly expressed, thus pointing toward a potential genetic explanation of sex differences (Deng et al., 2014). Additionally, microglial function was recently also shown to be affected

by environmental factors such as stress (Chagas et al., 2020). Taken together, the classical believe of sex hormones as the primary constitutive factor for sexual dimorphism might not yield an exhaustive explanation. Given that studies testing estradiol to „feminize" the CNS have only proved inconsistently successful in animal studies (Sampei et al., 2000; Li et al., 2011; Cai et al., 2014) and post-stroke supplementation of estradiol in menopausal women has not been successful in clinical trials (Viscoli et al., 2001), a multifaceted understanding of both, hormonal and non-hormonal cues as drivers behind the sexual differentiation of microglia cells might be more in order instead.

A different therapeutic approach might present the modulation of metabolism via dieting. There is accumulating evidence on dietary patterns influencing metabolic alterations (Grooms et al., 2013; Micha et al., 2017; Sacks et al., 2017; Lacstusu et al., 2019). Specifically, a ketogenic diet was recently demonstrated to inhibit microglia cell activation (Gzielo et al., 2019) and preliminary data suggests that supplementing taurine, an endogenous amino acid with antioxidant and neuroprotective effects (Menzie et al., 2013; Rafiee et al., 2022), could amend stroke outcome by improving mitochondrial function (He et al., 2021). Taken together, there might be considerable therapeutic leverage in appropriate post-stroke dieting to help alleviate CNS injury and thus ameliorate disease severity.

4.4 Concluding remarks

Understanding the causes and mechanisms of sex bias in neuropathological diseases might not only open up new therapeutic avenues but also hone existing strategies by adequately accounting for diverging sexual dimorphisms. To our knowledge, this study is the first to draw a tentative link between sex-specific microglial bioenergetics and activity in stroke. However, further mechanistic studies are warranted to substantiate this claim. Specifically, investigating lactate deposition in female and male microglia as a product of glycolysis or assessing mitochondrial dysfunction and overall cellular metabolic activity in both sexes post-stroke could provide deeper insights into different microglial metabolic phenotypes. Additionally, pharmacologic modulation of metabolic pathway activation in microglia by either OXPHOS inhibition (Antimycin A/Retenone) or glycolysis inhibition (2-deoxy-glucose, 2DG) might prove a promising step toward translational treatment options in stroke.

List of abbreviations

(c)DNA	(complimentary) Desoxyribonucleic Acid
(i)DTR	(inducible) Diphtherie Toxin Receptor
(RT-)qPCR	(Riverse transcriptase-) quantitative Polymerase Chain Reaction
ACA	Anterior Cerebral Artery
ACC	Common Carotid Artery
ACE	External Carotid Artery
ACHA	Anterior Choroidal Artery
ACI	Internal Carotid Artery
AD	Alzheimer's Disease
ADP	Adenosine Diphosphate
AICA	Anterior Inferior Cerebellar Artery
AMP	Adenosine Monophosphate
ATP	Adenosine Triphosphate
BBB	Blood Brain Barrier
BW	Bodyweight
CNS	Central Cervous System
CoA	Coenzyme A
DC	Dendritic Cell
DE(G)	Differentially Expressed (Genes)
DTx	Diphtheria Toxin
EC	Endothelial Cells
ECM	Extracellular Matrix
EDTA	Ethylenediaminetetraacetic acid
eYFP	enhanced Yellow Fluorescent Protein
F	Female
FC	Fold Change
FACS	Flourescence-Activated Cell Sorting
FDR	False Discovery Rate
GSEA	Gene set enrichment analysis
i.p.	intraperitoneal
Iba1	Ionized calcium binding adaptor molecule 1
IL	Interleukin
LPS	Lipopolysaccharide

LSA	Lenticulostriate Artery
M	Male
MCA	Middle Cerebral Artery
MG-	Microglia-, i.e. microglia-depleted
MG+	Microglia+, i.e. non microglia-depleted
MMP	Metalloprotease
NaCl	Sodium Chloride
NCX	Na^{+}/Ca^{2+} exchanger
NO	Nitric Oxide
NOD	Nucleotide Oligomerization Domain
NVU	Neurovascular Unit
ORA	Overrepresentation Analysis
OXPHOS	Oxidative phosphorylation
PBS	Phosphate Buffered Saline
PCA	Posterior Cerebral Artery
PCA	Principal Component Analysis
PFA	Paraformaldehyde
PICA	Posterior Inferior Cerebellar Artery
PRR	Pattern Recognition Receptor
RIG-1	Retinoic acid-Inducible Gene 1
RIN	RNA Integrity Number
RNA	Ribonucleic Acid
RNA-Seq	RNA-Sequencing
ROS	Reactive Oxygen Species
rpm	rotations per minute
RT	Room Temperature
SCA	Superior Cerebellar Artery
TAE	Tris-Acetate-EDTA
TAM	Tamoxifen
TCA	Tricarboxylic Acid
TCR	T Cell Receptor
tg	transgene
TLR	Toll-Like Receptor
tMCAO	transient Middle Cerebral Artery Occlusion

tPA	Tissue Plasminogen Activator
TTC	2,3,5-Triphenyltetrazolium chloride
WT	Wild-type

References

Abdullahi, W., Tripathi, D., Ronaldson, P. T. Blood-brain barrier dysfunction in ischemic stroke: targeting tight junctions and transporters for vascular protection. *Am J Physiol Cell Physiol* **315**, C343–56 (2018)

Abhayaratna, W. P., Seward, J. B., Appleton, C. P., Douglas, P. S., Oh, J. K., Tajik, A. J., et al. Left atrial size: physiologic determinants and clinical applications. *J Am Coll Cardiol* **47**, 2357–63 (2006)

Adrover, J. M., Aroca-Crevillén, A., Crainiciuc, G., Ostos, F., Rojas-Vega, Y., Rubio-Ponce, A., Cilloniz, C., Bonzón-Kulichenko, E., Calvo, E., Rico, D., Moro, M. A., Weber, C., Lizasoaín, I., et al. Programmed 'disarming' of the neutrophil proteome reduces the magnitude of inflammation. *Nat Immunol* **21**, 135-144 (2020)

Altaee, R., Gibson, C. L. Sexual dimorphism following in vitro ischemia in the response to neurosteroids and mechanisms of injury. *BMC Neurosci* **21**, 5 (2020)

Ames, A. 3rd. CNS energy metabolism as related to function. *Brain Res Brain Res Rev.* **34**(1-2), 42-68 (2000)

Arumugam, T., Chan, S., Jo, DG. *et al.* Gamma secretase–mediated Notch signaling worsens brain damage and functional outcome in ischemic stroke. *Nat Med* **12**, 621–623 (2006)

Baik, S. H., Kang, S., Lee, W., Choi, H., Chung, S., Kim, J. I., Mook-Jung, I. A Breakdown in Metabolic Reprogramming Causes Microglia Dysfunction in Alzheimer's Disease. *Cell Metab* **30**, 493-507.e6 (2019)

Bakker, J. The Sexual Differentiation of the Human Brain: Role of Sex Hormones Versus Sex Chromosomes. *Curr Top Behav Neurosci* **43**, 45-67 (2018)

Baron, J. C. Protecting the ischaemic penumbra as an adjunct to thrombectomy for acute stroke. *Nat Rev Neurol.* **14**, 325-337 (2018)

Becker, K. J., Tanzi, P., Zierath, D., Buckwalter, M. S. Antibodies to myelin basic protein are associated with cognitive decline after stroke. *J Neuroimmuno* **296**, 9-11 (2016)

Belov Kirdajova, D., Kriska, J., Tureckova, J., Anderova, M. Ischemia-Triggered Glutamate Excitotoxicity From the Perspective of Glial Cells. *Front Cell Neurosci.* **19**, 51 (2020)

Bernier, L.-P., York, E. M., Kamyabi, Choi, A. H. B., Weilinger, N. L., MacVicar, B. A. Microglial metabolic flexibility supports immune surveillance of the brain parenchyma. *Nat Commun* **11**, 1559 (2020)

Bertram, R., Gram Pedersen, M., Luciani, D. S., Sherman, A. A simplified model for mitochondrial ATP production. *J Theor Biol.* **243**, 575-86 (2006)

Blanco, L. P., Wang, X., Carlucci, P. M., Torres-Ruiz, J. J., Romo-Tena, J., Sun, H. W., Hafner, M., Kaplan, M. J. RNA Externalized by Neutrophil Extracellular Traps Promotes Inflammatory Pathways in Endothelial Cells. *Arthritis Rheumatol* **73**, 2282-2292 (2021)

Boekhoff, T. M., Ensinger, E. M., Carlson, R., Bock, P., Baumgärtner, W., Rohn, K., Tipold, A., Stein, V. M. Microglial contribution to secondary injury evaluated in a large animal model of human spinal cord trauma. *J Neurotrauma* **29**, 1000-11 (2012)

Bonkhoff, A.K., Schirmer, M.D., Bretzner, M. *et al.* Outcome after acute ischemic stroke is linked to sex-specific lesion patterns. *Nat Commun* **12**, 3289 (2021)

Bordt, E. A., Ceasrine, A. M., Bilbo, S. D. Microglia and sexual differentiation of the developing brain: A focus on ontogeny and intrinsic factors. *Glia* **68**, 1085-1099 (2020)

Brekke, E., Morken, T. S., Sonnewald, U. Glucose metabolism and astrocyte-neuron interactions in the neonatal brain. *Neurochem Int* **82**, 33-41 (2015)

Brostjan, C., Oehler, R. The role of neutrophil death in chronic inflammation and cancer. *Cell Death Discov.* **6**, 26 (2020)

Bruttger, J., Karram, K., Wörtge, S., Regen, T., Marini, F., Hoppmann, N., Klein, M., Blank, T., Yona, S., Wolf, Y., Mack, M., Pinteaux, E., Müller, W., Zipp, F., Binder, H., Bopp, T., Prinz, M., Jung, S., Waisman, A. Genetic Cell Ablation Reveals Clusters of Local Self-Renewing Microglia in the Mammalian Central Nervous System. *Immunity* **43**, 92-106 (2015)

Burgess, K., Bennett, C., Mosnier, H., Kwatra, N., Bethel, F., Jadavji, N. M. The Antioxidant Role of One-Carbon Metabolism on Stroke. *Antioxidants* **9**, 1141 (2020)

Busch, M., Kühner R. 12-Month prevalence of stroke or chronic consequences of stroke in Germany. *J of Health Monit* **2**, 64-69 (2017)

Cai, M., Ma, Y. L., Qin, P., Li, Y., Zhang, L. X., Nie, H., Peng, Z., Dong, H., Dong, H. L., Hou, W. G., Xiong, L. Z. The loss of estrogen efficacy against cerebral ischemia in aged postmenopausal female mice. *Neurosci Lett* **558**, 115-9 (2014)

Cai, W., Liu, S., Hu, M., Huang, F., Zhu, Q., Qiu, W., Hu, X., Colello, J., Zheng, S. G., Lu, Z. Functional Dynamics of Neutrophils After Ischemic Stroke. *Transl Stroke Res* **11**, 108-121 (2020)

Campbell, B. C. V., De Silva, D. A., Macleod, M. R. *et al.* Ischaemic stroke. *Nat Rev Dis Primers* **5**, 70 (2019)

Chagas, L. D. S., Sandre, P. C., Ribeiro, E., Ribeiro, N. C. A., Marcondes, H., Oliveira Silva, P., Savino, W., Serfaty, C. A. Environmental Signals on Microglial Function during Brain Development, Neuroplasticity, and Disease. *Int J Mol Sci* **21**, 2111 (2020)

Charchar, F. J., Tomaszewski, M., Padmanabhan, S., Lacka, B., Upton, M. N., Inglis, G. C., et al. The Y chromosome effect on blood pressure in two European populations. *Hypertension* **39**, 353–6 (2002)

Chen, E. Y., Tan, C. M., Kou, Y., Duan, Q., Wang, Z., Meirelles, G. V., Clark, N. R., Ma'ayan, A. Enrichr: interactive and collaborative HTML5 gene list enrichment analysis tool. *BMC Bioinformatics* **14**, 128 (2013)

Chen, J., Zhang, Z., Chen, L., Feng, X., Hu, W., Ge, W., Li, X., Jin, P., Shao, B. Correlation of Changes in Leukocytes Levels 24 Hours after Intravenous Thrombolysis With Prognosis in Patients With Acute Ischemic Stroke. *J Stroke Cerebrovasc Dis* **27**, 2857-2862 (2018)

Chen, R., Zhang, X., Gu, L., Zhu, H., Zhong, Y., Ye, Y., Xiong, X., Jian, Z. New Insight Into Neutrophils: A Potential Therapeutic Target for Cerebral Ischemia. *Front Immunol* **12**, 692061 (2021)

Chen, Y., Bodhankar, S., Murphy, S. J., Vandenbark, A. A., Alkayed, N. J., Offner, H. Intrastriatal B-cell administration limits infarct size after stroke in B-cell deficient mice. *Metab Brain Dis* **27**, 487-93 (2012)

Chen, Y., Hallenbeck, J. M., Ruetzler, C., Bol, D., Thomas, K., Berman, N. E. Overexpression of monocyte chemoattractant protein 1 in the brain exacerbates ischemic brain injury and is associated with recruitment of inflammatory cells. *J Cereb Blood Flow Metab* **23**, 748-755 (2003)

Chenais, B., Morjani, H., Drapier, J. C. Impact of endogenous nitric oxide on microglial cell energy metabolism and labile iron pool. *Journal of neurochemistry* **81**, 615-23 (2002)

Cheng, J., Alkayed, N. J., Hurn, P. D. Deleterious effects of dihydrotestosterone on cerebral ischemic injury. *J Cereb Blood Flow Metab* **27**, 1553–62 (2007)

Clark, D. D., Sokoloff, L. in Basic Neurochemistry: Molecular, Cellular and Medical Aspects, eds. Siegel, G. J., Agranoff, B. W., Albers, R. W., Fisher, S. K. & Uhler, M. D. (Lippincott, Philadelphia), pp. 637–670 (1999)

Conway, S. E., Roy-O'Reilly, M., Friedler, B., Staff, I., Fortunato, G., McCullough, L. D. Sex differences and the role of IL-10 in ischemic stroke recovery. *Biol Sex Differ* **12**, 6-17 (2015)

Cordonnier, C., Sprigg, N., Sandset, E. C., Pavlovic, A., Sunnerhagen, K. S., Caso, V., Christensen, H.; Women Initiative for Stroke in Europe (WISE) group. Stroke in women - from evidence to inequalities. *Nat Rev Neurol* **13**, 521-532 (2017)

Crawford, D. R., Sinha, S., Nair, N. U., Ryan, B. M., Barnholtz-Sloan, J. S., Mount, S. M., Erez, A., Aldape, K., Castle, P. E., Rajagopal, P. S., Day, C. P., Schäffer, A. A., Ruppin, E. Sex Biases in Cancer and Autoimmune Disease Incidence Are Strongly Positively Correlated with Mitochondrial Gene Expression across Human Tissues. *Cancers* **14**, 5885 (2022)

Cuartero, M. I., Ballesteros, I., Moraga, A., Nombela, F., Vivancos, J., Hamilton, J. A., Corbí, Á. L., Lizasoain, I., Moro, M. A. N2 neutrophils, novel players in brain inflammation after stroke: modulation by the PPARγ agonist rosiglitazone*. Stroke* **44**, 3498-508 (2013)

Darzi, Y., Letunic, I., Bork, P., Yamada, T. iPath3.0: interactive pathways explorer v3. *Nucleic Acids Research* **46**, W510–W513 (2018)

Davison, M. A., Ouyang, B., Keppetipola, K. M., Chen, M. Arterial diameter and the gender disparity in stroke thrombectomy outcomes. *Journal of NeuroInterventional Surgery* **10,** 949-952 (2018)

Deng, X., Berletch, J. B., Nguyen, D. K., Disteche, C. M. X chromosome regulation: diverse patterns in development, tissues and disease. *Nat Rev Genet* **15**, 367-78 (2014)

Di Carlo, A., Lamassa, M., Baldereschi, M., Pracucci, G., Basile, A. M., Wolfe, C. D., Giroud, M., Rudd, A., Ghetti, A., Inzitari, D.; European BIOMED Study of Stroke Care Group. Sex differences in the clinical presentation, resource use, and 3-month outcome of acute stroke in Europe: data from a multicenter multinational hospital-based registry. *Stroke* **34**, 1114-9 (2003)

Dobin, A., Davis, C. A., Schlesinger, F., Drenkow, J., Zaleski, C., Jha, S., Batut, P., Chaisson, M., Gingeras, T. R. STAR: ultrafast universal RNA-seq aligner. *Bioinformatics* **29**, 15-21 (2013)

Dotson, A. L., Wang, J., Chen, Y., Manning, D., Nguyen, H., Saugstad, J. A., Offner, H. Sex differences and the role of PPAR alpha in experimental stroke. *Metab Brain Dis* **31**, 539-47 (2016)

Doyle, K. P., Buckwalter, M. S. Does B lymphocyte-mediated autoimmunity contribute to post-stroke dementia? *Brain Behav Immun* **64**, 1–8 (2017)

Doyle, K. P., Quach, L. N., Solé, M., Axtell, R. C., Nguyen, T.-V. V., Soler-Llavina, G. J. et al. B-lymphocyte-mediated delayed cognitive impairment following stroke. *J Neurosci* **35**, 2133–2145 (2015)

Du, L., Zhang, Y., Chen, Y., Zhu, J., Yang, Y., Zhang, H. L. Role of Microglia in Neurological Disorders and Their Potentials as a Therapeutic Target. *Mol Neurobiol* **54**, 7567-7584 (2017)

Duffy, M. F., Collier, T. J., Patterson, J. R., Kemp, C. J., Luk, K. C., Tansey, M. G., Paumier, K. L., Kanaan, N. M., Fischer, D. L., Polinski, N. K., Barth, O. L., Howe, J. W., Vaikath, N. N., Majbour, N. K., El-Agnaf, O. M. A., Sortwell, C. E. Lewy body-like alpha-synuclein inclusions trigger reactive microgliosis prior to nigral degeneration. *J Neuroinflammation* **15**, 129 (2018)

Emberson, J., Lees, K. R., Lyden, P., Blackwell, L., Albers, G., Bluhmki, E., Brott, T., Cohen, G., Davis, S., Donnan, G., Grotta, J., Howard, G., Kaste, M., Koga, M., von Kummer, R., Lansberg, M., Lindley, R. I., Murray, G., Olivot, J. M., Parsons, M., Tilley, B., Toni, D., Toyoda, K., Wahlgren, N., Wardlaw, J., Whiteley, W., del Zoppo, G. J., Baigent, C., Sandercock, P., Hacke, W.; Stroke Thrombolysis Trialists' Collaborative Group. Effect of treatment delay, age, and stroke severity on the effects of intravenous thrombolysis with alteplase for acute ischaemic stroke: a meta-analysis of individual patient data from randomised trials. *Lancet* **384**, 1929-35 (2014)

Feigin, V. L., Nguyen, G., Cercy, K., Johnson, C. O., Alam, T., Parmar, P. G., Abajobir, A. A., Abate, K. H., Abd-Allah, F., Abejie, A. N., Abyu, G. Y., Ademi, Z., et al.; GBD 2016 Lifetime Risk of Stroke Collaborators. Global, regional, and country-specific lifetime risks of stroke, 1990 and 2016. *N Engl J Med* **379**, 2429–2437 (2018)

Felger, J. C., Abe, T., Kaunzner, U. W., Gottfied-Blackmore, A., Gal-Toth J., McEwan B. S., Iadecola C., Bulloch K. Brain dendritic cells in ischemic stroke: Time course, activation state, and origin. *Brain Behav Immun* **24**, 724-737 (2010)

Fenn, A. M., Hall, J. C., Gensel, J. C., Popovich, P. G., Godbout, J. P. IL-4 signaling drives a unique arginase+/IL-1β+ microglia phenotype and recruits macrophages to the inflammatory CNS: consequences of age-related deficits in IL-4Rα after traumatic spinal cord injury. *J Neurosci.* **34**, 8904-17 (2014)

Ferriero, D. M., Fullerton, H. J., Bernard, T. J., Billinghurst, L., Daniels, S. R., DeBaun, M. R., deVeber, G., Ichord, R. N., Jordan, L. C., Massicotte, P., Meldau, J., Roach, E. S., Smith, E. R.; American Heart Association Stroke Council and Council on Cardiovascular and Stroke Nursing. Management of Stroke

in Neonates and Children: A Scientific Statement From the American Heart Association/American Stroke Association. *Stroke* **50**, e51-e96 (2019)

Flannigan, K. L., Ngo, V. L., Geem, D., Harusato, A., Hirota, S. A., Parkos, C. A., Lukacs, N. W., Nusrat A., Gaboriau-Routhiau, V., Cerf-Benussan, N., Gerwitz, A. T., Denning, T. L. IL-17A-mediated neutrophil recruitment limits expansion of segmented filamentous bacteria. *Mucosal Immunology* **10**, 673–684 (2017)

Flowers, A., Bell-Temin, H., Jalloh, A., Stevens, S. M. Jr., Bickford, P. C. Proteomic anaysis of aged microglia: shifts in transcription, bioenergetics, and nutrient response. *J of neuroinflammation* **14**, 96 (2017)

Fricker, M., Tolkovsky, A. M., Borutaite, V., Coleman, M., Brown, G. C. Neuronal Cell Death. *Physiol Rev.* **98**, 813-880 (2018)

Füger, P., Hefendehl, J. K., Veeraraghavalu, K., Wendeln, A. C., Schlosser, C., Obermüller, U., Wegenast-Braun, B. M., Neher, J. J., Martus, P., Kohsaka, S., Thunemann, M., Feil, R., Sisodia, S. S., Skodras, A., Jucker, M. Microglia turnover with aging and in an Alzheimer's model via long-term in vivo single-cell imaging. *Nat Neurosci* **20**, 1371-1376 (2017)

Fumagalli, M., Lombardi, M., Gressens, P., Verderio, C. How to reprogram microglia toward beneficial functions. *Glia* **66**, 2531-2549 (2018)

Gallizioli M., Miró-Mur F., Otxoa-de-Amezaga A., Cugota R., Salas-Pedomo A., Justicia C., Brait V. H., Ruiz-Jaén F., Arbaizar-Rovirosa M., Pedregosa J., Bonfill-Teixidor E., Gelderblom M., Magnus T., Cano E., del Fresno C., Sancho D., Planas A. M. Dendritic cells and microglia have non-redundant functions in the inflamed brain with protective effects of type 1 cDCs. *Cell Rep* **33**, 108291 (2020)

Garcia, J. H., Liu, K. F., Yoshida, Y., Lian, J., Chen, S., del Zoppo, G. J. Influx of leukocytes and platelets in an evolving brain infarct (Wistar rat). *Am J Pathol* **144**, 188-199 (1994)

Garcia-Bonilla, L., Moore, J. M., Racchumi, G., Zhou, P., Butler, J. M., Iadecola, C., Anrather, J. Inducible nitric oxide synthase in neutrophils and endothelium contributes to ischemic brain injury in mice. *J Immunol* **193**, 2531-7 (2014)

García-Rodríguez, D., Giménez-Cassina, A. Ketone Bodies in the Brain Beyond Fuel Metabolism: From Excitability to Gene Expression and Cell Signaling. *Front Mol Neurosci.* **14**, 732120 (2021)

Gelderblom M., Leypoldt, F., Steinbach, K., Behrens, D., Choe, C. U., Siler, D. A., Arumugam, T. V., Orthey, E., Gerloff, C., Tolosa, E., Magnus, T. Temporal and spatial dynamics of cerebral immune cell accumulation in stroke. *Stroke* **40**, 1849-57 (2009)

Gelderblom, M., Weymar, A., Bernreuther, C., Velden, J., Arunachalam, P., Steinbach, K., Orthey, E., Arumugam, T. V., *et al.* Neutralization of the IL-17 axis diminishes neutrophil invasion and protects from ischemic stroke. *Blood* **120**, 3793-802 (2012)

Gelderblom, M., Gallizioli, M., Ludewig, P., Thom, V., Arunachalam, P., Rissiek, B., Bernreuther, C., Glatzel, M., Korn, T., Arumugam, T. V., Sedlacik, J., Gerloff, C., Tolosa, E., Planas, A. M., Magnus T. IL-23 (Interleukin-23)-Producing Conventional Dendritic Cells Control the Detrimental IL-17 (Interleukin-17) Response in Stroke. *Stroke* **49**, 155-164 (2018)

Ghosh, S., Castillo, E., Frias, E. S., Swanson, R. A. Bioenergetic regulation of microglia. *Glia* **66**, 1200-1212 (2018)

Gimeno-Bayon, J., Lopez-Lopez, A., Rodriguez, M. J., Mahy, N. Glucose pathways adaptation supports acquisition of activated microglia phenotype. *Journal of neuroscience research* **92**, 723-31 (2014)

Ginhoux, F., Greter, M., Leboeuf, M., Nandi, S., See, P., Gokhan, S., Mehler, M. F., Conway, S. J., Ng, L. G., Stanley, E. R., et al. Fate mapping analysis reveals that adult microglia derive from primitive macrophages. *Science* **330**, 841–845 (2010)

Glen C. Jickling, G. C., Dziedzic, T. Neutrophil count is related to stroke outcome following endovascular therapy. *Neurology* **93**, 194-195 (2019)

Gliem, M., Mausberg, A. K., Lee, J. I., Simiantonakis, I., van Roojien, N., Hartung, H. P. Macrophages prevent haemorrhagic infarct transformation in murine stroke models. *Ann Neurol* **71**, 743-752 (2012)

Gold, S. M., Willing, A., Leypoldt, F., Paul, F., Friese, M. A. Sex differences in autoimmune disorders of the central nervous system. *Semin Immunopathol* **41**, 177-188 (2019)

Gotoh, H., Nomura, T., Ono, K.: Glycogen serves as an energy source that maintains astrocyte cell proliferation in the neonatal telencephalon. *J Cereb Blood Flow Metab.* **37**, 2294-2307 (2017)

Gouix, E., Buisson, A., Nieoullon, A., Kerkerian-Le Goff, L., Tauskela, J. S., Blondeau, N., Had-Aissouni, L. Oxygen glucose deprivation-induced astrocyte dysfunction provokes neuronal death through oxidative stress. *Pharmacol Res.* **87**, 8-17 (2014)

Grissi, M., Boudot, C., Assem, M., Candellier, A., Lando, M., Poirot-Leclercq, S., Boullier, A., Bennis, Y., Lenglet, G., Avondo, C., Lalau, J. D., Choukroun, G., Massy, Z. A., Kamel, S., Chillon, J. M., Hénaut, L. Metformin prevents stroke damage in non-diabetic female mice with chronic kidney disease. *Sci Rep* **11**, 7464 (2021)

Grooms, K. N., Ommerborn, M. J., Pham, D. Q., Djoussé, L., Clark, C. R. Dietary fiber intake and cardiometabolic risks among US adults, NHANES 1999-2010. *Am J Med* **126**, 1059- 67 (2013)

Grubman, A., Choo, X.Y., Chew, G. *et al.* Transcriptional signature in microglia associated with Aβ plaque phagocytosis. *Nat Commun* **12**, 3015 (2021).

Guillot-Sestier, M.-V., Araiz, A. R., Mela, V., Gaban, A. S., O'Neill, E., Joshi, L., E. T., Chouchani, E. L., Mills, M., Lynch, A. Microglial metabolism is a pivotal factor in sexual dimorphism in Alzheimer's disease. *Commun Biol* **4**, 711 (2021)

Gzielo, K., Soltys, Z., Rajfur, Z., Setkowicz, Z. K. The Impact of the Ketogenic Diet on Glial Cells Morphology. A Quantitative Morphological Analysis. *Neuroscience* **413**, 239-251 (2019)

Hammond, T. R., Dufort, C., Dissing-Olesen, L., Giera, S., Young, A., Wysoker, A., Walker, A. J., Gergits, F., Segel, M., Nemesh, J., Marsh, S. E., Saunders, A., Macosko, E., Ginhoux, F., et al. Single-Cell RNA Sequencing of Microglia throughout the Mouse Lifespan and in the Injured Brain Reveals Complex Cell-State Changes. *Immunity* **50**, 253-271.e6 (2019)

Han, D., Liu, H., Gao, Y. The role of peripheral monocytes and macrophages in ischemic stroke. *Neurol Sci* **41**, 3589–3607 (2020)

Han, J., Fan, Y., Zhou, K., Blomgren, K., Harris, R. A. Uncovering sex differences of rodent microglia. *J Neuroinflammation* **18**, 74 (2021)

Han, L., Shen, W. J., Bittner, S., Kraemer, F. B., Azhar, S. PPARs: regulators of metabolism and as therapeutic targets in cardiovascular disease. Part II: PPAR-β/δ and PPAR-γ. *Future Cardiol* **13**, 279-296 (2017)

Hanamsagar, R., Alter, M. D., Block, C. S., Sullivan, H., Bolton, J. L., Bilbo, S. D. Generation of a microglial developmental index in mice and in humans reveals a sex difference in maturation and immune reactivity. *Glia* **65**, 1504–1520 (2017)

He, W., Tian, X., Zhang, K., Wang, H. Taurine promotes axonal sprouting through mitochondrial improvement in stroke. *Research Square* 1-13 (2021)

Holland, R., McIntosh, A. L., Finucane, O. M., Mela, V., Rubio-Araiz, A., Timmons, G., McCarthy, S. A., Gun'ko, Y. K., Lynch, M. A.. Inflammatory microglia are glycolytic and iron retentive and typify the microglia in APP/PS1 mice. *Brain Behav Immun* **68**, 183-196 (2018)

Howard, V. J., Cushman, M., Pulley, L., Gomez, C. R., Go, R. C., Prineas, R. J., et al. The reasons for geographic and racial differences in stroke study: objectives and design. *Neuroepidemiology* **25**, 135–43 (2005)

Jha, M. K., Jo, M., Kim, J. H., Suk, K. Microglia-Astrocyte Crosstalk: An Intimate Molecular Conversation. *Neuroscientist* **25**, 227-240 (2019)

Jolivel, V., Bicker, F., Binamé, F., Ploen, R., Keller, S., Gollan, R., Jurek, B., Birkenstock, J., Poisa-Beiro, L., Bruttger, J., Opitz, V., Thal, S. C., Waisman, A., Bäuerle, T., et al. Perivascular microglia promote blood vessel disintegration in the ischemic penumbra. *Acta Neuropathol* **129**, 279-95 (2015)

Ju, H., Park, K. W., Kim, I. D., Cave, J. W., Cho, S. Phagocytosis converts infiltrated monocytes to microglia-like phenotype in experimental brain ischemia. *J Neuroinflammation* **19**, 190 (2022)

Kabba, J. A., Xu, Y., Christian, H., Ruan, W., Chenai, K., Xiang, Y., et al. Microglia: housekeeper of the central nervous system. *Cell Mol Neurobiol.* **38**, 53–71 (2018)

Karlen, S.J., Miller, E. B., Wang, X. et al. Monocyte infiltration rather than microglia proliferation dominates the early immune response to rapid photoreceptor degeneration. *J Neuroinflammation* **15**, 344 (2018)

Kavanagh, K., Davis, M. A., Zhang, L., Wilson, M. D., Register, T. C., Adams, M. R., Rudel, L. L., Wagner, J. D. Estrogen decreases atherosclerosis in part by reducing hepatic acyl-CoA:cholesterol acyltransferase 2 (ACAT2) in monkeys. *Arterioscler Thromb Vasc Biol* **29**, 1471-7 (2009)

Kent, D. M., Price, L. L., Ringleb, P., Hill, M. D., Selker, H. P. Sex-based differences in response to recombinant tissue plasminogen activator in acute ischemic stroke: a pooled analysis of randomized clinical trials. *Stroke* **36**, 62–65 (2005)

Keren-Shaul, H., Spinrad, A., Weiner, A., Matcovitch-Natan, O., Dvir-Szternfeld, R., Ulland, T. K., David, E., Baruch, K., Lara-Astaiso, D., Toth, B., Itzkovitz, S., Colonna, M., Schwartz, M., Amit, I. A Unique Microglia Type Associated with Restricting Development of Alzheimer's Disease. *Cell* **169**, 1276-1290.e17 (2017)

Kharlamov, A, Kharlamov, E., Armstrong, D. M. Age-dependent increase in infarct volume following photochemically induced cerebral infarction: putative role of astroglia. *J Gerontol A Biol Sci Med Sci* **55**, B135-43 (2000)

Khatri R, McKinney AM, Swenson B, Janardhan V. Blood-brain barrier, reperfusion injury, and hemorrhagic transformation in acute ischemic stroke. *Neurology* **79**, 3 (2012)

Kierdorf, K., Erny, D., Goldmann, T., Sander, V., Schulz, C., Perdiguero, E. G., Wieghofer, P., Heinrich, A., Riemke, P., Hölscher, C., et al. Microglia emerge from erythromyeloid precursors via Pu.1- and Irf-8-dependent pathways. *Nat Neurosci* **16**, 273–280 (2013)

Kim, Y. R., Kim, Y. M., Lee, J., Park, J., Lee, J. E., Hyun, Y. M. Neutrophils Return to Bloodstream Through the Brain Blood Vessel After Crosstalk With Microglia During LPS-Induced Neuroinflammation. *Front Cell Dev Biol.* **8**, 613733 (2020)

Klein, S. L. Immune cells have sex and so should journal articles. *Endocrinology* **153**, 2544–50 (2012)

Klein, S. L., Flanagan, K. L. Sex differences in immune responses. *Nat Rev Immunol* **16**, 626–638 (2016)

Kleinbongard, P., Lieder, H., Skyschally, A., Heusch, G. No sex-related differences in infarct size, no-reflow and protection by ischaemic preconditioning in Göttingen minipigs. *Cardiovasc Res* **15**, cvac062 (2022)

Kleinschnitz, C., Schwab, N., Kraft, P., Hagedorn, I., Dreykluft, A., Schwarz, T., Austinat, M., Nieswandt, B., Wiendl, H., Stoll, G. Early detrimental T-cell effects in experimental cerebral ischemia are neither related to adaptive immunity nor thrombus formation. *Blood* **115**, 3835-42 (2010)

Koenigsknecht, J., Landreth, G. Microglial phagocytosis of fibrillar beta-amyloid through a beta1 integrin-dependent mechanism. *J Neurosci* **24**, 9838-46 (2004)

Kopec, A. M., Smith, C. J., Ayre, N. R., Sweat, S. C., Bilbo, S. D. Microglial dopamine receptor elimination defines sex-specific nucleus accumbens development and social behavior in adolescent rats. *Nat Commun* **9**, 3769 (2018)

Krasemann, S., Madore, C., Cialic, R., Baufeld, C., Calcagno, N., El Fatimy, R., Beckers, L., O'Loughlin, E., Xu, Y., Fanek, Z., Greco, D. J., Smith, S. T., Tweet, G., Humulock, Z., Zrzavy, T., Conde-Sanroman, P., et al. The TREM2-APOE Pathway Drives the Transcriptional Phenotype of Dysfunctional Microglia in Neurodegenerative Diseases. *Immunity* **47**, 566-581.e9 (2017)

Kuleshov, M. V., Jones, M. R., Rouillard, A. D., Fernandez, N. F., Duan, Q., Wang, Z., Koplev, S., Jenkins, S. L., Jagodnik, K. M., Lachmann, A., McDermott, M. G., Monteiro, C. D., Gundersen, G. W., Ma'ayan, A. Enrichr: a comprehensive gene set enrichment analysis web server 2016 update. *Nucleic Acids Res* **44**, W90-7 (2016)

Lăcătușu, C. M., Grigorescu, E. D., Floria, M., Onofriescu, A., Mihai, B. M. The Mediterranean Diet: From an Environment-Driven Food Culture to an Emerging Medical Prescription. *Int J Environ Res Public Health* **16**, 942 (2019)

Lee, J. W., Profant. M., Wang, C. Metabolic Sex Dimorphism of the Brain at the Gene, Cell, and Tissue Level. *J Immunol* **208**, 212–220 (2022)

LeGates, T. A., Kvarta, M. D., Thompson, S. M. Sex differences in antidepressant efficacy. *Neuropsychopharmacology* **44**, 140–154 (2019)

Lenz, K. M., McCarthy, M. M. A starring role for microglia in brain sex differences. *Neuroscientist* **21**, 306–321 (2015)

Lenz, K. M., Nugent, B. M., Haliyur, R., McCarthy, M. M. Microglia are essential to masculinization of brain and behavior. *J Neurosci* **33**, 2761-72 (2013)

Lenz, K. M., Pickett, L. A., Wright, C. L., Davis, K. T., Joshi, A., McCarthy, M. M. Mast Cells in the Developing Brain Determine Adult Sexual Behavior. *J Neurosci* **38**, 8044-8059 (2018)

Leppert, M. H., Burke, J. F., Lisabeth, L. D., Madsen, T. E., Kleindorfer, D. O., Sillau, S., Schwamm, L. H., Daugherty, S. L., Bradley, C. J., Ho, P. M., Poisson, S. N. Systematic Review of Sex Differences in Ischemic Strokes Among Young Adults: Are Young Women Disproportionately at Risk? *Stroke* **53**, 319-327 (2022)

Li, L. Z., Huang, Y. Y., Yang, Z. H., Zhang, S. J., Han, Z. P., Luo, Y. M. Potential microglia-based interventions for stroke. *CNS Neurosci Ther.* **26**, 288-296 (2020)

Li, J., Siegel, M., Yuan, M., Zeng, Z., Finnucan, L., Persky, R., Hurn, P. D., McCullough, L. D. Estrogen enhances neurogenesis and behavioral recovery after stroke. *J Cereb Blood Flow Metab* **31**, 413-25 (2011)

Li, Q., Barres, B. A. Microglia and macrophages in brain homeostasis and disease. *Nat Rev Immunol* **18**, 225–242 (2018)

Li, R., Sun, X., Shu, Y., Mao, Z., Xiao, L., Qiu, W., Lu, Z., Hu, X. Sex differences in outcomes of disease-modifying treatments for multiple sclerosis: a systematic review. *Mult Scler Relat Disord* **12**, 23–28 (2017)

Li, Y., He, X., Kawaguchi, R., Zhang, Y., Wang, Q., Monavarfeshani, A., Yang, Z., Chen, B., Shi, Z., et al. Microglia-organized scar-free spinal cord repair in neonatal mice. *Nature* **587**, 613-618 (2020)

Liao, Y., Smyth, G. K., Shi, W. featureCounts: an efficient general purpose program for assigning sequence reads to genomic features. *Bioinformatics* **30**, 923-30 (2014)

Liesz, A., Suri-Payer, E., Veltkamp, C., Doerr, H., Sommer, C., Rivest, S., Giese, T., Veltkamp, R. Regulatory T cells are key cerebroprotective immunomodulators in acute experimental stroke. *Nat Med* **15**,192-9 (2009)

Liu, R., Pan, M.-X., Tang, J.-C., Zhang, Y., Liao, H.-B., Zhuang, Y., et al. Role of neuroinflammation in ischemic stroke. *Neuroimmunol Neuroinflammation* **4**, 158 (2017)

Lorenzano, S., Ahmed, N., Falcou, A., Mikulik, R., Tatlisumak, T., Roffe, C., et al. Does sex influence the response to intravenous thrombolysis in ischemic stroke?: answers from safe implementation of treatments in Stroke-International Stroke Thrombolysis Register. *Stroke* **44**, 3401–6 (2013)

Love, M. I., Huber, W., Anders, S. Moderated estimation of fold change and dispersion for RNA-seq data with DESeq2. *Genome Biol* **15**, 550 (2014)

Lu, J., Zhou, W., Dou, F., Wang, C., Yu, Z. TRPV1 sustains microglial metabolic reprogramming in Alzheimer's disease. *EMBO Rep* **22**, e52013 (2021)

Lund, H., Pieber, M., Parsa, R. et al. Competitive repopulation of an empty microglial niche yields functionally distinct subsets of microglia-like cells. *Nat Commun* **9**, 4845 (2018)

Lynch, M. A. Exploring Sex-Related Differences in Microglia May Be a Game-Changer in Precision Medicine. *Front Aging Neurosci* **14**, 868448 (2022)

MacLusky, N. J., Naftolin, F. Sexual differentiation of the central nervous system. *Science* **211**, 1294-302 (1981)

Manwani, B., Bentivegna, K., Benashski, S. E., Venna, V. R., Xu, Y., Arnold, A. P., McCullough, L. D. Sex differences in ischemic stroke sensitivity are influenced by gonadal hormones, not by sex chromosome complement. *J Cereb Blood Flow Metab* **35**, 221-9 (2015)

Mao, R., Zong, N., Hu, Y. *et al.* Neuronal Death Mechanisms and Therapeutic Strategy in Ischemic Stroke. *Neurosci. Bull.* **38**, 1229–1247 (2022).

Marinelli, S., Basilico, B., Marrone, M. C., Ragozzino, D. Microglia-neuron crosstalk: Signaling mechanism and control of synaptic transmission. *Semin Cell Dev Biol* **94**, 138-151 (2019)

Márquez, E. J., Chung, C. H., Marches, R., Rossi, R. J., Nehar-Belaid, D., Eroglu, A., Mellert, D. J., Kuchel, G. A., Banchereau, J., Ucar, D. Sexual-dimorphism in human immune system aging. *Nat Commun* **11**, 751 (2020)

Martínez-Reyes, I., Chandel, N. S. Mitochondrial one-carbon metabolism maintains redox balance during hypoxia. *Cancer Discov* **4**, 1371-3 (2014)

McConell, H. L., Kersch, C. N., Woltjer, R. L., Neuwelt, E. A. The translational significance oft he neurovascular unit. *J Biol Chem* **292**, 767-770 (2017)

McKenna, M. C., Schuck, P. F., Ferreira, G. C. Fundamentals of CNS energy metabolism and alterations in lysosomal storage diseases. *J Neurochem* **148**, 590-599 (2019)

Meng, H., Zhao, H., Cao, X., Hao, J., Zhang, H., Liu, Y., Zhu, M. S., Fan, L., Weng, L., Qian, L., Wang, X., Xu, Y. Double-negative T cells remarkably promote neuroinflammation after ischemic stroke. *Proc Natl Acad Sci U S A* **116**, 5558-5563 (2019)

Menzie, J., Prentice, H., Wu, J. Y. Neuroprotective Mechanisms of Taurine against Ischemic Stroke. *Brain Sci* **3**, 877-907 (2013)

Merali, Z., Huang, K., Mikulis, D., Silver, F., and Kassner, A. Evolution of blood-brain-barrier permeability after acute ischemic stroke. *PLoS One* **12**, e0171558 (2017)

Merico, D., Isserlin, R., Stueker, O., Emili, A., Bader, G. D. Enrichment map: a network-based method for gene-set enrichment visualization and interpretation. *PLoS One* **5**, e13984 (2010)

Metzemaekers, M., Gouwy, M., Proost, P. Neutrophil chemoattractant receptors in health and disease: double-edged swords. *Cell Mol Immunol* **17**, 433-450 (2020)

Micha, R., Peñalvo, J. L., Cudhea, F., Imamura, F., Rehm, C. D., Mozaffarian, D. Association Between Dietary Factors and Mortality From Heart Disease, Stroke, and Type 2 Diabetes in the United States. *JAMA* **317**, 912-924 (2017)

Minhas, P. S., Latif-Hernandez, A., McReynolds, M. R., Durairaj, A. S., Wang, Q., Rubin, A., Joshi, A. U., He, J. Q., Gauba, E., Liu, L., et al. Restoring metabolism of myeloid cells reverses cognitive decline in ageing. *Nature* **590**, 122–128 (2021)

Miró-Mur, F., Pérez-de-Puig, I., Ferrer-Ferrer, M., Urra, X., Justicia, C., Chamorro, A., Planas, A. M. Immature monocytes recruited to the ischemic mouse brain differentiate into macrophages with features of alternative activation. *Brain Behav Immun* **53**, 18-33 (2016)

Moss, D. W., Bates, T. E. Activation of murine microglial cell lines by lipopolysaccharide and interferon-gamma causes NO-mediated decreases in mitochondrial and cellular function. *The European journal of neuroscience* **13**, 529-38 (2001)

Muzio, L., Viotti, A., Martino, G. Microglia in Neuroinflammation and Neurodegeneration: From Understanding to Therapy. *Front Neurosci* **15**, 742065 (2021)

Nehlig, A. Brain uptake and metabolism of ketone bodies in animal models. *Prostaglandins Leikot. Essent. Fatty Acids* **70**, 265-275 (2004)

Nelson, L. H., Warden, S., Lenz, K. M. Sex differences in microglial phagocytosis in the neonatal hippocampus. *Brain Behav Immun* **64**, 11-22 (2017)

Neumann, J., Sauerzweig, S., Rönicke, R., Gunzer, F., Dinkel, K., Ullrich, O., Gunzer, M., Reymann, K. G. Microglia cells protect neurons by direct engulfment of invading neutrophil granulocytes: a new mechanism of CNS immune privilege. *J Neurosci* **28**, 5965-75 (2008)

Nuñez, J. Sex and steroid hormones in early brain injury. *Rev Endocr Metab Disord* **13**, 173-86 (2012)

Oliva, M., Muñoz-Aguirre, M., Kim-Hellmuth, S., Wucher, V., Gewirtz, A. D. H., Cotter, D. J., Parsana, P., Kasela, S., Balliu, B., Viñuela, A.; GTEx Consortium. The impact of sex on gene expression across human tissues. *Science* **369**, eaba3066 (2020)

Olthuis, S. G. H., Pirson, F. A. V., Pinckaers, F. M. E., Hinsenveld, W. H., Nieboer, D., Ceulemans, A., *et al.* MR CLEAN-LATE investigators. Endovascular treatment versus no endovascular treatment after 6-24 h in patients with ischaemic stroke and collateral flow on CT angiography (MR CLEAN-LATE) in the Netherlands: a multicentre, open-label, blinded-endpoint, randomised, controlled, phase 3 trial. *Lancet* **401**, 1371-1380 (2023)

Ortega, S. B., Torres, V. O., Latchney, S. E., Whoolery, C. W., Noorbhai, I. Z., Poinsatte, K., Selvaraj, U. M., Benson, M. A., Meeuwissen, A. J. M., Plautz, E. J., Kong, X., Ramirez, D. M., Ajay, A. D., Meeks, J.

P., Goldberg, M. P., Monson, N. L., Eisch, A. J., Stowe, A. M. B cells migrate into remote brain areas and support neurogenesis and functional recovery after focal stroke in mice. *Proc Natl Acad Sci USA* **117**, 4983-4993 (2020)

Otxoa-de-Amezaga, A., Miró-Mur, F., Pedragosa, J., Gallizioli, M., Justicia, C., Gaja-Capdevila, N., Ruíz-Jaen, F., Salas-Perdomo, A., Bosch, A., et al. Microglial cell loss after ischemic stroke favors brain neutrophil accumulation. *Acta Neuropathol* **137**, 321-341 (2019)

Paolicelli, R. C., Bolasco, G., Pagani, F., Maggi, L., Scianni, M., Panzanelli, P., Giustetto, M., Ferreira, T. A., Guiducci, E., Dumas, L., Ragozzino, D., Gross, C. T. Synaptic pruning by microglia is necessary for normal brain development. *Science* **333**, 1456-8 (2011)

Paolicelli, R. C., Ferretti, M. T. Function and Dysfunction of Microglia during Brain Development: Consequences for Synapses and Neural Circuits. *Front Synaptic Neurosci* **10**, 9 (2017)

Parkhurst, C. N., Yang, G., Ninan, I., Savas, J. N., Yates, J. R. 3rd, Lafaille, J. J., Hempstead, B. L., Littman, D. R., Gan, W. B. Microglia promote learning-dependent synapse formation through brain-derived neurotrophic factor. *Cell* **155**, 1596-609 (2013)

Pedragosa, J., Miró-Mur, F., Otxoa-de-Amezaga, A., Justicia, C., Ruíz-Jaén, F., Ponsaerts, P., Pasparakis, M., Planas, A. M. CCR2 deficiency in monocytes impairs angiogenesis and functional recovery after ischemic stroke in mice. *J Cereb Blood Flow Metab* **40**, 98-116 (2020)

Perez-de-Puig, I., Miro-Mur, F., Ferrer-Ferrer, M., Gelpi E., Pedragosa, J., Justicia, C., Urra, X., Chamorro, A., Planas, A. M. Neutrophil recruitment to the brain in mouse and human ischemic stroke. *Acta Neuropathol* **129**, 239–257 (2015)

Pfeiffer, T., Schuster, S., Bonhoeffer, S. Cooperation and competition in the evolution of ATP-producing pathways. *Science* **292**, 504-7 (2001)

Plass, D., Vos, T., Hornberg, C., Scheidt-Nave, C., Zeeb, H., Krämer, A. Trends in disease burden in Germany–results, implications and limitations of the Global Burden of Disease Study. *Dtsch Arztebl Int* **111**, 629–38 (2014)

Qiu, S., Xu, Y. Guidelines for Acute Ischemic Stroke Treatment. *Neurosci Bull.* **36**, 1229-1232 (2020)

Rafiee, Z., García-Serrano, A.M., Duarte, J. M. N. Taurine Supplementation as a Neuroprotective Strategy upon Brain Dysfunction in Metabolic Syndrome and Diabetes. *Nutrients* **14***,* 1292 (2022)

Redondo-Castro, E., Hernández, J., Mahy, N., Navarro, X. Phagocytic microglial phenotype induced by glibenclamide improves functional recovery but worsens hyperalgesia after spinal cord injury in adult rats. *Eur J Neurosci* **38**, 3786-98 (2013)

Ren, X., Akiyoshi, K., Dziennis, S., Vandenbark, A. A., Herson, P. S., Hurn, P. D., Offner, H. Regulatory B cells limit CNS inflammation and neurologic deficits in murine experimental stroke. *J Neurosci* **31**, 8556-63 (2011)

Réu, P., Khosravi, A., Bernard, S., Mold, J. E., Salehpour, M., Alkass, K., Perl, S., Tisdale, J., Possnert, G., Druid, H., Frisén, J. The Lifespan and Turnover of Microglia in the Human Brain. *Cell Rep* **20**, 779-784 (2017)

Ritzel, R. M., Lai, Y. J., Crapser, J. D., Patel, A. R., Schrecengost, A., Grenier, J. M., Mancini, N. S., Patrizz, A., Jellison, E. R., Morales-Scheihing, D., Venna, V. R., Kofler, J. K., Liu, F., Verma, R., McCullough, L. D. Aging alters the immunological response to ischemic stroke. *Acta Neuropathol* **136**, 89-110 (2018)

Rivoal, J., Hanson, A. D. Metabolic Control of Anaerobic Glycolysis (Overexpression of Lactate Dehydrogenase in Transgenic Tomato Roots Supports the Davies-Roberts Hypothesis and Points to a Critical Role for Lactate Secretion. *Plant Physiol.* **106**, 1179-1185 (1994)

Ruhnau, J., Schulze, J., Dressel, A., Vogelgesang, A. Thrombosis, Neuroinflammation, and Poststroke Infection: The Multifaceted Role of Neutrophils in Stroke. *J Immunol Res* **27**, 5140679 (2017)

Sacks, F. M., Lichtenstein, A. H., Wu, J. H. Y., Appel, L. J., Creager, M. A., Kris-Etherton, P. M., Miller, M., Rimm, E. B., Rudel, L. L., Robinson, J. G., Stone, N. J., Van Horn, L. V.; American Heart Association. Dietary Fats and Cardiovascular Disease: A Presidential Advisory From the American Heart Association. *Circulation* **136**, e1-e23 (2017)

Saini, V., Guada, L., Yavagal, D. R. Global Epidemiology of Stroke and Access to Acute Ischemic Stroke Interventions. *Neurology* **97**, 6-16 (2021)

Salter, M. W., Stevens, B. Microglia emerge as central players in brain disease. *Nat Med* **23**, 1018-1027 (2017)

Sampei, K., Goto, S., Alkayed, N. J., Crain, B. J., Korach, K. S., Traystman, R. J., Demas, G. E., Nelson, R. J., Hurn, P. D. Stroke in estrogen receptor-alpha-deficient mice. *Stroke* **31**, 738-744 (2000)

Sarraj, A., Hassan, A. E., Abraham, M. G., *et al.* Trial of Endovascular Thrombectomy for Large Ischemic Strokes. *N Engl J Med* **388**, 1259-1271 (2023)

Schafer, D. P., Lehrman, E. K., Kautzman, A. G., Koyama, R., Mardinly, A. R., Yamasaki, R., Ransohoff, R. M., Greenberg, M. E., Barres, B. A., Stevens, B. Microglia sculpt postnatal neural circuits in an activity and complement-dependent manner. *Neuron* **74**, 691-705 (2012)

Schnitzer, A., McGovern, N., Ginhoux, F. Dendritic cells and monocyte-derived cells: Two complementary and integrated functional systems. *Semin Cell Dev Biol* **41**, 9-22 (2015)

Schulze, J., Gellrich, J., Kirsch, M., Dressel, A., Vogelgesang, A. Central Nervous System-Infiltrating T Lymphocytes in Stroke Are Activated via Their TCR (T-Cell Receptor) but Lack CD25 Expression. *Stroke* **52**, 2939-2947 (2021)

Schwarz, J. M., Sholar, P. W., Bilbo, S. D. Sex differences in microglial colonization of the developing rat brain. *J Neurochem* **120**, 948-63 (2012)

Scott-Hewitt, N., Perrucci, F., Morini, R., Erreni, M., Mahoney, M., Witkowska, A., Carey, A., Faggiani, E., Schuetz, L. T., Mason, S., Tamborini, M., Bizzotto, M., Passoni, L., Filipello, F., Jahn, R., Stevens, B., Matteoli, M. Local externalization of phosphatidylserine mediates developmental synaptic pruning by microglia. *EMBO J* **39**, e105380 (2020)

Selvamani, A., Sohrabji, F. Reproductive age modulates the impact of focal ischemia on the forebrain as well as the effects of estrogen treatment in female rats. *Neurobiol Aging* **31**, 1618-28 (2010)

Shi, L., Sun, Z., Su, W., Xu, F., Xie, D., Zhang, Q., Dai, X., et al. Treg cell-derived osteopontin promotes microglia-mediated white matter repair after ischemic stroke. *Immunity* **54**, 1527-1542.e8 (2021)

Shimakura, A., Kamanaka, Y., Ikeda, Y., Kondo, K., Suzuki, Y., Umemura, K. Neutrophil elastase inhibition reduces cerebral ischemic damage in the middle cerebral artery occlusion. *Brain Res* **858**, 55–60 (2000)

Song, S., Yu, L., Hasan, M. N., Paruchuri, S. S., Mullett, S. J., Sullivan, M. L. G., Fiesler, V. M., Young, C. B., Stolz, D. B., Wendell, S. G., Sun, D. Elevated microglial oxidative phosphorylation and phagocytosis stimulate post-stroke brain remodeling and cognitive function recovery in mice. *Commun Biol* **5**, 35 (2022)

Spiller, K. J., Restrepo, C. R., Khan, T., Dominique, M. A., Fang, T. C., Canter, R. G., Roberts, C. J., Miller, K. R., Ransohoff, R. M., Trojanowski, J. Q., Lee, V. M. Microglia-mediated recovery from ALS-relevant motor neuron degeneration in a mouse model of TDP-43 proteinopathy. *Nat Neurosci* **21**, 329-340 (2018)

Strbian, D., Durukan, A., Pitkonen, M., Marinkovic, I., Tatlisumak, E., Pedrono, E., Abo-Ramadan, U., Tatlisumak, T. The blood-brain barrier is continuously open for several weeks following transient focal cerebral ischemia. *Neuroscience* **153**, 175-81 (2008)

Sun, J. C., Beilke, J. N., Lanier, L. L. Adaptive immune features of natural killer cells. *Nature* **457**, 557-61 (2009)

Szepesi, Z., Manouchehrian, O., Bachiller, S., Deierborg, T. Bidirectional Microglia-Neuron Communication in Health and Disease. *Front Cell Neurosci.* **12**, 323 (2018)

Theofilatos, K., Korfiati, A., Mavroudi, S., Cowperthwaite, M. C., Shpak, M. Discovery of stroke-related blood biomarkers from gene expression network models. *BMC Med Genomics* **12**, 118 (2019)

Thiebaut, A. M., Hedou, E., Marciniak, S. J., Vivien, D., Roussel, B. D. Proteostasis During Cerebral Ischemia. *Front Neurosci.* **13**, 637 (2019)

Tian, Y., Stamova, B., Jickling, G. C., Liu, D., Ander, B. P., Bushnell, C., et al. Effects of gender on gene expression in the blood of ischemic stroke patients. *J Cereb Blood Flow Metab* **32**, 780–91 (2012)

Van den Bossche, J., Baardman, J., Otto, N. A., van der Velden, S., Neele, A. E., van den Berg, S. M., Luque-Martin, R., Chen, H. J., Boshuizen, M. C., Ahmed, M., Hoeksema, M. A., de Vos, A. F., de Winther, M. P. Mitochondrial dysfunction prevents repolarization of inflammatory macrophages. *Cell Rep* **17**, 684-696 (2016)

van der Poel, M., Ulas, T., Mizee, M. R., Hsiao, C. C., Miedema, S. S. M., Adelia, Schuurman, K. G., Helder, B., Tas, S. W., Schultze, J. L., Hamann, J., Huitinga, I. Transcriptional profiling of human microglia reveals grey-white matter heterogeneity and multiple sclerosis-associated changes. *Nat Commun* **10**, 1139 (2019)

VanRyzin, J. W., Pickett, L. A., McCarthy, M. M. Microglia: Driving critical periods and sexual differentiation of the brain. *Dev Neurobiol* **78**, 580-592 (2018)

Vazana, U., Veksler, R., Pell, G. S., Prager, O., Fassler, M., Chassidim, Y., Roth, Y., Shahar, H., Zangen, A., Raccah, R., Onesti, E., Ceccanti, M., Colonnese, C., Santoro, A., Salvati, M., D'Elia, A., Nucciarelli, V., Inghilleri, M., Friedman, A. Glutamate-Mediated Blood-Brain Barrier Opening: Implications for Neuroprotection and Drug Delivery. *J Neurosci* **36**, 7727-39 (2016)

Villa, A., Gelosa, P., Castiglioni, L., Cimino, M., Rizzi, N., Pepe, G., Lolli, F., Marcello, E., Sironi, L., Vegeto, E., Maggi, A. Sex-specific features of microglia from adult mice. *Cell Rep* **23**, 3501–11 (2018)

Villapol, S., Loane, D. J., Burns, M. P. Sexual dimorphism in the inflammatory response to traumatic brain injury. *Glia* **65**: 1423–1438 (2017)

Viscoli, C. M., Brass, L. M., Kernan, W. N., Sarrel, P. M., Suissa, S., Horwitz, R. I. A clinical trial of estrogen-replacement therapy after ischemic stroke. *N Engl J Med* **345**, 1243-9 (2021)

Wang, X., Xuan, W., Zhu, Z. Y., *et al.* The evolving role of neuro-immune interaction in brain repair after cerebral ischemic stroke. *CNS Neurosci Ther*. **24**, 1100-1114 (2018)

Weaver, C. T., Elson, C. O., Fouser, L. A., Kolls, J. K. The Th17 pathway and inflammatory diseases of the intestines, lungs, and skin. *Annu Rev Pathol* **8**, 477–512 (2013)

Wenger, N. K., Speroff, L., Packard, B. Cardiovascular health and disease in women. *N Engl J Med.* **329**, 247-56 (1993)

Werner, Y., Mass, E., Kumar, P. A., Ulas, T., Händler, K., Horne, A., Klee, K., Lupp, A., *et al.* Cxcr4 distinguishes HSC-derived monocytes from microglia and reveals monocyte immune responses to experimental stroke. *Nat Neurosci* **23**, 351–362 (2020)

Wheeler, T. J. ATP does not regulate the reconstituted glucose transporter. *Biochemistry* **28**, 3413-20 (1989)

Wong, C. H., Jenne, C. N., Lee, W. Y., Léger, C., Kubes, P. Functional innervation of hepatic iNKT cells is immunosuppressive following stroke. *Science* **334**, 101-5 (2011)

Wong, C. H., Jenne, C. N., Tam, P. P., Léger, C., Venegas, A., Ryckborst, K., Hill, M. D., Kubes, P. Prolonged Activation of Invariant Natural Killer T Cells and T_H2-Skewed Immunity in Stroke Patients. *Front Neurol* **8**, 6 (2017)

Xia, H. J., Zhang, G. H., Wang, R. R., Zheng, Y. T. The influence of age and sex on the cell counts of peripheral blood leukocyte subpopulations in Chinese rhesus macaques. *Cell Mol Immunol* **6**, 433–40 (2009)

Xiang, X., Wind, K., Wiedemann, T., Blume, T., Shi, Y., Briel, N., Beyer, L., Biechele, G., Eckenweber, F., Zatcepin, A., Lammich, S., Ribicic, S., Tahirovic, S., et al. Microglial activation states drive glucose uptake and FDG-PET alterations in neurodegenerative diseases. *Sci Transl Med* **13**, eabe5640 (2021)

Xie, Z., Bailey, A., Kuleshov, M. V., Clarke, D. J. B., Evangelista, J. E., Jenkins, S. L., Lachmann, A., Wojciechowicz, M. L., Kropiwnicki, E., Jagodnik, K. M., Jeon, M., Ma'ayan, A. Gene Set Knowledge Discovery with Enrichr. *Curr Protoc* **1**, e90 (2021)

Xing, C., Arai, K., Lo, E. H., Hommel, M. Pathophysiologic cascades in ischemic stroke. *Int J Stroke* **7**, 378–85 (2012)

Yang, Y., Rosenberg, G. A. Blood-brain barrier breakdown in acute and chronic cerebrovascular disease. *Stroke* **42**, 3323–8 (2011)

Yilmaz, G., Arumugam T. V., Stokes. K. Y., Granger, D. N. Role of T lymphocytes and interferon-gamma in ischemic stroke. *Circulation* **113**, 2105-12 (2006)

Yu, X., Ji, C., Shao, A. Neurovascular Unit Dysfunction and Neurodegenerative Disorders. *Front Neurosci.* **14**, 334 (2020)

Zhang, Y., Chen, K., Sloan, S. A., Bennett, M. L., Scholze, A. R., O'Keeffe, S., et al. An RNA sequencing transcriptome and splicing database of glia, neurons, and vascular cells of the cerebral cortex. *The Journal of neuroscience: the official journal of the Society for Neuroscience* **34**, 11929-47 (2014)

Zhang, Z., Zhou, C., Liu, M. *et al.* Neutrophil counts and the risk of first stroke in general hypertensive adults. *Hypertens Res* **44**, 830–839 (2021)

Zhao, Y., Xu, H. Microglial lactate metabolism as a potential therapeutic target for Alzheimer's disease. *Mol Neurodegeneration* **17**, 36 (2022)

Zhu, B., Pan, Y., Jing, J., Meng, X., Zhao, X., Liu, L., et al. Neutrophil counts, neutrophil ratio, and new stroke in minor ischemic stroke or TIA. *Neurology* **90**, e1870–8 (2018)

Zhu, M. L., Bakhru, P., Conley, B., Nelson, J. S., Free, M., Martin, A., Starmer, J., Wilson, E. M., Su, M. A. Sex bias in CNS autoimmune disease mediated by androgen control of autoimmune regulator. *Nat Commun* **7**, 11350 (2016)

Supplementary information

Supplementary Figure 1: Effects of microglia-specific cell depletion in females and males

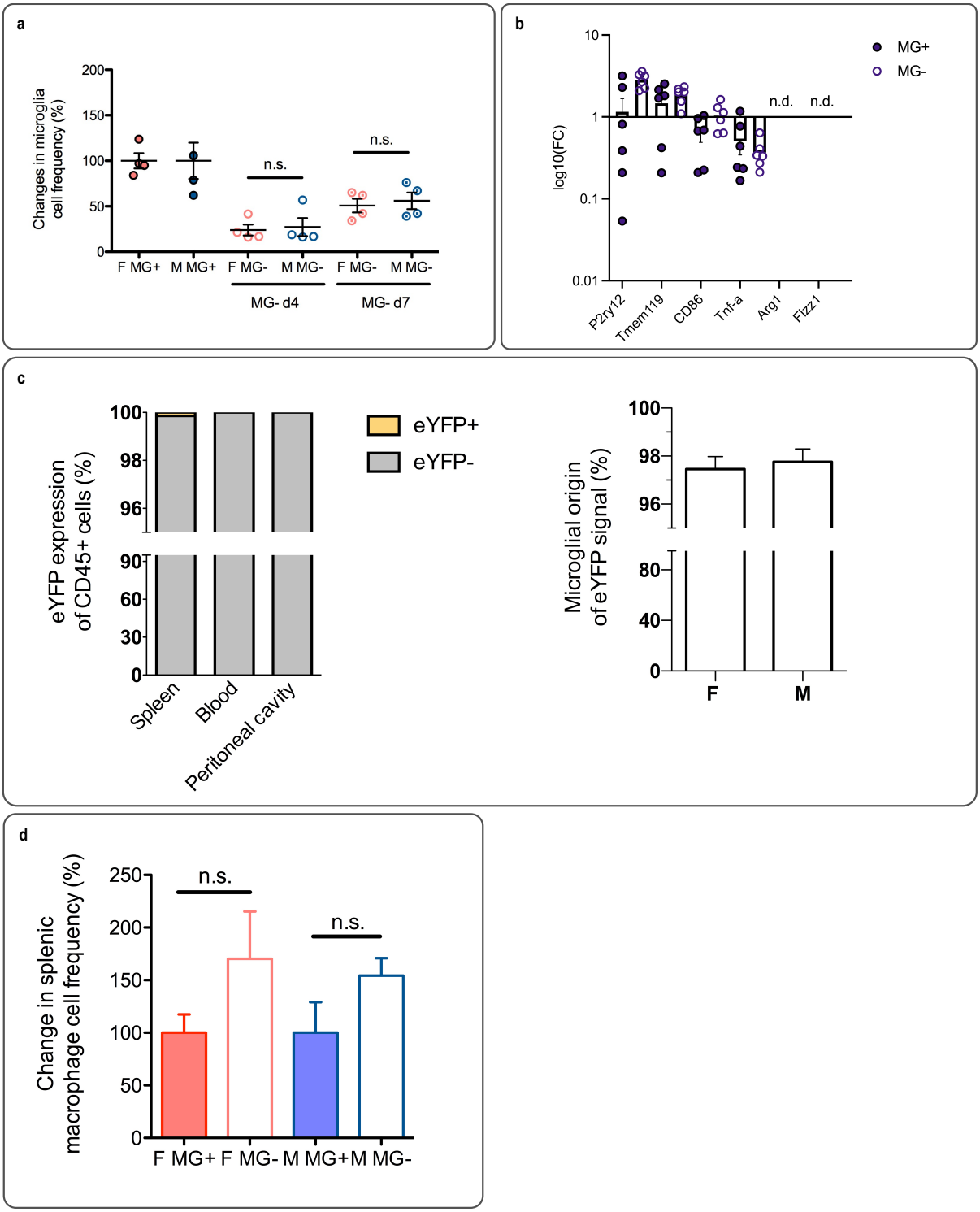

Supplementary Figure 1 | a, Sex-specific microglia cell dynamics after depletion and upon repopulation. Ordinary one-way ANOVA between groups: n = 4 per group; $F(5, 23) = 9.182$, $p = 0.0002$. Tukey's multiple comparison test: F MG- d4 versus M MG- d4, $p = 0.2907$; F MG- d7 versus M MG- d7, $p = 0.4720$. The bars show mean values ± s.e.m. **b**, qPCR quantification of relevant homeostatic microglia marker genes (*P2ry12*, *Tmem119*), pro-inflammatory marker genes (*Cd86*, *Tnf-a*), and anti-inflammatory marker genes (*Arg1*, *Fizz1*) on FACS isolated microglia samples from Cx3cr1-cre^{ERT2} x iDTR$^{-/-}$ x eYFP$^{+/-}$ (MG+) and Cx3cr1-cre^{ERT2} x iDTR$^{+/-}$ x eYFP$^{+/-}$ (MG-) mice on d4 of DTx-induced microglia depletion. Bars show mean values ± s.e.m. **c**, Microglia-specificity in female and male Cx3cr1-cre^{ERT2} x iDTR$^{-/-}$ x eYFP$^{+/-}$ (MG+) and Cx3cr1-cre^{ERT2} x iDTR$^{+/-}$ x eYFP$^{+/-}$ (MG-) mice: no to only marginal eYFP expression in circulating monocytes (blood), tissue-resident macrophages (spleen), or circulating macrophages (peritoneal cavity) before DTx treatment (left); microglia cells as the origin of CNS-detectable eYFP signal (right): n = 4 per group; no quantifications. Bars show mean values (left) ± s.e.m. (right). **d**, Effect of DTx treatment on peripheral tissue-resident macrophages on d4. Two-tailed, two-sample *t*-test for females ($t(6) = 1.454$, $p = 0.196$) and males ($t(6) = 1.623$, $p = 0.1557$) respectively; n = 4 MG-depleted versus n = 4 wild-type littermate controls for each female and male mice. The bars show mean values ± s.e.m.

Supplementary Figure 2: Quality control and supporting data on microglia RNA profiling

a

Condition	Time	Sex	Pooled?	RIN	RNA (ng)	Infarct size (%)
tMCAO	1d	f	No	7,5	3,135	10
			No	7,6	1,095	80
			No	8,4	1,14	70
			No	7,8	2,085	50
		m	No	8,6	124,785	45
			No	9,1	43,125	15
			No	9,4	30,6	40
	3d	f	No	7,8	2,565	40
			No	7,5	2,995	70
			No	8,8	3,54	70
			No	7,4	3,705	70
		m	No	8,2	142,74	90
			No	8,5	134,78	90
			No	8,4	19,17	70
	7d	m	No	8	105,225	15
			No	7,4	2,685	30
			No	8,7	8,145	45
	14d	m	No	8,9	22,53	95
			No	8,2	135,36	85
			No	8,2	119,7	75
sham	1d	f	No	7,6	0,58	
			No	7,8	0,425	
			No	8,1	1,24	
		m	Yes (2)	7,2	6,69	
			Yes (2)	7,1	24,915	
			Yes (3)	7,3	40,14	
	3d	f	No	8,4	0,825	
			No	8,6	1,495	
			No	7,5	0,885	
		m	Yes (2)	7,1	29,07	
			Yes (2)	7	70,65	
			No	7,1	34,635	
	7d	m	Yes (2)	7,4	94,25	
			Yes (2)	7,6	70,49	
			No	7,3	13,89	
	14d	m	No	7,5	90,765	
			No	7,5	29,175	
			No	7,1	47,595	

Supplementary Figure 2 | b-d, analyses provided by NIG. **a**, Overview of samples used for RNA-Seq. **b**, PCA of samples from male mice after tMCAO (stroke d1, d3, d7, d14) and corresponding sham surgery (sham d1, d3, d7, d14). **c**, PCA of samples from female mice after tMCAO (stroke d1, d3) and corresponding sham surgery (sham d1, d3). **d**, Clustering analyses of male (left) and female (right) RNA-Seq samples. **e-h**, Overview of all DE genes from male mice on post-stroke day one **(e)**, day three **(f)**, and DE genes from female mice on post stroke day one **(g)** and day three **(h)** used for ORA. **i**, Top ten most significantly regulated KEGG pathways in female (red) and male (blue) microglia from C57Bl6/J wild-type mice at day one and three (pooled) after sham surgery with respective FDR-adjusted *P* values. Enrichr adjusted for multiple comparisons by FDR; *n* = 6 female mice, *n* = 12 male mice. **j-k**, KEGG metabolic network for female (**j**) and male (**k**) microglia on day one after tMCAO; enriched pathways are highlighted. Line width, upregulation. Done using iPath3 (Darzi et al., 2018).

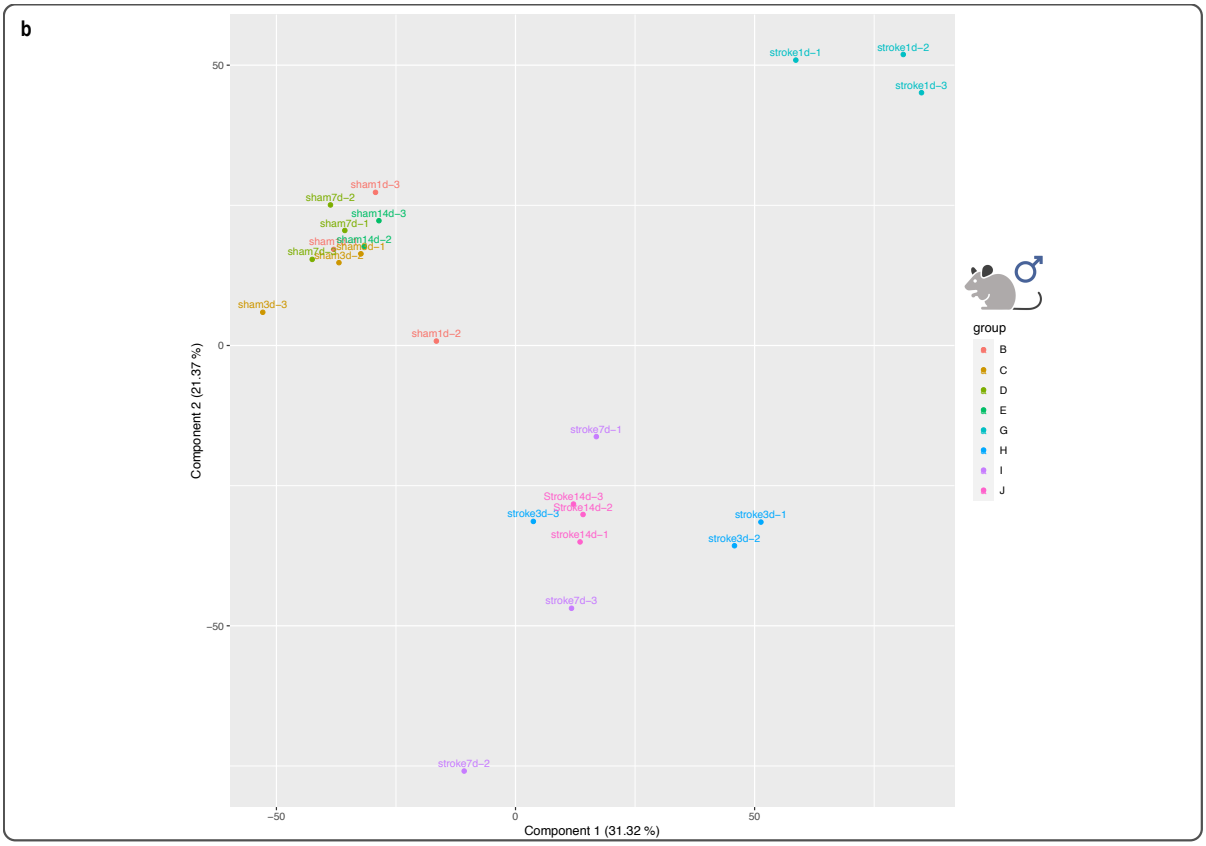
b
stroke1d−1
stroke1d−2
stroke1d−3
sham1d−3
sham7d−2
sham14d−3
sham7d−1
sham14d−2
sham3d−3
sham1d−2
stroke7d−1
Stroke14d−3
stroke3d−3
Stroke14d−2
stroke14d−1
stroke3d−1
stroke3d−2
stroke7d−3
stroke7d−2
Component 2 (21.37 %)
Component 1 (31.32 %)
group
B
C
D
E
G
H
I
J

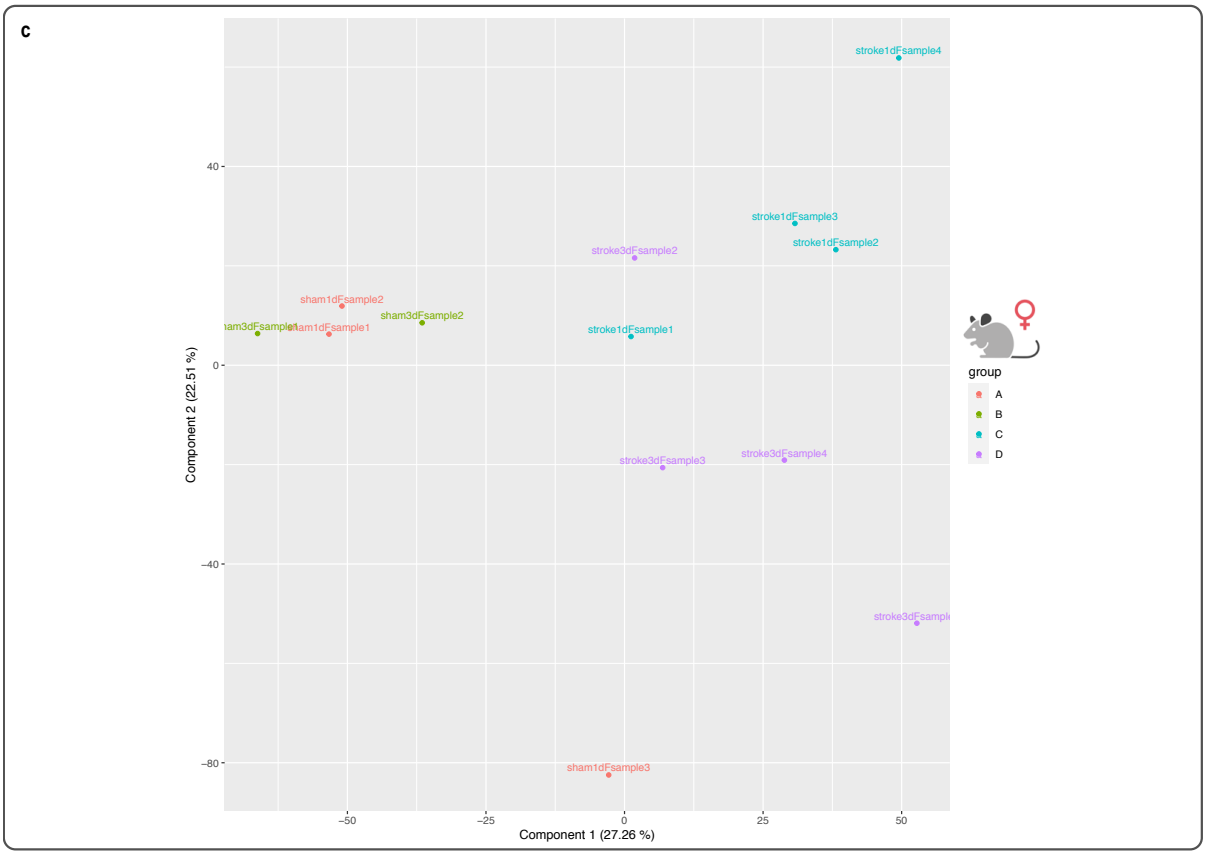
c
stroke1dFsample4
stroke1dFsample3
stroke1dFsample2
stroke3dFsample2
sham1dFsample2
sham3dFsample2
sham1dFsample1
stroke1dFsample1
stroke3dFsample3
stroke3dFsample4
sham1dFsample3
Component 2 (22.51 %)
Component 1 (27.26 %)
group
A
B
C
D

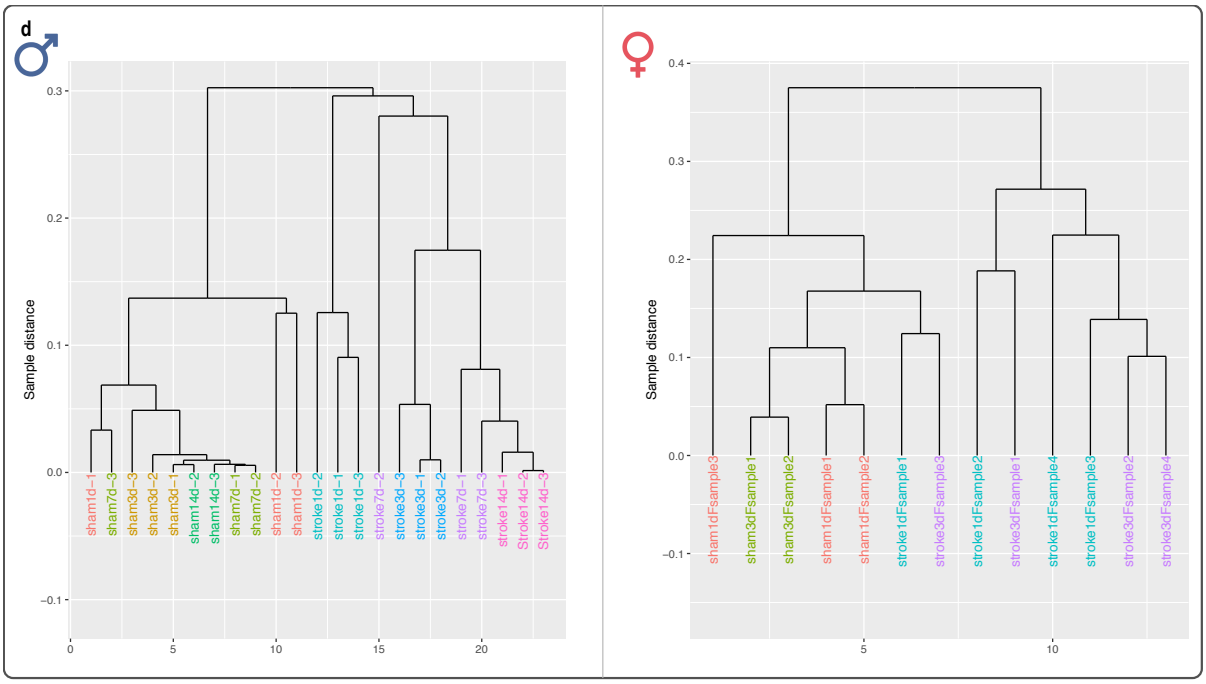

e

gene_id	gene_name	log2FoldChange
ENSMUSG00000030994	**D7Ertd443e**	-4,41
ENSMUSG00000022357	**Klhl38**	-3,86
ENSMUSG00000022496	**Tnfrsf17**	-3,73
ENSMUSG00000049436	**Upk1b**	-3,57
ENSMUSG00000021303	**Gng4**	-3,42
ENSMUSG00000040016	**Ptger3**	-3,41
ENSMUSG00000021356	**Irf4**	-3,37
ENSMUSG00000003949	**Hlf**	-3,35
ENSMUSG00000047419	**Cmya5**	-3,29
ENSMUSG00000030165	**Klrd1**	-3,26
ENSMUSG00000036036	**Zfp57**	-3,13
ENSMUSG00000026489	**Coq8a**	-3,13
ENSMUSG00000075225	**Ccdc162**	-3,12
ENSMUSG00000058022	**Adtrp**	-3,08
ENSMUSG00000034353	**Ramp1**	-3,08
ENSMUSG00000055102	**Zfp819**	-3,07
ENSMUSG00000050473	**Slc35d3**	-3,07
ENSMUSG00000022376	**Adcy8**	-3,05
ENSMUSG00000048424	**Ranbp3l**	-3,05
ENSMUSG00000028654	**Mycl**	-3,02
ENSMUSG00000025175	**Fn3k**	-2,99
ENSMUSG00000021880	**Rnase6**	-2,99
ENSMUSG00000080485	**Gm23493**	-2,99
ENSMUSG00000004359	**Spic**	-2,97
ENSMUSG00000001300	**Efnb2**	-2,94

ENSMUSG00000104918	**Gm42944**	-2,94
ENSMUSG00000051590	**Map3k19**	-2,94
ENSMUSG00000027200	**Sema6d**	-2,94
ENSMUSG00000084964	**Gm15503**	-2,89
ENSMUSG00000038026	**Kcnj9**	-2,87
ENSMUSG00000043795	**Prr33**	-2,85
ENSMUSG00000076621	**Ighj1**	-2,83
ENSMUSG00000109799	**Gm45515**	-2,82
ENSMUSG00000028989	**Angptl7**	-2,81
ENSMUSG00000038201	**Kcna7**	-2,80
ENSMUSG00000021198	**Unc79**	-2,77
ENSMUSG00000042678	**Myo15**	-2,77
ENSMUSG00000018427	**Ypel2**	-2,77
ENSMUSG00000018102	**H2bc4**	-2,74
ENSMUSG00000050138	**Kcnk12**	-2,74
ENSMUSG00000035085	**1700020L24Rik**	-2,73
ENSMUSG00000036181	**H1f2**	-2,73
ENSMUSG00000070868	**Skint3**	-2,71
ENSMUSG00000035686	**Thrsp**	-2,71
ENSMUSG00000003882	**Il7r**	-2,70
ENSMUSG00000058385	**H2bc8**	-2,70
ENSMUSG00000027224	**Duoxa1**	-2,69
ENSMUSG00000050103	**Agmo**	-2,68
ENSMUSG00000022026	**Olfm4**	-2,67
ENSMUSG00000028976	**Slc2a5**	-2,67
ENSMUSG00000038068	**Rnf144b**	-2,66
ENSMUSG00000034009	**Rxfp1**	-2,66
ENSMUSG00000021130	**Galnt16**	-2,66
ENSMUSG00000039103	**Nexn**	-2,65
ENSMUSG00000031779	**Ccl22**	-2,65
ENSMUSG00000036353	**P2ry12**	-2,65
ENSMUSG00000034686	**Prr7**	-2,65
ENSMUSG00000113856	**Gm10790**	-2,64
ENSMUSG00000102674	**8030442B05Rik**	-2,62
ENSMUSG00000084803	**5830444B04Rik**	-2,62
ENSMUSG00000067199	**Frat1**	-2,62
ENSMUSG00000076618	**Ighj4**	-2,61
ENSMUSG00000051627	**H1f4**	-2,61
ENSMUSG00000087006	**Gm13889**	-2,61
ENSMUSG00000110195	**Pde2a**	-2,59
ENSMUSG00000067577	**A430093F15Rik**	-2,58
ENSMUSG00000028766	**Alpl**	-2,57
ENSMUSG00000048249	**Crebrf**	-2,57
ENSMUSG00000047146	**Tet1**	-2,56
ENSMUSG00000042182	**Bend6**	-2,56
ENSMUSG00000047867	**Gimap6**	-2,55
ENSMUSG00000113216	**Gm40841**	-2,55

ENSMUSG00000022311	**Csmd3**	-2,55
ENSMUSG00000037972	**Snn**	-2,55
ENSMUSG00000041132	**N4bp2l1**	-2,55
ENSMUSG00000020798	**Spns3**	-2,54
ENSMUSG00000027217	**Tspan18**	-2,54
ENSMUSG00000052565	**H1f3**	-2,54
ENSMUSG00000001552	**Jup**	-2,54
ENSMUSG00000090257	**Gm4524**	-2,54
ENSMUSG00000020593	**Lpin1**	-2,53
ENSMUSG00000020264	**Slc36a2**	-2,53
ENSMUSG00000031955	**Bcar1**	-2,51
ENSMUSG00000033717	**Adra2a**	-2,51
ENSMUSG00000020682	**Mmp28**	-2,50
ENSMUSG00000028497	**Hacd4**	-2,50
ENSMUSG00000086782	**E130102H24Rik**	-2,49
ENSMUSG00000036040	**Adamtsl2**	-2,48
ENSMUSG00000025196	**Cpn1**	-2,48
ENSMUSG00000006586	**Runx1t1**	-2,48
ENSMUSG00000095385	**D630033O11Rik**	-2,47
ENSMUSG00000004668	**Abca13**	-2,47
ENSMUSG00000042371	**Slc5a10**	-2,46
ENSMUSG00000024548	**Setbp1**	-2,45
ENSMUSG00000031210	**Gpr165**	-2,45
ENSMUSG00000059824	**Dbp**	-2,44
ENSMUSG00000059336	**Slc14a1**	-2,44
ENSMUSG00000001053	**N4bp3**	-2,44
ENSMUSG00000085881	**Gm15912**	-2,43
ENSMUSG00000074570	**Cass4**	-2,43
ENSMUSG00000087362	**Gm13710**	-2,43
ENSMUSG00000035274	**Tpbg**	-2,42
ENSMUSG00000023328	**Ache**	-2,42
ENSMUSG00000051497	**Kcnj16**	-2,42
ENSMUSG00000029368	**Alb**	-2,41
ENSMUSG00000041797	**Abca9**	-2,41
ENSMUSG00000060402	**Chst8**	-2,41
ENSMUSG00000091472	**Gm3739**	-2,40
ENSMUSG00000015829	**Tnr**	-2,40
ENSMUSG00000051504	**Siglech**	-2,40
ENSMUSG00000050447	**Lypd6**	-2,40
ENSMUSG00000111212	**Gm47087**	-2,39
ENSMUSG00000040694	**Apobec2**	-2,39
ENSMUSG00000027843	**Ptpn22**	-2,39
ENSMUSG00000030592	**Ryr1**	-2,38
ENSMUSG00000100147	**1700047M11Rik**	-2,38
ENSMUSG00000020774	**Aspa**	-2,38
ENSMUSG00000060459	**Kng2**	-2,38
ENSMUSG00000071226	**Cecr2**	-2,37

ENSMUSG00000039765	**Cc2d2a**	-2,37
ENSMUSG00000031173	**Otc**	-2,36
ENSMUSG00000118370	**Gm41750**	-2,35
ENSMUSG00000118423	**Lrrc70**	-2,35
ENSMUSG00000036862	**Dchs1**	-2,35
ENSMUSG00000019768	**Esr1**	-2,35
ENSMUSG00000042246	**Tmc7**	-2,35
ENSMUSG00000042451	**Mybph**	-2,35
ENSMUSG00000020037	**Rfx4**	-2,34
ENSMUSG00000040899	**Ccr6**	-2,33
ENSMUSG00000030054	**Gp9**	-2,33
ENSMUSG00000064373	**Selenop**	-2,33
ENSMUSG00000076620	**Ighj2**	-2,33
ENSMUSG00000100502	**Gm28286**	-2,33
ENSMUSG00000099145	**Mir8116**	-2,33
ENSMUSG00000031425	**Plp1**	-2,32
ENSMUSG00000074272	**Ceacam1**	-2,32
ENSMUSG00000034472	**Rasd2**	-2,32
ENSMUSG00000053024	**Cntn2**	-2,32
ENSMUSG00000024975	**Pdcd4**	-2,32
ENSMUSG00000100627	**A830008E24Rik**	-2,32
ENSMUSG00000067203	**H2-K2**	-2,32
ENSMUSG00000021573	**Tppp**	-2,31
ENSMUSG00000095139	**Pou3f2**	-2,31
ENSMUSG00000047880	**Cxcr5**	-2,30
ENSMUSG00000032017	**Grik4**	-2,30
ENSMUSG00000064901	**Snora21**	-2,30
ENSMUSG00000022240	**Ctnnd2**	-2,30
ENSMUSG00000028644	**Ermap**	-2,30
ENSMUSG00000029299	**Abcg3**	-2,30
ENSMUSG00000106379	**Lhfpl3**	-2,30
ENSMUSG00000044749	**Abca6**	-2,30
ENSMUSG00000100183	**Gm28512**	-2,30
ENSMUSG00000091311	**Spata31d1b**	-2,30
ENSMUSG00000056602	**Fry**	-2,29
ENSMUSG00000038151	**Prdm1**	-2,29
ENSMUSG00000021983	**Atp8a2**	-2,28
ENSMUSG00000086938	**4930481A15Rik**	-2,28
ENSMUSG00000030650	**Tmc5**	-2,28
ENSMUSG00000021280	**Exoc3l4**	-2,28
ENSMUSG00000074203	**G430095P16Rik**	-2,27
ENSMUSG00000101942	**Gm19582**	-2,27
ENSMUSG00000108024	**Gm43912**	-2,26
ENSMUSG00000022358	**Fbxo32**	-2,26
ENSMUSG00000026572	**Tbx19**	-2,26
ENSMUSG00000030283	**St8sia1**	-2,26
ENSMUSG00000090185	**Gm15523**	-2,25

ENSMUSG00000029650	**Slc46a3**	-2,25
ENSMUSG00000031431	**Tsc22d3**	-2,24
ENSMUSG00000006362	**Cbfa2t3**	-2,24
ENSMUSG00000032254	**Kif23**	-2,23
ENSMUSG00000056880	**Gadl1**	-2,23
ENSMUSG00000070498	**Tmem132b**	-2,23
ENSMUSG00000090691	**Gm3667**	-2,22
ENSMUSG00000045515	**Pou3f3**	-2,22
ENSMUSG00000094628	**Gm3252**	-2,22
ENSMUSG00000040488	**Ltbp4**	-2,21
ENSMUSG00000097887	**Gm26542**	-2,21
ENSMUSG00000024697	**Gna14**	-2,21
ENSMUSG00000086006	**Gm13293**	-2,20
ENSMUSG00000024617	**Camk2a**	-2,20
ENSMUSG00000041670	**Rims1**	-2,20
ENSMUSG00000050035	**Fhl4**	-2,20
ENSMUSG00000114422	**Gm30411**	-2,20
ENSMUSG00000018819	**Lsp1**	-2,20
ENSMUSG00000117916	**9630028I04Rik**	-2,20
ENSMUSG00000084199	**Gm12422**	-2,20
ENSMUSG00000050640	**Tmem150c**	-2,20
ENSMUSG00000026170	**Cyp27a1**	-2,20
ENSMUSG00000028630	**Dyrk2**	-2,20
ENSMUSG00000035355	**Kcnh4**	-2,20
ENSMUSG00000027858	**Tspan2**	-2,19
ENSMUSG00000020889	**Nr1d1**	-2,19
ENSMUSG00000024897	**Apba1**	-2,19
ENSMUSG00000101903	**Gm29291**	-2,19
ENSMUSG00000085852	**Gm13807**	-2,18
ENSMUSG00000034858	**Fam214a**	-2,18
ENSMUSG00000043556	**Fbxl7**	-2,18
ENSMUSG00000036949	**Slc39a12**	-2,17
ENSMUSG00000104517	**Gm18407**	-2,17
ENSMUSG00000009731	**Kcnd1**	-2,16
ENSMUSG00000111014	**Gm47795**	-2,16
ENSMUSG00000026587	**Astn1**	-2,16
ENSMUSG00000047604	**Frat2**	-2,16
ENSMUSG00000002732	**Fkbp7**	-2,16
ENSMUSG00000031523	**Dlc1**	-2,16
ENSMUSG00000019944	**Rhobtb1**	-2,16
ENSMUSG00000048376	**F2r**	-2,16
ENSMUSG00000103043	**Gm37306**	-2,16
ENSMUSG00000026589	**Sec16b**	-2,15
ENSMUSG00000015396	**Cd83**	-2,15
ENSMUSG00000032238	**Rora**	-2,15
ENSMUSG00000041538	**H2-Ob**	-2,15
ENSMUSG00000086491	**Gm13291**	-2,15

ENSMUSG00000041798	**Gck**	-2,14
ENSMUSG00000025993	**Slc40a1**	-2,14
ENSMUSG00000041287	**Sox15**	-2,14
ENSMUSG00000061353	**Cxcl12**	-2,14
ENSMUSG00000027457	**Snph**	-2,14
ENSMUSG00000037211	**Spry1**	-2,14
ENSMUSG00000034684	**Sema3f**	-2,14
ENSMUSG00000043448	**Gjc2**	-2,13
ENSMUSG00000096001	**2610528A11Rik**	-2,13
ENSMUSG00000029343	**Crybb1**	-2,13
ENSMUSG00000047246	**H2bc6**	-2,13
ENSMUSG00000035681	**Kcnc2**	-2,13
ENSMUSG00000054850	**Smim10l2a**	-2,13
ENSMUSG00000062901	**Klhl24**	-2,13
ENSMUSG00000109498	**Gm45222**	-2,13
ENSMUSG00000036295	**Lrrn3**	-2,13
ENSMUSG00000058183	**Mmel1**	-2,12
ENSMUSG00000045573	**Penk**	-2,12
ENSMUSG00000081906	**Rpl9-ps1**	-2,12
ENSMUSG00000025573	**6030468B19Rik**	-2,11
ENSMUSG00000025887	**Casp12**	-2,11
ENSMUSG00000107846	**Gm43963**	-2,11
ENSMUSG00000091996	**BC049352**	-2,11
ENSMUSG00000024109	**Nrxn1**	-2,10
ENSMUSG00000041202	**Pla2g2d**	-2,10
ENSMUSG00000029419	**Ajm1**	-2,10
ENSMUSG00000029095	**Ablim2**	-2,10
ENSMUSG00000032411	**Tfdp2**	-2,10
ENSMUSG00000028211	**Trp53inp1**	-2,10
ENSMUSG00000034614	**Pik3ip1**	-2,10
ENSMUSG00000102752	**Gm7694**	-2,10
ENSMUSG00000039137	**Whrn**	-2,10
ENSMUSG00000018604	**Tbx3**	-2,09
ENSMUSG00000087543	**Gm16576**	-2,09
ENSMUSG00000028088	**Fmo5**	-2,09
ENSMUSG00000051359	**Ncald**	-2,08
ENSMUSG00000062257	**Opcml**	-2,08
ENSMUSG00000027583	**Zbtb46**	-2,08
ENSMUSG00000009551	**6330409D20Rik**	-2,07
ENSMUSG00000026546	**Cfap45**	-2,07
ENSMUSG00000021281	**Tnfaip2**	-2,06
ENSMUSG00000084340	**Gm14766**	-2,06
ENSMUSG00000118265	**Gm50211**	-2,06
ENSMUSG00000058297	**Spock2**	-2,06
ENSMUSG00000087674	**4930447M23Rik**	-2,06
ENSMUSG00000074923	**Pak6**	-2,06
ENSMUSG00000009214	**Mymk**	-2,06

ENSMUSG00000098197	**BC051537**	-2,06
ENSMUSG00000044770	**Scml4**	-2,05
ENSMUSG00000044522	**A730020M07Rik**	-2,05
ENSMUSG00000044313	**Mab21l3**	-2,05
ENSMUSG00000024049	**Myom1**	-2,05
ENSMUSG00000113591	**4930447K03Rik**	-2,05
ENSMUSG00000099583	**H3c4**	-2,05
ENSMUSG00000048163	**Selplg**	-2,04
ENSMUSG00000040229	**Gpr34**	-2,04
ENSMUSG00000061859	**Patj**	-2,04
ENSMUSG00000031618	**Nr3c2**	-2,04
ENSMUSG00000046031	**Calhm6**	-2,04
ENSMUSG00000021318	**Gli3**	-2,04
ENSMUSG00000030711	**Sult1a1**	-2,04
ENSMUSG00000029231	**Pdgfra**	-2,03
ENSMUSG00000048978	**Nrsn1**	-2,03
ENSMUSG00000045664	**Cdc42ep2**	-2,03
ENSMUSG00000076439	**Mog**	-2,03
ENSMUSG00000072618	**Gm10384**	-2,03
ENSMUSG00000021186	**Fbln5**	-2,03
ENSMUSG00000056716	**Gm5420**	-2,03
ENSMUSG00000109675	**Nxpe1-ps**	-2,03
ENSMUSG00000039830	**Olig2**	-2,02
ENSMUSG00000043388	**Tmem130**	-2,02
ENSMUSG00000038065	**Mturn**	-2,02
ENSMUSG00000100465	**Gm29264**	-2,02
ENSMUSG00000042671	**Rgs8**	-2,02
ENSMUSG00000106665	**Gm43389**	-2,02
ENSMUSG00000060550	**H2-Q7**	-2,02
ENSMUSG00000114709	**Gm47920**	-2,02
ENSMUSG00000087355	**Gm13187**	-2,02
ENSMUSG00000079481	**Nhsl2**	-2,01
ENSMUSG00000031778	**Cx3cl1**	-2,01
ENSMUSG00000022840	**Adcy5**	-2,01
ENSMUSG00000012819	**Cdh23**	-2,00
ENSMUSG00000035671	**Zswim4**	-2,00
ENSMUSG00000108912	**E230020D15Rik**	-2,00
ENSMUSG00000073409	**H2-Q6**	-2,00
ENSMUSG00000031494	**Cd209a**	-2,00
ENSMUSG00000014773	**Dll1**	-2,00
ENSMUSG00000074794	**Arrdc3**	-2,00
ENSMUSG00000037855	**Zfp365**	-2,00
ENSMUSG00000026303	**Mlph**	-2,00
ENSMUSG00000072720	**Myo18b**	-2,00
ENSMUSG00000091275	**Gm3248**	-2,00
ENSMUSG00000070577	**Gm572**	-2,00
ENSMUSG00000025044	**Msr1**	7,08

ENSMUSG00000029304	**Spp1**	6,86
ENSMUSG00000025473	**Adam8**	6,78
ENSMUSG00000049723	**Mmp12**	6,36
ENSMUSG00000050370	**Ch25h**	6,25
ENSMUSG00000015568	**Lpl**	5,87
ENSMUSG00000022102	**Dok2**	5,20
ENSMUSG00000022246	**Rai14**	5,14
ENSMUSG00000004709	**Cd244a**	5,10
ENSMUSG00000026390	**Marco**	5,09
ENSMUSG00000026228	**Htr2b**	4,68
ENSMUSG00000055214	**Pld5**	4,62
ENSMUSG00000057337	**Chst3**	4,52
ENSMUSG00000028459	**Cd72**	4,50
ENSMUSG00000022150	**Dab2**	4,45
ENSMUSG00000076441	**Ass1**	4,45
ENSMUSG00000023830	**Igf2r**	4,41
ENSMUSG00000068699	**Flnc**	4,40
ENSMUSG00000009376	**Met**	4,37
ENSMUSG00000050335	**Lgals3**	4,35
ENSMUSG00000026193	**Fn1**	4,27
ENSMUSG00000028121	**Bcar3**	4,27
ENSMUSG00000040026	**Saa3**	4,18
ENSMUSG00000028327	**Stra6l**	4,17
ENSMUSG00000034641	**Cd300ld**	4,05
ENSMUSG00000004891	**Nes**	4,03
ENSMUSG00000002944	**Cd36**	4,01
ENSMUSG00000028678	**Kif2c**	3,97
ENSMUSG00000040711	**Sh3pxd2b**	3,88
ENSMUSG00000027737	**Slc7a11**	3,81
ENSMUSG00000025854	**Fam20c**	3,81
ENSMUSG00000015854	**Cd5l**	3,79
ENSMUSG00000026536	**Ifi211**	3,77
ENSMUSG00000079339	**Ifit1bl1**	3,75
ENSMUSG00000027276	**Jag1**	3,74
ENSMUSG00000032715	**Trib3**	3,70
ENSMUSG00000026981	**Il1rn**	3,70
ENSMUSG00000033721	**Vav3**	3,69
ENSMUSG00000044162	**Tnip3**	3,68
ENSMUSG00000068220	**Lgals1**	3,63
ENSMUSG00000066684	**Pilrb1**	3,62
ENSMUSG00000079243	**Xirp1**	3,60
ENSMUSG00000015340	**Cybb**	3,56
ENSMUSG00000027750	**Postn**	3,52
ENSMUSG00000021508	**Cxcl14**	3,48
ENSMUSG00000022094	**Slc39a14**	3,46
ENSMUSG00000023046	**Igfbp6**	3,40
ENSMUSG00000032997	**Chpf**	3,32

ENSMUSG00000035352	**Ccl12**	3,31
ENSMUSG00000037148	**Arhgap10**	3,25
ENSMUSG00000034459	**Ifit1**	3,23
ENSMUSG00000032220	**Myo1e**	3,21
ENSMUSG00000026437	**Cdk18**	3,21
ENSMUSG00000022303	**Dcstamp**	3,21
ENSMUSG00000028494	**Plin2**	3,20
ENSMUSG00000030208	**Emp1**	3,19
ENSMUSG00000027514	**Zbp1**	3,19
ENSMUSG00000029752	**Asns**	3,17
ENSMUSG00000073489	**Ifi204**	3,15
ENSMUSG00000057191	**AB124611**	3,15
ENSMUSG00000072621	**Slfn10-ps**	3,11
ENSMUSG00000073490	**Ifi207**	3,10
ENSMUSG00000046591	**Ticrr**	3,09
ENSMUSG00000020841	**Cpd**	3,08
ENSMUSG00000005087	**Cd44**	3,05
ENSMUSG00000075297	**H60b**	3,05
ENSMUSG00000097352	**C920009B18Rik**	3,05
ENSMUSG00000041390	**Mdfic**	3,04
ENSMUSG00000039994	**Timeless**	3,02
ENSMUSG00000041827	**Oasl1**	3,01
ENSMUSG00000037474	**Dtl**	3,00
ENSMUSG00000039981	**Zc3h12d**	3,00
ENSMUSG00000045502	**Hcar2**	2,99
ENSMUSG00000001228	**Uhrf1**	2,98
ENSMUSG00000047798	**Cd300lf**	2,98
ENSMUSG00000031146	**Plp2**	2,96
ENSMUSG00000002289	**Angptl4**	2,96
ENSMUSG00000020641	**Rsad2**	2,95
ENSMUSG00000113769	**5033406O09Rik**	2,94
ENSMUSG00000006221	**Hspb7**	2,92
ENSMUSG00000028874	**Fgr**	2,92
ENSMUSG00000022636	**Alcam**	2,91
ENSMUSG00000037280	**Galnt6**	2,91
ENSMUSG00000034591	**Slc41a2**	2,90
ENSMUSG00000026435	**Slc45a3**	2,90
ENSMUSG00000026728	**Vim**	2,90
ENSMUSG00000090319	**Gm4462**	2,90
ENSMUSG00000105987	**AI506816**	2,87
ENSMUSG00000050967	**Creg2**	2,87
ENSMUSG00000001227	**Sema6b**	2,86
ENSMUSG00000063193	**Cd300lb**	2,86
ENSMUSG00000059956	**Serpinb12**	2,85
ENSMUSG00000056737	**Capg**	2,84
ENSMUSG00000020638	**Cmpk2**	2,82
ENSMUSG00000037849	**Ifi206**	2,81

ENSMUSG00000067206	**Lrrc66**	2,81
ENSMUSG00000059089	**Fcgr4**	2,79
ENSMUSG00000050578	**Mmp13**	2,77
ENSMUSG00000025001	**Hells**	2,76
ENSMUSG00000004105	**Angptl2**	2,76
ENSMUSG00000035455	**Fignl1**	2,76
ENSMUSG00000042828	**Trim72**	2,76
ENSMUSG00000021260	**Hhipl1**	2,73
ENSMUSG00000031506	**Ptpn7**	2,73
ENSMUSG00000023045	**Soat2**	2,71
ENSMUSG00000040658	**Dnph1**	2,71
ENSMUSG00000029762	**Akr1b8**	2,69
ENSMUSG00000032724	**Abtb2**	2,68
ENSMUSG00000020089	**Ppa1**	2,68
ENSMUSG00000025355	**Mmp19**	2,68
ENSMUSG00000074896	**Ifit3**	2,66
ENSMUSG00000086712	**AI427809**	2,65
ENSMUSG00000097558	**Gm26902**	2,65
ENSMUSG00000032911	**Cspg4**	2,64
ENSMUSG00000030536	**Iqgap1**	2,63
ENSMUSG00000027313	**Chac1**	2,63
ENSMUSG00000050737	**Ptges**	2,61
ENSMUSG00000041308	**Sntb2**	2,59
ENSMUSG00000027490	**E2f1**	2,59
ENSMUSG00000099757	**BE692007**	2,58
ENSMUSG00000027994	**Mcub**	2,57
ENSMUSG00000111118	**Gm6545**	2,56
ENSMUSG00000028108	**Ecm1**	2,55
ENSMUSG00000028069	**Gpatch4**	2,55
ENSMUSG00000002835	**Chaf1a**	2,53
ENSMUSG00000028238	**Atp6v0d2**	2,53
ENSMUSG00000026271	**Gpr35**	2,53
ENSMUSG00000074785	**Plxnc1**	2,52
ENSMUSG00000005667	**Mthfd2**	2,52
ENSMUSG00000005410	**Mcm5**	2,52
ENSMUSG00000030830	**Itgal**	2,51
ENSMUSG00000028718	**Stil**	2,50
ENSMUSG00000035049	**Rrp12**	2,50
ENSMUSG00000037679	**Inf2**	2,49
ENSMUSG00000020053	**Igf1**	2,49
ENSMUSG00000058470	**Gm8369**	2,49
ENSMUSG00000031328	**Flna**	2,48
ENSMUSG00000009687	**Fxyd5**	2,48
ENSMUSG00000031762	**Mt2**	2,48
ENSMUSG00000035493	**Tgfbi**	2,47
ENSMUSG00000052353	**Cemip**	2,47
ENSMUSG00000052688	**Rab7b**	2,46

ENSMUSG00000053137	**Mapk11**	2,46
ENSMUSG00000047959	**Kcna3**	2,45
ENSMUSG00000097487	**Ptges3l**	2,45
ENSMUSG00000028583	**Pdpn**	2,43
ENSMUSG00000007080	**Pole**	2,42
ENSMUSG00000066682	**Pilrb2**	2,42
ENSMUSG00000114687	**Gm5452**	2,41
ENSMUSG00000033581	**Igf2bp2**	2,40
ENSMUSG00000032656	**Marchf3**	2,40
ENSMUSG00000053746	**Ptrh1**	2,39
ENSMUSG00000053801	**Grwd1**	2,39
ENSMUSG00000044042	**Fmn1**	2,39
ENSMUSG00000002847	**Pla1a**	2,38
ENSMUSG00000103308	**Gm37800**	2,38
ENSMUSG00000025969	**Nrp2**	2,38
ENSMUSG00000025498	**Irf7**	2,37
ENSMUSG00000024640	**Psat1**	2,37
ENSMUSG00000029553	**Tfec**	2,36
ENSMUSG00000054404	**Slfn5**	2,36
ENSMUSG00000040034	**Nup43**	2,36
ENSMUSG00000030785	**Cox6a2**	2,35
ENSMUSG00000104913	**Gm6560**	2,35
ENSMUSG00000028671	**Gale**	2,35
ENSMUSG00000030107	**Usp18**	2,35
ENSMUSG00000022218	**Tgm1**	2,35
ENSMUSG00000001918	**Slc1a5**	2,35
ENSMUSG00000044703	**Phf11a**	2,34
ENSMUSG00000056145	**Al504432**	2,34
ENSMUSG00000031438	**Rnf128**	2,33
ENSMUSG00000031304	**Il2rg**	2,33
ENSMUSG00000040528	**Milr1**	2,33
ENSMUSG00000048612	**Myof**	2,32
ENSMUSG00000027698	**Nceh1**	2,32
ENSMUSG00000053338	**Tarm1**	2,31
ENSMUSG00000079419	**Ms4a6c**	2,31
ENSMUSG00000020334	**Slc22a4**	2,29
ENSMUSG00000010048	**Ifrd2**	2,29
ENSMUSG00000070305	**Mpzl3**	2,28
ENSMUSG00000029591	**Ung**	2,28
ENSMUSG00000021591	**Glrx**	2,28
ENSMUSG00000048498	**Cd300e**	2,27
ENSMUSG00000096960	**A230028O05Rik**	2,27
ENSMUSG00000040675	**Mthfd1l**	2,27
ENSMUSG00000047721	**Bola2**	2,26
ENSMUSG00000028633	**Ctps**	2,26
ENSMUSG00000030789	**Itgax**	2,25
ENSMUSG00000025403	**Shmt2**	2,25

ENSMUSG00000056888	**Glipr1**	2,25
ENSMUSG00000112023	**Lilr4b**	2,24
ENSMUSG00000032294	**Pkm**	2,24
ENSMUSG00000027748	**Trpc4**	2,24
ENSMUSG00000060950	**Trmt61a**	2,23
ENSMUSG00000026796	**Fam129b**	2,23
ENSMUSG00000026558	**Uck2**	2,23
ENSMUSG00000021565	**Slc6a19**	2,23
ENSMUSG00000024066	**Xdh**	2,22
ENSMUSG00000044719	**E230025N22Rik**	2,21
ENSMUSG00000054203	**Ifi205**	2,20
ENSMUSG00000034612	**Chst11**	2,20
ENSMUSG00000024679	**Ms4a6d**	2,20
ENSMUSG00000026068	**Il18rap**	2,20
ENSMUSG00000030657	**Xylt1**	2,19
ENSMUSG00000105954	**Gm42793**	2,19
ENSMUSG00000112006	**Gm48633**	2,19
ENSMUSG00000078452	**Raet1d**	2,18
ENSMUSG00000031562	**Dctd**	2,16
ENSMUSG00000028587	**Orc1**	2,16
ENSMUSG00000025492	**Ifitm3**	2,16
ENSMUSG00000034993	**Vat1**	2,15
ENSMUSG00000068697	**Myoz1**	2,15
ENSMUSG00000057135	**Scimp**	2,15
ENSMUSG00000037572	**Wdhd1**	2,14
ENSMUSG00000029338	**Antxr2**	2,14
ENSMUSG00000037759	**Ptger2**	2,13
ENSMUSG00000005465	**Il27ra**	2,13
ENSMUSG00000027712	**Anxa5**	2,12
ENSMUSG00000025153	**Fasn**	2,12
ENSMUSG00000023988	**Bysl**	2,12
ENSMUSG00000026355	**Mcm6**	2,12
ENSMUSG00000046245	**Pilra**	2,12
ENSMUSG00000028044	**Cks1b**	2,11
ENSMUSG00000096971	**4930556M19Rik**	2,11
ENSMUSG00000004929	**Thop1**	2,11
ENSMUSG00000036894	**Rap2b**	2,10
ENSMUSG00000019987	**Arg1**	2,10
ENSMUSG00000115219	**Eef1akmt4**	2,10
ENSMUSG00000029561	**Oasl2**	2,09
ENSMUSG00000079445	**B3gnt7**	2,09
ENSMUSG00000021458	**Aopep**	2,09
ENSMUSG00000025395	**Prim1**	2,09
ENSMUSG00000011008	**Mcoln2**	2,08
ENSMUSG00000035834	**Polr3g**	2,08
ENSMUSG00000052776	**Oas1a**	2,08
ENSMUSG00000042660	**Wdr55**	2,07

ENSMUSG00000051439	**Cd14**	2,07
ENSMUSG00000086499	**Gm16217**	2,06
ENSMUSG00000010609	**Psen2**	2,06
ENSMUSG00000031821	**Gins2**	2,06
ENSMUSG00000097245	**Gm5421**	2,06
ENSMUSG00000021091	**Serpina3n**	2,05
ENSMUSG00000012519	**Mlkl**	2,05
ENSMUSG00000006442	**Srm**	2,04
ENSMUSG00000001707	**Eef1e1**	2,04
ENSMUSG00000036875	**Dna2**	2,03
ENSMUSG00000030835	**Nomo1**	2,03
ENSMUSG00000054932	**Afp**	2,02
ENSMUSG00000001542	**Ell2**	2,02
ENSMUSG00000041313	**Slc7a1**	2,02
ENSMUSG00000032012	**Nectin1**	2,02
ENSMUSG00000071537	**Klrg2**	2,02
ENSMUSG00000032431	**Crtap**	2,01
ENSMUSG00000005481	**Ddx39**	2,01
ENSMUSG00000027454	**Gins1**	2,01
ENSMUSG00000018986	**Slfn3**	2,00
ENSMUSG00000039577	**Nphp4**	2,00
ENSMUSG00000006732	**Mettl1**	2,00
ENSMUSG00000020834	**Dhrs13**	2,00

f

gene_id	gene_name	log2FoldChange
ENSMUSG00000015854	**Cd5l**	6,73
ENSMUSG00000029304	**Spp1**	5,89
ENSMUSG00000029816	**Gpnmb**	5,73
ENSMUSG00000050370	**Ch25h**	5,72
ENSMUSG00000040026	**Saa3**	5,60
ENSMUSG00000021091	**Serpina3n**	5,34
ENSMUSG00000019987	**Arg1**	4,91
ENSMUSG00000026193	**Fn1**	4,90
ENSMUSG00000026228	**Htr2b**	4,63
ENSMUSG00000097558	**Gm26902**	4,62
ENSMUSG00000027533	**Fabp5**	4,60
ENSMUSG00000044338	**Aplnr**	4,42
ENSMUSG00000021362	**Gcm2**	4,40
ENSMUSG00000030022	**Adamts9**	4,36
ENSMUSG00000079017	**Ifi27l2a**	4,36
ENSMUSG00000044258	**Ctla2a**	4,34
ENSMUSG00000028108	**Ecm1**	4,11
ENSMUSG00000031170	**Slc38a5**	4,10
ENSMUSG00000022246	**Rai14**	4,10
ENSMUSG00000023031	**Cela1**	4,10

ENSMUSG00000004709	**Cd244a**	4,07
ENSMUSG00000072980	**Oip5**	4,06
ENSMUSG00000048572	**Tmem252**	4,04
ENSMUSG00000023505	**Cdca3**	4,04
ENSMUSG00000020676	**Ccl11**	3,99
ENSMUSG00000028356	**Ambp**	3,94
ENSMUSG00000017716	**Birc5**	3,87
ENSMUSG00000068220	**Lgals1**	3,86
ENSMUSG00000026580	**Selp**	3,86
ENSMUSG00000028459	**Cd72**	3,85
ENSMUSG00000018126	**Baiap2l2**	3,84
ENSMUSG00000027331	**Knstrn**	3,82
ENSMUSG00000047592	**Nxpe5**	3,82
ENSMUSG00000032548	**Slco2a1**	3,81
ENSMUSG00000064057	**Scgb3a1**	3,81
ENSMUSG00000037628	**Cdkn3**	3,79
ENSMUSG00000032218	**Ccnb2**	3,77
ENSMUSG00000040564	**Apoc1**	3,77
ENSMUSG00000044703	**Phf11a**	3,77
ENSMUSG00000030111	**A2m**	3,76
ENSMUSG00000027875	**Hmgcs2**	3,75
ENSMUSG00000068129	**Cst7**	3,74
ENSMUSG00000027379	**Bub1**	3,72
ENSMUSG00000028364	**Tnc**	3,68
ENSMUSG00000034773	**Hrob**	3,67
ENSMUSG00000037872	**Ackr1**	3,65
ENSMUSG00000024989	**Cep55**	3,63
ENSMUSG00000031502	**Col4a1**	3,62
ENSMUSG00000025044	**Msr1**	3,59
ENSMUSG00000032400	**Zwilch**	3,59
ENSMUSG00000026683	**Nuf2**	3,59
ENSMUSG00000036067	**Slc2a6**	3,56
ENSMUSG00000036256	**Igfbp7**	3,54
ENSMUSG00000020330	**Hmmr**	3,53
ENSMUSG00000015880	**Ncapg**	3,53
ENSMUSG00000041731	**Pgm5**	3,53
ENSMUSG00000030117	**Gdf3**	3,51
ENSMUSG00000078452	**Raet1d**	3,51
ENSMUSG00000031503	**Col4a2**	3,48
ENSMUSG00000005397	**Nid1**	3,46
ENSMUSG00000027469	**Tpx2**	3,46
ENSMUSG00000036875	**Dna2**	3,46
ENSMUSG00000028718	**Stil**	3,45
ENSMUSG00000050063	**Klk6**	3,43
ENSMUSG00000040204	**Pclaf**	3,43
ENSMUSG00000028873	**Cdca8**	3,42
ENSMUSG00000068101	**Cenpm**	3,42

ENSMUSG00000030867	**Plk1**	3,41
ENSMUSG00000019997	**Ccn2**	3,41
ENSMUSG00000029163	**Emilin1**	3,40
ENSMUSG00000002289	**Angptl4**	3,38
ENSMUSG00000035683	**Melk**	3,38
ENSMUSG00000045328	**Cenpe**	3,38
ENSMUSG00000037035	**Inhbb**	3,37
ENSMUSG00000027514	**Zbp1**	3,36
ENSMUSG00000003484	**Cyp4f18**	3,35
ENSMUSG00000032911	**Cspg4**	3,34
ENSMUSG00000041431	**Ccnb1**	3,33
ENSMUSG00000027715	**Ccna2**	3,32
ENSMUSG00000045930	**Clec14a**	3,32
ENSMUSG00000020897	**Aurkb**	3,31
ENSMUSG00000034311	**Kif4**	3,31
ENSMUSG00000037544	**Dlgap5**	3,30
ENSMUSG00000001131	**Timp1**	3,30
ENSMUSG00000001930	**Vwf**	3,29
ENSMUSG00000035365	**Parpbp**	3,29
ENSMUSG00000020649	**Rrm2**	3,28
ENSMUSG00000019942	**Cdk1**	3,27
ENSMUSG00000026622	**Nek2**	3,26
ENSMUSG00000022033	**Pbk**	3,26
ENSMUSG00000018339	**Gpx3**	3,24
ENSMUSG00000028327	**Stra6l**	3,24
ENSMUSG00000096971	**4930556M19Rik**	3,23
ENSMUSG00000023015	**Racgap1**	3,23
ENSMUSG00000027412	**Lpin3**	3,22
ENSMUSG00000024538	**Ppic**	3,22
ENSMUSG00000040084	**Bub1b**	3,20
ENSMUSG00000004105	**Angptl2**	3,20
ENSMUSG00000056481	**Cd248**	3,16
ENSMUSG00000001403	**Ube2c**	3,16
ENSMUSG00000001555	**Fkbp10**	3,16
ENSMUSG00000020808	**Pimreg**	3,14
ENSMUSG00000027306	**Nusap1**	3,14
ENSMUSG00000029710	**Ephb4**	3,14
ENSMUSG00000037725	**Ckap2**	3,14
ENSMUSG00000029070	**Mxra8**	3,13
ENSMUSG00000044201	**Cdc25c**	3,13
ENSMUSG00000028494	**Plin2**	3,12
ENSMUSG00000034883	**Lrr1**	3,11
ENSMUSG00000068699	**Flnc**	3,11
ENSMUSG00000020932	**Gfap**	3,10
ENSMUSG00000026669	**Mcm10**	3,09
ENSMUSG00000022021	**Diaph3**	3,09
ENSMUSG00000046295	**Ankle1**	3,08

ENSMUSG00000073489	**Ifi204**	3,06
ENSMUSG00000026390	**Marco**	3,06
ENSMUSG00000020493	**Prr11**	3,05
ENSMUSG00000097254	**C430042M11Rik**	3,05
ENSMUSG00000042116	**Vwa1**	3,05
ENSMUSG00000022661	**Cd200**	3,04
ENSMUSG00000046186	**Cd109**	3,04
ENSMUSG00000026285	**Pdcd1**	3,04
ENSMUSG00000004098	**Col5a3**	3,04
ENSMUSG00000027326	**Knl1**	3,02
ENSMUSG00000022322	**Shcbp1**	3,02
ENSMUSG00000028763	**Hspg2**	3,02
ENSMUSG00000003779	**Kif20a**	3,02
ENSMUSG00000017146	**Brca1**	3,02
ENSMUSG00000025383	**Il23a**	3,01
ENSMUSG00000009687	**Fxyd5**	3,00
ENSMUSG00000048922	**Cdca2**	3,00
ENSMUSG00000045932	**Ifit2**	3,00
ENSMUSG00000027323	**Rad51**	3,00
ENSMUSG00000031262	**Cenpi**	3,00
ENSMUSG00000079339	**Ifit1bl1**	2,99
ENSMUSG00000098318	**Lockd**	2,99
ENSMUSG00000041498	**Kif14**	2,98
ENSMUSG00000020674	**Pxdn**	2,97
ENSMUSG00000031004	**Mki67**	2,97
ENSMUSG00000028121	**Bcar3**	2,96
ENSMUSG00000036777	**Anln**	2,96
ENSMUSG00000039187	**Fanci**	2,96
ENSMUSG00000029414	**Kntc1**	2,95
ENSMUSG00000074476	**Spc24**	2,95
ENSMUSG00000015568	**Lpl**	2,95
ENSMUSG00000042489	**Clspn**	2,94
ENSMUSG00000044303	**Cdkn2a**	2,93
ENSMUSG00000051379	**Flrt3**	2,93
ENSMUSG00000020914	**Top2a**	2,93
ENSMUSG00000052776	**Oas1a**	2,92
ENSMUSG00000030677	**Kif22**	2,92
ENSMUSG00000002055	**Spag5**	2,92
ENSMUSG00000039396	**Neil3**	2,92
ENSMUSG00000002068	**Ccne1**	2,91
ENSMUSG00000023830	**Igf2r**	2,91
ENSMUSG00000020427	**Igfbp3**	2,91
ENSMUSG00000068744	**Psrc1**	2,91
ENSMUSG00000034205	**Loxl2**	2,91
ENSMUSG00000030249	**Abcc9**	2,90
ENSMUSG00000027490	**E2f1**	2,90
ENSMUSG00000006398	**Cdc20**	2,90

ENSMUSG00000051378	**Kif18b**	2,90
ENSMUSG00000027074	**Slc43a3**	2,90
ENSMUSG00000024791	**Cdca5**	2,90
ENSMUSG00000033350	**Chst2**	2,89
ENSMUSG00000036223	**Ska1**	2,89
ENSMUSG00000022146	**Osmr**	2,88
ENSMUSG00000028597	**Gpx7**	2,87
ENSMUSG00000036768	**Kif15**	2,87
ENSMUSG00000020641	**Rsad2**	2,86
ENSMUSG00000050335	**Lgals3**	2,86
ENSMUSG00000039981	**Zc3h12d**	2,86
ENSMUSG00000029096	**Htra3**	2,86
ENSMUSG00000035455	**Fignl1**	2,85
ENSMUSG00000038943	**Prc1**	2,85
ENSMUSG00000024056	**Ndc80**	2,85
ENSMUSG00000055044	**Pdlim1**	2,85
ENSMUSG00000028044	**Cks1b**	2,85
ENSMUSG00000028678	**Kif2c**	2,85
ENSMUSG00000097352	**C920009B18Rik**	2,84
ENSMUSG00000027883	**Gpsm2**	2,84
ENSMUSG00000020357	**Flt4**	2,84
ENSMUSG00000049871	**Nlrc3**	2,83
ENSMUSG00000024640	**Psat1**	2,83
ENSMUSG00000047798	**Cd300lf**	2,83
ENSMUSG00000023046	**Igfbp6**	2,82
ENSMUSG00000029177	**Cenpa**	2,82
ENSMUSG00000037358	**Dipk2b**	2,81
ENSMUSG00000047534	**Mis18bp1**	2,81
ENSMUSG00000092074	**Dynlt1a**	2,81
ENSMUSG00000022440	**C1qtnf6**	2,81
ENSMUSG00000024440	**Pcdh12**	2,80
ENSMUSG00000027994	**Mcub**	2,80
ENSMUSG00000030346	**Rad51ap1**	2,80
ENSMUSG00000021903	**Galnt15**	2,79
ENSMUSG00000036446	**Lum**	2,78
ENSMUSG00000002900	**Lamb1**	2,78
ENSMUSG00000079553	**Kifc1**	2,78
ENSMUSG00000022945	**Chaf1b**	2,78
ENSMUSG00000086712	**AI427809**	2,78
ENSMUSG00000045273	**Cenph**	2,78
ENSMUSG00000051669	**AU021092**	2,77
ENSMUSG00000029591	**Ung**	2,77
ENSMUSG00000021922	**Itih4**	2,76
ENSMUSG00000037625	**Cldn11**	2,76
ENSMUSG00000020841	**Cpd**	2,76
ENSMUSG00000070323	**Mmp27**	2,76
ENSMUSG00000025492	**Ifitm3**	2,76

ENSMUSG00000001240	**Ramp2**	2,75
ENSMUSG00000050737	**Ptges**	2,75
ENSMUSG00000028583	**Pdpn**	2,74
ENSMUSG00000006715	**Gmnn**	2,74
ENSMUSG00000026779	**Mastl**	2,74
ENSMUSG00000069792	**Wfdc17**	2,74
ENSMUSG00000040711	**Sh3pxd2b**	2,73
ENSMUSG00000058046	**4933430I17Rik**	2,73
ENSMUSG00000074896	**Ifit3**	2,73
ENSMUSG00000026890	**Lhx6**	2,72
ENSMUSG00000054435	**Gimap4**	2,71
ENSMUSG00000050410	**Tcf19**	2,71
ENSMUSG00000037095	**Lrg1**	2,71
ENSMUSG00000001228	**Uhrf1**	2,71
ENSMUSG00000028551	**Cdkn2c**	2,71
ENSMUSG00000022034	**Esco2**	2,71
ENSMUSG00000092349	**Smim40**	2,71
ENSMUSG00000005824	**Tnfsf14**	2,71
ENSMUSG00000071847	**Apcdd1**	2,71
ENSMUSG00000005233	**Spc25**	2,70
ENSMUSG00000034459	**Ifit1**	2,70
ENSMUSG00000026039	**Sgo2a**	2,69
ENSMUSG00000006014	**Prg4**	2,69
ENSMUSG00000039062	**Anpep**	2,69
ENSMUSG00000111171	**Gm47815**	2,69
ENSMUSG00000019647	**Sema6a**	2,69
ENSMUSG00000022548	**Apod**	2,68
ENSMUSG00000026043	**Col3a1**	2,68
ENSMUSG00000034591	**Slc41a2**	2,68
ENSMUSG00000033644	**Piwil2**	2,67
ENSMUSG00000002835	**Chaf1a**	2,66
ENSMUSG00000050105	**Grrp1**	2,66
ENSMUSG00000090231	**Cfb**	2,65
ENSMUSG00000033355	**Rtp4**	2,64
ENSMUSG00000033191	**Tie1**	2,63
ENSMUSG00000021176	**Efcab11**	2,63
ENSMUSG00000041378	**Cldn5**	2,63
ENSMUSG00000022483	**Col2a1**	2,63
ENSMUSG00000033788	**Dysf**	2,62
ENSMUSG00000026185	**Igfbp5**	2,62
ENSMUSG00000035860	**Cdhr3**	2,62
ENSMUSG00000026728	**Vim**	2,62
ENSMUSG00000075602	**Ly6a**	2,62
ENSMUSG00000052688	**Rab7b**	2,62
ENSMUSG00000068758	**Il3ra**	2,62
ENSMUSG00000027654	**Fam83d**	2,61
ENSMUSG00000032783	**Troap**	2,61

ENSMUSG00000026437	**Cdk18**	2,60
ENSMUSG00000045502	**Hcar2**	2,60
ENSMUSG00000001946	**Esam**	2,60
ENSMUSG00000027699	**Ect2**	2,60
ENSMUSG00000038379	**Ttk**	2,60
ENSMUSG00000054404	**Slfn5**	2,60
ENSMUSG00000032254	**Kif23**	2,60
ENSMUSG00000028702	**Rad54l**	2,59
ENSMUSG00000024084	**Qpct**	2,58
ENSMUSG00000024899	**Papss2**	2,57
ENSMUSG00000030353	**Tead4**	2,57
ENSMUSG00000032586	**Traip**	2,56
ENSMUSG00000075266	**Cenpw**	2,56
ENSMUSG00000062488	**Ifit3b**	2,56
ENSMUSG00000029661	**Col1a2**	2,56
ENSMUSG00000036098	**Myrf**	2,56
ENSMUSG00000045031	**Cetn4**	2,55
ENSMUSG00000031756	**Cenpn**	2,55
ENSMUSG00000046179	**E2f8**	2,55
ENSMUSG00000074336	**Apoc4**	2,55
ENSMUSG00000028175	**Depdc1a**	2,54
ENSMUSG00000020014	**Cfap54**	2,53
ENSMUSG00000017724	**Etv4**	2,53
ENSMUSG00000032231	**Anxa2**	2,53
ENSMUSG00000029561	**Oasl2**	2,53
ENSMUSG00000033031	**Cip2a**	2,53
ENSMUSG00000072812	**Ahnak2**	2,52
ENSMUSG00000033952	**Aspm**	2,52
ENSMUSG00000021391	**Cenpp**	2,52
ENSMUSG00000046768	**Rhoj**	2,52
ENSMUSG00000063060	**Sox7**	2,51
ENSMUSG00000027463	**Slc52a3**	2,51
ENSMUSG00000027496	**Aurka**	2,51
ENSMUSG00000039814	**Xkr5**	2,51
ENSMUSG00000036356	**Csgalnact1**	2,50
ENSMUSG00000030785	**Cox6a2**	2,50
ENSMUSG00000032221	**Mns1**	2,49
ENSMUSG00000076437	**Selenoh**	2,49
ENSMUSG00000037313	**Tacc3**	2,48
ENSMUSG00000034471	**Caskin2**	2,48
ENSMUSG00000024066	**Xdh**	2,48
ENSMUSG00000037849	**Ifi206**	2,48
ENSMUSG00000046470	**Sox18**	2,47
ENSMUSG00000009545	**Kcnq1**	2,47
ENSMUSG00000058773	**H1f5**	2,47
ENSMUSG00000031486	**Adgra2**	2,46
ENSMUSG00000029082	**Bst1**	2,46

ENSMUSG00000019929	**Dcn**	2,46
ENSMUSG00000025498	**Irf7**	2,46
ENSMUSG00000031871	**Cdh5**	2,46
ENSMUSG00000049916	**2610318N02Rik**	2,46
ENSMUSG00000017861	**Mybl2**	2,45
ENSMUSG00000011008	**Mcoln2**	2,45
ENSMUSG00000026389	**Steap3**	2,44
ENSMUSG00000023972	**Ptk7**	2,44
ENSMUSG00000005470	**Asf1b**	2,44
ENSMUSG00000028037	**Ifi44**	2,43
ENSMUSG00000027803	**Wwtr1**	2,43
ENSMUSG00000044229	**Nxpe4**	2,43
ENSMUSG00000030123	**Plxnd1**	2,43
ENSMUSG00000037759	**Ptger2**	2,42
ENSMUSG00000021360	**Gcnt2**	2,42
ENSMUSG00000022941	**Ripply3**	2,42
ENSMUSG00000001020	**S100a4**	2,41
ENSMUSG00000020185	**E2f7**	2,41
ENSMUSG00000021994	**Wnt5a**	2,41
ENSMUSG00000031821	**Gins2**	2,41
ENSMUSG00000025001	**Hells**	2,40
ENSMUSG00000031803	**B3gnt3**	2,40
ENSMUSG00000038775	**Vill**	2,40
ENSMUSG00000000682	**Cd52**	2,40
ENSMUSG00000026921	**Egfl7**	2,39
ENSMUSG00000061577	**Adgrg5**	2,39
ENSMUSG00000039055	**Eme1**	2,39
ENSMUSG00000079419	**Ms4a6c**	2,39
ENSMUSG00000010830	**Kdelr3**	2,39
ENSMUSG00000070858	**Gm1673**	2,38
ENSMUSG00000037031	**Tspan15**	2,38
ENSMUSG00000102918	**Pcdhgc3**	2,38
ENSMUSG00000031838	**Ifi30**	2,38
ENSMUSG00000054690	**Emcn**	2,38
ENSMUSG00000079685	**Ulbp1**	2,37
ENSMUSG00000021485	**Mxd3**	2,37
ENSMUSG00000001517	**Foxm1**	2,37
ENSMUSG00000020241	**Col6a2**	2,37
ENSMUSG00000034329	**Brip1**	2,37
ENSMUSG00000027435	**Cd93**	2,37
ENSMUSG00000037474	**Dtl**	2,36
ENSMUSG00000040373	**Cacng5**	2,36
ENSMUSG00000035273	**Hpse**	2,35
ENSMUSG00000113769	**5033406O09Rik**	2,35
ENSMUSG00000050994	**Adgb**	2,35
ENSMUSG00000037337	**Map4k1**	2,35
ENSMUSG00000029762	**Akr1b8**	2,34

ENSMUSG00000037679	**Inf2**	2,34
ENSMUSG00000021294	**Kif26a**	2,34
ENSMUSG00000048612	**Myof**	2,34
ENSMUSG00000042029	**Ncapg2**	2,34
ENSMUSG00000026429	**Ube2t**	2,34
ENSMUSG00000036617	**Etl4**	2,33
ENSMUSG00000030365	**Clec2i**	2,33
ENSMUSG00000051375	**Pcdh1**	2,33
ENSMUSG00000080303	**Gm12419**	2,32
ENSMUSG00000026442	**Nfasc**	2,32
ENSMUSG00000022754	**Tmem45a**	2,32
ENSMUSG00000035493	**Tgfbi**	2,32
ENSMUSG00000025351	**Cd63**	2,32
ENSMUSG00000042429	**Adora1**	2,31
ENSMUSG00000062515	**Fabp4**	2,31
ENSMUSG00000026981	**Il1rn**	2,31
ENSMUSG00000041548	**Hspb8**	2,31
ENSMUSG00000038264	**Sema7a**	2,31
ENSMUSG00000039167	**Adgrl4**	2,31
ENSMUSG00000037572	**Wdhd1**	2,30
ENSMUSG00000026640	**Plxna2**	2,30
ENSMUSG00000079298	**Klrb1b**	2,30
ENSMUSG00000021714	**Cenpk**	2,29
ENSMUSG00000007080	**Pole**	2,29
ENSMUSG00000038252	**Ncapd2**	2,29
ENSMUSG00000019846	**Lama4**	2,29
ENSMUSG00000004552	**Ctse**	2,28
ENSMUSG00000003534	**Ddr1**	2,28
ENSMUSG00000030162	**Olr1**	2,28
ENSMUSG00000001506	**Col1a1**	2,28
ENSMUSG00000070436	**Serpinh1**	2,28
ENSMUSG00000021965	**Ska3**	2,27
ENSMUSG00000002602	**Axl**	2,27
ENSMUSG00000002847	**Pla1a**	2,27
ENSMUSG00000039994	**Timeless**	2,27
ENSMUSG00000025747	**Tyms**	2,27
ENSMUSG00000023940	**Sgo1**	2,26
ENSMUSG00000037370	**Enpp1**	2,26
ENSMUSG00000032125	**Robo4**	2,26
ENSMUSG00000025574	**Tk1**	2,26
ENSMUSG00000056145	**Al504432**	2,25
ENSMUSG00000057191	**AB124611**	2,25
ENSMUSG00000031538	**Plat**	2,25
ENSMUSG00000049409	**Prokr1**	2,24
ENSMUSG00000001119	**Col6a1**	2,24
ENSMUSG00000022816	**Fstl1**	2,24
ENSMUSG00000041736	**Tspo**	2,24

ENSMUSG00000056737	**Capg**	2,24
ENSMUSG00000024420	**Zfp521**	2,23
ENSMUSG00000059089	**Fcgr4**	2,23
ENSMUSG00000027698	**Nceh1**	2,23
ENSMUSG00000036853	**Mcoln3**	2,23
ENSMUSG00000025854	**Fam20c**	2,23
ENSMUSG00000055333	**Fat2**	2,23
ENSMUSG00000031734	**Irx3**	2,22
ENSMUSG00000027935	**Rab13**	2,22
ENSMUSG00000048489	**Depp1**	2,22
ENSMUSG00000024675	**Ms4a4c**	2,21
ENSMUSG00000026582	**Sele**	2,21
ENSMUSG00000031465	**Angpt2**	2,20
ENSMUSG00000014329	**Bicc1**	2,20
ENSMUSG00000046610	**Oacyl**	2,20
ENSMUSG00000020895	**Tmem107**	2,20
ENSMUSG00000054932	**Afp**	2,20
ENSMUSG00000025494	**Sigirr**	2,20
ENSMUSG00000031239	**Itm2a**	2,19
ENSMUSG00000018845	**Unc45b**	2,19
ENSMUSG00000034206	**Polq**	2,19
ENSMUSG00000025289	**Prdx4**	2,18
ENSMUSG00000021707	**Dhfr**	2,18
ENSMUSG00000024590	**Lmnb1**	2,18
ENSMUSG00000002985	**Apoe**	2,18
ENSMUSG00000027238	**Frmd5**	2,18
ENSMUSG00000028111	**Ctsk**	2,18
ENSMUSG00000040616	**Tmem51**	2,18
ENSMUSG00000069808	**Fam57a**	2,18
ENSMUSG00000025324	**Atp10a**	2,17
ENSMUSG00000030247	**Kcnj8**	2,17
ENSMUSG00000073405	**H2-T-ps**	2,17
ENSMUSG00000022385	**Gtse1**	2,17
ENSMUSG00000025420	**Katnal2**	2,17
ENSMUSG00000021569	**Trip13**	2,17
ENSMUSG00000031799	**Tpm4**	2,16
ENSMUSG00000027555	**Car13**	2,16
ENSMUSG00000074793	**Hspa12b**	2,16
ENSMUSG00000047959	**Kcna3**	2,16
ENSMUSG00000026873	**Phf19**	2,16
ENSMUSG00000042842	**Serpinb6b**	2,16
ENSMUSG00000079037	**Prnp**	2,15
ENSMUSG00000108118	**Gm34312**	2,15
ENSMUSG00000044921	**Rassf9**	2,15
ENSMUSG00000015027	**Galns**	2,15
ENSMUSG00000027419	**Pcsk2**	2,15
ENSMUSG00000099757	**BE692007**	2,15

ENSMUSG00000102418	**Sh2d1b1**	2,14
ENSMUSG00000041134	**Cyyr1**	2,14
ENSMUSG00000004891	**Nes**	2,14
ENSMUSG00000028438	**Kif24**	2,14
ENSMUSG00000073418	**C4b**	2,14
ENSMUSG00000026335	**Pam**	2,14
ENSMUSG00000066842	**Hmcn1**	2,14
ENSMUSG00000020473	**Aebp1**	2,14
ENSMUSG00000022220	**Adcy4**	2,13
ENSMUSG00000028965	**Tnfrsf9**	2,13
ENSMUSG00000118138	**Gm50322**	2,13
ENSMUSG00000066861	**Oas1g**	2,13
ENSMUSG00000025473	**Adam8**	2,13
ENSMUSG00000019899	**Lama2**	2,13
ENSMUSG00000026072	**Il1r1**	2,13
ENSMUSG00000021565	**Slc6a19**	2,12
ENSMUSG00000035413	**Tmem98**	2,12
ENSMUSG00000001507	**Itga3**	2,12
ENSMUSG00000031375	**Bgn**	2,12
ENSMUSG00000026605	**Cenpf**	2,12
ENSMUSG00000029910	**Mad2l1**	2,12
ENSMUSG00000044562	**Rasip1**	2,12
ENSMUSG00000080743	**Gm7150**	2,12
ENSMUSG00000030208	**Emp1**	2,11
ENSMUSG00000000317	**Bcl6b**	2,11
ENSMUSG00000017446	**C1qtnf1**	2,11
ENSMUSG00000079445	**B3gnt7**	2,11
ENSMUSG00000069793	**Slfn9**	2,11
ENSMUSG00000032815	**Fanca**	2,10
ENSMUSG00000005763	**Cd247**	2,10
ENSMUSG00000006403	**Adamts4**	2,10
ENSMUSG00000036545	**Adamts2**	2,10
ENSMUSG00000085636	**Gm11769**	2,09
ENSMUSG00000027800	**Tm4sf1**	2,09
ENSMUSG00000024903	**Lao1**	2,09
ENSMUSG00000040605	**Bace2**	2,09
ENSMUSG00000015850	**Adamtsl4**	2,08
ENSMUSG00000040907	**Atp1a3**	2,08
ENSMUSG00000047907	**Tshz2**	2,08
ENSMUSG00000035578	**Iqcg**	2,07
ENSMUSG00000070691	**Runx3**	2,07
ENSMUSG00000030107	**Usp18**	2,07
ENSMUSG00000020826	**Nos2**	2,07
ENSMUSG00000041390	**Mdfic**	2,06
ENSMUSG00000026536	**Ifi211**	2,06
ENSMUSG00000024935	**Slc1a1**	2,06
ENSMUSG00000027375	**Mal**	2,06

ENSMUSG00000086690	**4933406J10Rik**	2,06
ENSMUSG00000022762	**Ncam2**	2,06
ENSMUSG00000028212	**Ccne2**	2,06
ENSMUSG00000078773	**Rad54b**	2,06
ENSMUSG00000060591	**Ifitm2**	2,06
ENSMUSG00000027954	**Efna1**	2,06
ENSMUSG00000064262	**Gimap8**	2,05
ENSMUSG00000054580	**Pla2r1**	2,05
ENSMUSG00000028195	**Ccn1**	2,05
ENSMUSG00000098098	**Bvht**	2,05
ENSMUSG00000045679	**Pqlc3**	2,05
ENSMUSG00000040658	**Dnph1**	2,05
ENSMUSG00000040528	**Milr1**	2,04
ENSMUSG00000036894	**Rap2b**	2,04
ENSMUSG00000027322	**Siglec1**	2,04
ENSMUSG00000032113	**Chek1**	2,04
ENSMUSG00000062082	**Cd200r4**	2,04
ENSMUSG00000105954	**Gm42793**	2,04
ENSMUSG00000040562	**Gstm2**	2,04
ENSMUSG00000021175	**Cdca7l**	2,04
ENSMUSG00000023913	**Pla2g7**	2,03
ENSMUSG00000020186	**Csrp2**	2,03
ENSMUSG00000037605	**Adgrl3**	2,03
ENSMUSG00000034037	**Fgd5**	2,03
ENSMUSG00000067377	**Tspan6**	2,03
ENSMUSG00000072082	**Ccnf**	2,03
ENSMUSG00000022479	**Vdr**	2,03
ENSMUSG00000079293	**Clec7a**	2,03
ENSMUSG00000038402	**Foxf2**	2,03
ENSMUSG00000044469	**Tnfaip8l1**	2,03
ENSMUSG00000031246	**Sh3bgrl**	2,03
ENSMUSG00000037466	**Tedc1**	2,03
ENSMUSG00000060913	**Trim55**	2,02
ENSMUSG00000004371	**Il11**	2,02
ENSMUSG00000032028	**Nxpe2**	2,02
ENSMUSG00000021493	**Pdlim7**	2,02
ENSMUSG00000025743	**Sdc3**	2,01
ENSMUSG00000041362	**Shtn1**	2,01
ENSMUSG00000016024	**Lbp**	2,01
ENSMUSG00000028909	**Ptpru**	2,01
ENSMUSG00000022074	**Tnfrsf10b**	2,01
ENSMUSG00000039748	**Exo1**	2,01
ENSMUSG00000042641	**Rgsl1**	2,01
ENSMUSG00000045333	**Zfp423**	2,00
ENSMUSG00000031616	**Ednra**	2,00
ENSMUSG00000050953	**Gja1**	2,00
ENSMUSG00000097654	**Gm26714**	2,00

ENSMUSG00000051517	**Arhgef39**	2,00
ENSMUSG00000022304	**Dpys**	2,00
ENSMUSG00000028587	**Orc1**	2,00
ENSMUSG00000022687	**Boc**	2,00
ENSMUSG00000027811	**4930579G24Rik**	2,00
ENSMUSG00000022212	**Cpne6**	-3,14
ENSMUSG00000090877	**Hspa1b**	-3,10
ENSMUSG00000029657	**Hsph1**	-2,90
ENSMUSG00000097266	**Gm26802**	-2,90
ENSMUSG00000022240	**Ctnnd2**	-2,85
ENSMUSG00000025014	**Dntt**	-2,83
ENSMUSG00000030539	**Sema4b**	-2,79
ENSMUSG00000008193	**Spib**	-2,77
ENSMUSG00000087442	**Gm14453**	-2,76
ENSMUSG00000091971	**Hspa1a**	-2,74
ENSMUSG00000079164	**Tlr5**	-2,65
ENSMUSG00000003379	**Cd79a**	-2,56
ENSMUSG00000017740	**Slc12a5**	-2,53
ENSMUSG00000101166	**Gm28496**	-2,51
ENSMUSG00000014030	**Pax5**	-2,49
ENSMUSG00000028222	**Calb1**	-2,49
ENSMUSG00000009394	**Syn2**	-2,46
ENSMUSG00000048251	**Bcl11b**	-2,46
ENSMUSG00000038026	**Kcnj9**	-2,46
ENSMUSG00000010803	**Gabra1**	-2,46
ENSMUSG00000007033	**Hspa1l**	-2,44
ENSMUSG00000030724	**Cd19**	-2,44
ENSMUSG00000032936	**Camkv**	-2,39
ENSMUSG00000095969	**Rnu1a1**	-2,38
ENSMUSG00000031210	**Gpr165**	-2,38
ENSMUSG00000111844	**Gm47097**	-2,37
ENSMUSG00000053025	**Sv2b**	-2,36
ENSMUSG00000078307	**AI593442**	-2,35
ENSMUSG00000091370	**5730435O14Rik**	-2,33
ENSMUSG00000036095	**Dgkb**	-2,33
ENSMUSG00000022055	**Nefl**	-2,30
ENSMUSG00000054459	**Vsnl1**	-2,30
ENSMUSG00000003032	**Klf4**	-2,29
ENSMUSG00000108614	**2610306O10Rik**	-2,29
ENSMUSG00000022054	**Nefm**	-2,28
ENSMUSG00000047842	**Diras2**	-2,28
ENSMUSG00000043384	**Gprasp1**	-2,26
ENSMUSG00000027273	**Snap25**	-2,25
ENSMUSG00000108486	**Gm44836**	-2,25
ENSMUSG00000034336	**Ina**	-2,23
ENSMUSG00000041202	**Pla2g2d**	-2,23
ENSMUSG00000029420	**Rimbp2**	-2,23

ENSMUSG00000040424	**Hipk4**	-2,22
ENSMUSG00000032609	**Klhdc8b**	-2,22
ENSMUSG00000072966	**Gprasp2**	-2,20
ENSMUSG00000042671	**Rgs8**	-2,19
ENSMUSG00000070880	**Gad1**	-2,19
ENSMUSG00000032503	**Arpp21**	-2,19
ENSMUSG00000097120	**Gm26887**	-2,18
ENSMUSG00000065987	**Cd209b**	-2,18
ENSMUSG00000024479	**Mal2**	-2,18
ENSMUSG00000085589	**A430078I02Rik**	-2,17
ENSMUSG00000051906	**Cd209f**	-2,17
ENSMUSG00000028488	**Sh3gl2**	-2,17
ENSMUSG00000024486	**Hbegf**	-2,16
ENSMUSG00000060882	**Kcnd2**	-2,15
ENSMUSG00000103593	**Gm37352**	-2,15
ENSMUSG00000061702	**Tmem91**	-2,14
ENSMUSG00000090185	**Gm15523**	-2,12
ENSMUSG00000070822	**Zscan18**	-2,11
ENSMUSG00000085802	**Gm16059**	-2,11
ENSMUSG00000075027	**4631405J19Rik**	-2,09
ENSMUSG00000105434	**Gm43359**	-2,09
ENSMUSG00000040950	**Mgl2**	-2,09
ENSMUSG00000026527	**Rgs7**	-2,07
ENSMUSG00000116604	**Gm49745**	-2,07
ENSMUSG00000034825	**Nrip3**	-2,07
ENSMUSG00000104150	**Gm44573**	-2,07
ENSMUSG00000025221	**Kcnip2**	-2,07
ENSMUSG00000045733	**Sprn**	-2,06
ENSMUSG00000026163	**Sphkap**	-2,06
ENSMUSG00000040536	**Necab1**	-2,05
ENSMUSG00000042589	**Cux2**	-2,05
ENSMUSG00000074968	**Ano3**	-2,05
ENSMUSG00000078816	**Prkcg**	-2,05
ENSMUSG00000104367	**Gm38079**	-2,05
ENSMUSG00000030994	**D7Ertd443e**	-2,04
ENSMUSG00000007944	**Ttc9b**	-2,04
ENSMUSG00000028785	**Hpca**	-2,03
ENSMUSG00000103976	**Gm37677**	-2,03
ENSMUSG00000033268	**Duox1**	-2,03
ENSMUSG00000008489	**Elavl2**	-2,03
ENSMUSG00000022454	**Nell2**	-2,03
ENSMUSG00000032564	**Cpne4**	-2,03
ENSMUSG00000097545	**Mir124a-1hg**	-2,03
ENSMUSG00000068696	**Gpr88**	-2,02
ENSMUSG00000016349	**Eef1a2**	-2,02
ENSMUSG00000061911	**Myt1l**	-2,02
ENSMUSG00000043463	**Rab9b**	-2,01

ENSMUSG00000049556	**Lingo1**	-2,01
ENSMUSG00000094626	**Tmem121b**	-2,01
ENSMUSG00000053693	**Mast1**	-2,01
ENSMUSG00000044122	**Proca1**	-2,01
ENSMUSG00000026589	**Sec16b**	-2,01
ENSMUSG00000111063	**Zkscan7**	-2,00
ENSMUSG00000043468	**Adam30**	-2,00

---

g

gene_id	gene_name	log2FoldChange
ENSMUSG00000055148	**Klf2**	-3,03
ENSMUSG00000051627	**H1f4**	-3,01
ENSMUSG00000020889	**Nr1d1**	-2,84
ENSMUSG00000047246	**H2bc6**	-2,83
ENSMUSG00000036181	**H1f2**	-2,80
ENSMUSG00000009214	**Mymk**	-2,80
ENSMUSG00000074207	**Adh1**	-2,77
ENSMUSG00000036040	**Adamtsl2**	-2,72
ENSMUSG00000027224	**Duoxa1**	-2,70
ENSMUSG00000027217	**Tspan18**	-2,68
ENSMUSG00000026866	**Kynu**	-2,67
ENSMUSG00000114864	**Gm41071**	-2,62
ENSMUSG00000028976	**Slc2a5**	-2,61
ENSMUSG00000022357	**Klhl38**	-2,53
ENSMUSG00000048163	**Selplg**	-2,50
ENSMUSG00000027326	**Knl1**	-2,49
ENSMUSG00000048424	**Ranbp3l**	-2,41
ENSMUSG00000073412	**Lst1**	-2,39
ENSMUSG00000051457	**Spn**	-2,38
ENSMUSG00000042675	**Ypel3**	-2,37
ENSMUSG00000106019	**Gm43672**	-2,34
ENSMUSG00000036353	**P2ry12**	-2,33
ENSMUSG00000035686	**Thrsp**	-2,32
ENSMUSG00000067235	**H2-Q10**	-2,31
ENSMUSG00000117916	**9630028I04Rik**	-2,30
ENSMUSG00000028989	**Angptl7**	-2,29
ENSMUSG00000100215	**Gm8292**	-2,29
ENSMUSG00000020377	**Ltc4s**	-2,26
ENSMUSG00000020593	**Lpin1**	-2,25
ENSMUSG00000062545	**Tlr12**	-2,25
ENSMUSG00000036594	**H2-Aa**	-2,24
ENSMUSG00000085881	**Gm15912**	-2,23
ENSMUSG00000005043	**Sgsh**	-2,22
ENSMUSG00000001741	**Il16**	-2,22
ENSMUSG00000052160	**Pld4**	-2,19
ENSMUSG00000060402	**Chst8**	-2,19

ENSMUSG00000109675	**Nxpe1-ps**	-2,19
ENSMUSG00000030148	**Clec4a2**	-2,19
ENSMUSG00000018819	**Lsp1**	-2,19
ENSMUSG00000040564	**Apoc1**	-2,16
ENSMUSG00000037548	**H2-DMb2**	-2,16
ENSMUSG00000101903	**Gm29291**	-2,15
ENSMUSG00000049436	**Upk1b**	-2,15
ENSMUSG00000071076	**Jund**	-2,14
ENSMUSG00000090665	**Gad1-ps**	-2,14
ENSMUSG00000038776	**Ephx1**	-2,14
ENSMUSG00000114784	**Gm47754**	-2,14
ENSMUSG00000051504	**Siglech**	-2,13
ENSMUSG00000048905	**Bnip5**	-2,13
ENSMUSG00000081809	**Gm15539**	-2,13
ENSMUSG00000036949	**Slc39a12**	-2,12
ENSMUSG00000060586	**H2-Eb1**	-2,12
ENSMUSG00000017493	**Igfbp4**	-2,12
ENSMUSG00000036526	**Card11**	-2,12
ENSMUSG00000050103	**Agmo**	-2,11
ENSMUSG00000028088	**Fmo5**	-2,11
ENSMUSG00000086914	**Gm16124**	-2,11
ENSMUSG00000041849	**Card6**	-2,10
ENSMUSG00000026489	**Coq8a**	-2,10
ENSMUSG00000026303	**Mlph**	-2,10
ENSMUSG00000021880	**Rnase6**	-2,09
ENSMUSG00000001552	**Jup**	-2,09
ENSMUSG00000090257	**Gm4524**	-2,08
ENSMUSG00000111147	**Gm33699**	-2,08
ENSMUSG00000048120	**Entpd1**	-2,07
ENSMUSG00000041797	**Abca9**	-2,06
ENSMUSG00000000753	**Serpinf1**	-2,06
ENSMUSG00000087355	**Gm13187**	-2,06
ENSMUSG00000068735	**Trp53i11**	-2,06
ENSMUSG00000018593	**Sparc**	-2,06
ENSMUSG00000114422	**Gm30411**	-2,06
ENSMUSG00000039496	**Cdnf**	-2,05
ENSMUSG00000079056	**Kcnip3**	-2,04
ENSMUSG00000022376	**Adcy8**	-2,04
ENSMUSG00000029650	**Slc46a3**	-2,03
ENSMUSG00000086158	**Ccpg1os**	-2,03
ENSMUSG00000049086	**Bmyc**	-2,03
ENSMUSG00000031785	**Adgrg1**	-2,02
ENSMUSG00000020682	**Mmp28**	-2,02
ENSMUSG00000023044	**Csad**	-2,01
ENSMUSG00000022496	**Tnfrsf17**	-2,01
ENSMUSG00000037972	**Snn**	-2,01
ENSMUSG00000030674	**Qprt**	-2,00

ENSMUSG00000059336	**Slc14a1**	-2,00
ENSMUSG00000050138	**Kcnk12**	-2,00
ENSMUSG00000025494	**Sigirr**	-2,00
ENSMUSG00000049723	**Mmp12**	6,52
ENSMUSG00000026981	**Il1rn**	5,60
ENSMUSG00000015568	**Lpl**	4,97
ENSMUSG00000022303	**Dcstamp**	4,84
ENSMUSG00000027737	**Slc7a11**	4,54
ENSMUSG00000002944	**Cd36**	4,37
ENSMUSG00000004891	**Nes**	4,22
ENSMUSG00000050370	**Ch25h**	4,09
ENSMUSG00000021701	**Plk2**	4,00
ENSMUSG00000026536	**Ifi211**	3,99
ENSMUSG00000028459	**Cd72**	3,99
ENSMUSG00000022246	**Rai14**	3,96
ENSMUSG00000028327	**Stra6l**	3,86
ENSMUSG00000001542	**Ell2**	3,79
ENSMUSG00000029304	**Spp1**	3,78
ENSMUSG00000072621	**Slfn10-ps**	3,74
ENSMUSG00000005087	**Cd44**	3,74
ENSMUSG00000022636	**Alcam**	3,73
ENSMUSG00000031488	**Rab11fip1**	3,64
ENSMUSG00000022237	**Ankrd33b**	3,61
ENSMUSG00000025473	**Adam8**	3,58
ENSMUSG00000052688	**Rab7b**	3,56
ENSMUSG00000057337	**Chst3**	3,55
ENSMUSG00000050335	**Lgals3**	3,54
ENSMUSG00000038179	**Slamf7**	3,50
ENSMUSG00000103966	**Gm37120**	3,44
ENSMUSG00000074802	**Gas2l3**	3,44
ENSMUSG00000030208	**Emp1**	3,43
ENSMUSG00000030162	**Olr1**	3,42
ENSMUSG00000105954	**Gm42793**	3,38
ENSMUSG00000015340	**Cybb**	3,38
ENSMUSG00000025582	**Nptx1**	3,37
ENSMUSG00000004296	**Il12b**	3,36
ENSMUSG00000112023	**Lilr4b**	3,31
ENSMUSG00000022150	**Dab2**	3,29
ENSMUSG00000111997	**Gm5176**	3,28
ENSMUSG00000063193	**Cd300lb**	3,26
ENSMUSG00000112657	**BC106175**	3,20
ENSMUSG00000079243	**Xirp1**	3,19
ENSMUSG00000054203	**Ifi205**	3,19
ENSMUSG00000050737	**Ptges**	3,18
ENSMUSG00000111118	**Gm6545**	3,17
ENSMUSG00000035352	**Ccl12**	3,15
ENSMUSG00000021508	**Cxcl14**	3,14

ENSMUSG00000026390	**Marco**	3,13
ENSMUSG00000030144	**Clec4d**	3,12
ENSMUSG00000053137	**Mapk11**	3,12
ENSMUSG00000023087	**Noct**	3,09
ENSMUSG00000106959	**Gm42548**	3,09
ENSMUSG00000022102	**Dok2**	3,07
ENSMUSG00000040026	**Saa3**	3,06
ENSMUSG00000084069	**Gm12306**	3,06
ENSMUSG00000025854	**Fam20c**	3,05
ENSMUSG00000028121	**Bcar3**	3,01
ENSMUSG00000042515	**Pwwp3b**	3,00
ENSMUSG00000041827	**Oasl1**	2,97
ENSMUSG00000103308	**Gm37800**	2,97
ENSMUSG00000026728	**Vim**	2,97
ENSMUSG00000022094	**Slc39a14**	2,94
ENSMUSG00000027555	**Car13**	2,93
ENSMUSG00000040711	**Sh3pxd2b**	2,91
ENSMUSG00000029379	**Cxcl3**	2,90
ENSMUSG00000022797	**Tfrc**	2,90
ENSMUSG00000042349	**Ikbke**	2,89
ENSMUSG00000056145	**AI504432**	2,86
ENSMUSG00000025044	**Msr1**	2,86
ENSMUSG00000043421	**Hilpda**	2,83
ENSMUSG00000017007	**Rbpjl**	2,82
ENSMUSG00000032715	**Trib3**	2,82
ENSMUSG00000041390	**Mdfic**	2,81
ENSMUSG00000026435	**Slc45a3**	2,79
ENSMUSG00000055202	**Zfp811**	2,79
ENSMUSG00000021458	**Aopep**	2,79
ENSMUSG00000019122	**Ccl9**	2,78
ENSMUSG00000032724	**Abtb2**	2,78
ENSMUSG00000024245	**Tmem178**	2,76
ENSMUSG00000092203	**1110038B12Rik**	2,75
ENSMUSG00000027276	**Jag1**	2,74
ENSMUSG00000096971	**4930556M19Rik**	2,72
ENSMUSG00000048279	**Sacs**	2,71
ENSMUSG00000037242	**Clic4**	2,70
ENSMUSG00000061878	**Sphk1**	2,70
ENSMUSG00000029752	**Asns**	2,69
ENSMUSG00000073490	**Ifi207**	2,69
ENSMUSG00000073274	**Gm14636**	2,68
ENSMUSG00000079293	**Clec7a**	2,66
ENSMUSG00000068220	**Lgals1**	2,66
ENSMUSG00000022126	**Acod1**	2,65
ENSMUSG00000021965	**Ska3**	2,64
ENSMUSG00000074785	**Plxnc1**	2,63
ENSMUSG00000032220	**Myo1e**	2,62

ENSMUSG00000002289	**Angptl4**	2,62
ENSMUSG00000024529	**Lox**	2,61
ENSMUSG00000111394	**Gm49759**	2,60
ENSMUSG00000016283	**H2-M2**	2,56
ENSMUSG00000000184	**Ccnd2**	2,55
ENSMUSG00000067931	**Zfp948**	2,54
ENSMUSG00000064899	**Snord118**	2,54
ENSMUSG00000042417	**Ccno**	2,54
ENSMUSG00000021591	**Glrx**	2,53
ENSMUSG00000025746	**Il6**	2,53
ENSMUSG00000028583	**Pdpn**	2,52
ENSMUSG00000002068	**Ccne1**	2,51
ENSMUSG00000097558	**Gm26902**	2,50
ENSMUSG00000032860	**P2ry2**	2,48
ENSMUSG00000059956	**Serpinb12**	2,48
ENSMUSG00000035373	**Ccl7**	2,48
ENSMUSG00000030142	**Clec4e**	2,47
ENSMUSG00000025059	**Gk**	2,46
ENSMUSG00000049907	**Rasl11b**	2,46
ENSMUSG00000042272	**Sestd1**	2,45
ENSMUSG00000034641	**Cd300ld**	2,44
ENSMUSG00000067206	**Lrrc66**	2,44
ENSMUSG00000034855	**Cxcl10**	2,44
ENSMUSG00000019558	**Slc6a8**	2,43
ENSMUSG00000023951	**Vegfa**	2,43
ENSMUSG00000110275	**Gm5905**	2,42
ENSMUSG00000089774	**Slc5a3**	2,42
ENSMUSG00000056749	**Nfil3**	2,41
ENSMUSG00000025355	**Mmp19**	2,41
ENSMUSG00000103313	**Gm38357**	2,40
ENSMUSG00000108053	**Gm43890**	2,39
ENSMUSG00000001918	**Slc1a5**	2,39
ENSMUSG00000020334	**Slc22a4**	2,39
ENSMUSG00000085894	**Gm15832**	2,38
ENSMUSG00000107320	**Gm42549**	2,37
ENSMUSG00000040152	**Thbs1**	2,36
ENSMUSG00000033967	**Rnf225**	2,36
ENSMUSG00000026193	**Fn1**	2,35
ENSMUSG00000034156	**Tspoap1**	2,35
ENSMUSG00000020641	**Rsad2**	2,34
ENSMUSG00000037849	**Ifi206**	2,34
ENSMUSG00000044162	**Tnip3**	2,34
ENSMUSG00000030641	**Ddias**	2,33
ENSMUSG00000108414	**Snhg1**	2,32
ENSMUSG00000004267	**Eno2**	2,32
ENSMUSG00000021493	**Pdlim7**	2,32
ENSMUSG00000052825	**Gm9892**	2,32

ENSMUSG00000063316	**Rpl27**	2,31
ENSMUSG00000020205	**Phlda1**	2,31
ENSMUSG00000106147	**Snord3a**	2,30
ENSMUSG00000020841	**Cpd**	2,30
ENSMUSG00000032113	**Chek1**	2,30
ENSMUSG00000030536	**Iqgap1**	2,29
ENSMUSG00000028128	**F3**	2,29
ENSMUSG00000085295	**4930430E12Rik**	2,29
ENSMUSG00000041308	**Sntb2**	2,29
ENSMUSG00000037280	**Galnt6**	2,28
ENSMUSG00000037148	**Arhgap10**	2,27
ENSMUSG00000020658	**Efr3b**	2,27
ENSMUSG00000034591	**Slc41a2**	2,26
ENSMUSG00000037573	**Tob1**	2,26
ENSMUSG00000020932	**Gfap**	2,26
ENSMUSG00000023830	**Igf2r**	2,25
ENSMUSG00000101166	**Gm28496**	2,25
ENSMUSG00000033721	**Vav3**	2,24
ENSMUSG00000106734	**Gm20559**	2,24
ENSMUSG00000096740	**Lbhd1**	2,23
ENSMUSG00000026437	**Cdk18**	2,23
ENSMUSG00000100813	**Gm28874**	2,23
ENSMUSG00000067869	**Tcea1-ps1**	2,23
ENSMUSG00000030103	**Bhlhe40**	2,23
ENSMUSG00000119262	**Snord3b1**	2,23
ENSMUSG00000034459	**Ifit1**	2,22
ENSMUSG00000110631	**Gm42047**	2,21
ENSMUSG00000075266	**Cenpw**	2,21
ENSMUSG00000077222	**Gm22270**	2,21
ENSMUSG00000104324	**Gm37320**	2,19
ENSMUSG00000112148	**Lilrb4a**	2,19
ENSMUSG00000097352	**C920009B18Rik**	2,19
ENSMUSG00000030657	**Xylt1**	2,18
ENSMUSG00000026558	**Uck2**	2,18
ENSMUSG00000085704	**4921531C22Rik**	2,18
ENSMUSG00000072620	**Slfn2**	2,18
ENSMUSG00000027313	**Chac1**	2,17
ENSMUSG00000024878	**Cbwd1**	2,17
ENSMUSG00000042265	**Trem1**	2,17
ENSMUSG00000064602	**Snora41**	2,16
ENSMUSG00000039981	**Zc3h12d**	2,16
ENSMUSG00000031246	**Sh3bgrl**	2,15
ENSMUSG00000067186	**Olfr132**	2,15
ENSMUSG00000089726	**Mir17hg**	2,14
ENSMUSG00000081603	**Gm14681**	2,14
ENSMUSG00000029553	**Tfec**	2,14
ENSMUSG00000037944	**Ccr7**	2,13

ENSMUSG00000025804	**Ccr1**	2,12
ENSMUSG00000000385	**Tmprss2**	2,12
ENSMUSG00000028494	**Plin2**	2,11
ENSMUSG00000027654	**Fam83d**	2,11
ENSMUSG00000031506	**Ptpn7**	2,10
ENSMUSG00000116673	**A630089N07Rik**	2,10
ENSMUSG00000097418	**Mir155hg**	2,10
ENSMUSG00000033581	**Igf2bp2**	2,09
ENSMUSG00000056888	**Glipr1**	2,09
ENSMUSG00000117869	**Snhg4**	2,09
ENSMUSG00000020359	**Phykpl**	2,09
ENSMUSG00000001473	**Tubb6**	2,08
ENSMUSG00000054598	**9130230L23Rik**	2,08
ENSMUSG00000109704	**Gm38414**	2,08
ENSMUSG00000042745	**Id1**	2,08
ENSMUSG00000074305	**Peak1**	2,08
ENSMUSG00000000555	**Itga5**	2,07
ENSMUSG00000044042	**Fmn1**	2,06
ENSMUSG00000026107	**Nabp1**	2,06
ENSMUSG00000003500	**Impdh1**	2,06
ENSMUSG00000028037	**Ifi44**	2,05
ENSMUSG00000001707	**Eef1e1**	2,05
ENSMUSG00000109244	**Gm44751**	2,04
ENSMUSG00000091021	**Gm17300**	2,04
ENSMUSG00000028238	**Atp6v0d2**	2,04
ENSMUSG00000021589	**Rhobtb3**	2,04
ENSMUSG00000032656	**Marchf3**	2,04
ENSMUSG00000016552	**Foxred2**	2,03
ENSMUSG00000032332	**Col12a1**	2,03
ENSMUSG00000031799	**Tpm4**	2,03
ENSMUSG00000091993	**B930036N10Rik**	2,03
ENSMUSG00000092444	**Gm18733**	2,02
ENSMUSG00000040528	**Milr1**	2,02
ENSMUSG00000028111	**Ctsk**	2,02
ENSMUSG00000079297	**Gm2223**	2,01
ENSMUSG00000039313	**Minar1**	2,01
ENSMUSG00000075297	**H60b**	2,01
ENSMUSG00000041313	**Slc7a1**	2,00
ENSMUSG00000085148	**Mir22hg**	2,00
ENSMUSG00000090125	**Pou3f1**	2,00

---

h

gene_id	gene_name	log2FoldChange
ENSMUSG00000030539	**Sema4b**	-2,73
ENSMUSG00000064441	**Snord37**	-2,62
ENSMUSG00000118125	**Gm50387**	-2,52

ENSMUSG00000020142	**Slc1a4**	-2,35
ENSMUSG00000091418	**Gm3164**	-2,31
ENSMUSG00000093445	**Lrch4**	-2,29
ENSMUSG00000006154	**Eps8l1**	-2,29
ENSMUSG00000103144	**Pcdhga1**	-2,20
ENSMUSG00000045252	**Zfp574**	-2,17
ENSMUSG00000040841	**Six5**	-2,12
ENSMUSG00000020793	**Galr2**	-2,11
ENSMUSG00000038037	**Socs1**	-2,10
ENSMUSG00000046541	**Zfp526**	-2,04
ENSMUSG00000023266	**Frs3**	-2,03
ENSMUSG00000040204	**Pclaf**	4,87
ENSMUSG00000032218	**Ccnb2**	4,78
ENSMUSG00000075266	**Cenpw**	4,71
ENSMUSG00000022033	**Pbk**	4,55
ENSMUSG00000020914	**Top2a**	4,48
ENSMUSG00000026683	**Nuf2**	4,44
ENSMUSG00000015880	**Ncapg**	4,41
ENSMUSG00000041498	**Kif14**	4,38
ENSMUSG00000039396	**Neil3**	4,38
ENSMUSG00000020808	**Pimreg**	4,35
ENSMUSG00000027331	**Knstrn**	4,31
ENSMUSG00000036067	**Slc2a6**	4,25
ENSMUSG00000031004	**Mki67**	4,22
ENSMUSG00000026669	**Mcm10**	4,18
ENSMUSG00000050370	**Ch25h**	4,16
ENSMUSG00000009687	**Fxyd5**	4,14
ENSMUSG00000079017	**Ifi27l2a**	4,13
ENSMUSG00000027326	**Knl1**	4,12
ENSMUSG00000068220	**Lgals1**	4,08
ENSMUSG00000020330	**Hmmr**	4,04
ENSMUSG00000027715	**Ccna2**	4,03
ENSMUSG00000040026	**Saa3**	3,96
ENSMUSG00000032254	**Kif23**	3,94
ENSMUSG00000024791	**Cdca5**	3,87
ENSMUSG00000045328	**Cenpe**	3,86
ENSMUSG00000027469	**Tpx2**	3,84
ENSMUSG00000044258	**Ctla2a**	3,83
ENSMUSG00000041431	**Ccnb1**	3,82
ENSMUSG00000037628	**Cdkn3**	3,80
ENSMUSG00000003484	**Cyp4f18**	3,80
ENSMUSG00000027379	**Bub1**	3,80
ENSMUSG00000028175	**Depdc1a**	3,79
ENSMUSG00000002055	**Spag5**	3,79
ENSMUSG00000044201	**Cdc25c**	3,77
ENSMUSG00000037544	**Dlgap5**	3,77
ENSMUSG00000001403	**Ube2c**	3,77

ENSMUSG00000028459	**Cd72**	3,76
ENSMUSG00000024989	**Cep55**	3,74
ENSMUSG00000068129	**Cst7**	3,71
ENSMUSG00000023505	**Cdca3**	3,68
ENSMUSG00000017146	**Brca1**	3,68
ENSMUSG00000020897	**Aurkb**	3,64
ENSMUSG00000040084	**Bub1b**	3,62
ENSMUSG00000026536	**Ifi211**	3,60
ENSMUSG00000022034	**Esco2**	3,57
ENSMUSG00000069792	**Wfdc17**	3,54
ENSMUSG00000098318	**Lockd**	3,53
ENSMUSG00000018339	**Gpx3**	3,51
ENSMUSG00000036777	**Anln**	3,51
ENSMUSG00000052688	**Rab7b**	3,50
ENSMUSG00000032400	**Zwilch**	3,50
ENSMUSG00000034311	**Kif4**	3,46
ENSMUSG00000073489	**Ifi204**	3,45
ENSMUSG00000035683	**Melk**	3,44
ENSMUSG00000051378	**Kif18b**	3,44
ENSMUSG00000037725	**Ckap2**	3,44
ENSMUSG00000032231	**Anxa2**	3,42
ENSMUSG00000004296	**Il12b**	3,41
ENSMUSG00000027306	**Nusap1**	3,38
ENSMUSG00000037474	**Dtl**	3,37
ENSMUSG00000047534	**Mis18bp1**	3,36
ENSMUSG00000019942	**Cdk1**	3,35
ENSMUSG00000028873	**Cdca8**	3,34
ENSMUSG00000079293	**Clec7a**	3,33
ENSMUSG00000021848	**Otx2**	3,33
ENSMUSG00000020493	**Prr11**	3,30
ENSMUSG00000023031	**Cela1**	3,30
ENSMUSG00000039187	**Fanci**	3,29
ENSMUSG00000026193	**Fn1**	3,29
ENSMUSG00000027514	**Zbp1**	3,28
ENSMUSG00000045273	**Cenph**	3,28
ENSMUSG00000003779	**Kif20a**	3,28
ENSMUSG00000031246	**Sh3bgrl**	3,27
ENSMUSG00000036875	**Dna2**	3,27
ENSMUSG00000026728	**Vim**	3,27
ENSMUSG00000022021	**Diaph3**	3,26
ENSMUSG00000047798	**Cd300lf**	3,25
ENSMUSG00000051627	**H1f4**	3,23
ENSMUSG00000005233	**Spc25**	3,22
ENSMUSG00000072980	**Oip5**	3,21
ENSMUSG00000074476	**Spc24**	3,19
ENSMUSG00000029177	**Cenpa**	3,19
ENSMUSG00000062980	**Cped1**	3,16

ENSMUSG00000027533	**Fabp5**	3,16
ENSMUSG00000036768	**Kif15**	3,16
ENSMUSG00000015854	**Cd5l**	3,15
ENSMUSG00000024675	**Ms4a4c**	3,15
ENSMUSG00000035365	**Parpbp**	3,15
ENSMUSG00000033952	**Aspm**	3,14
ENSMUSG00000028044	**Cks1b**	3,14
ENSMUSG00000027699	**Ect2**	3,14
ENSMUSG00000034317	**Trim59**	3,14
ENSMUSG00000030677	**Kif22**	3,14
ENSMUSG00000048327	**Ckap2l**	3,12
ENSMUSG00000030346	**Rad51ap1**	3,12
ENSMUSG00000107176	**Gm9794**	3,12
ENSMUSG00000032725	**Folr2**	3,11
ENSMUSG00000029304	**Spp1**	3,11
ENSMUSG00000029414	**Kntc1**	3,11
ENSMUSG00000017716	**Birc5**	3,11
ENSMUSG00000030867	**Plk1**	3,10
ENSMUSG00000026429	**Ube2t**	3,10
ENSMUSG00000024056	**Ndc80**	3,10
ENSMUSG00000023940	**Sgo1**	3,10
ENSMUSG00000026779	**Mastl**	3,09
ENSMUSG00000031506	**Ptpn7**	3,08
ENSMUSG00000028212	**Ccne2**	3,07
ENSMUSG00000020649	**Rrm2**	3,06
ENSMUSG00000022126	**Acod1**	3,06
ENSMUSG00000042489	**Clspn**	3,06
ENSMUSG00000030156	**Cd69**	3,06
ENSMUSG00000033031	**Cip2a**	3,05
ENSMUSG00000001228	**Uhrf1**	3,04
ENSMUSG00000024084	**Qpct**	3,02
ENSMUSG00000006398	**Cdc20**	3,01
ENSMUSG00000027323	**Rad51**	3,00
ENSMUSG00000022246	**Rai14**	2,99
ENSMUSG00000021728	**Emb**	2,98
ENSMUSG00000028718	**Stil**	2,98
ENSMUSG00000026981	**Il1rn**	2,97
ENSMUSG00000002289	**Angptl4**	2,97
ENSMUSG00000046179	**E2f8**	2,96
ENSMUSG00000025492	**Ifitm3**	2,96
ENSMUSG00000035455	**Fignl1**	2,95
ENSMUSG00000027490	**E2f1**	2,94
ENSMUSG00000037313	**Tacc3**	2,94
ENSMUSG00000032911	**Cspg4**	2,92
ENSMUSG00000099757	**BE692007**	2,92
ENSMUSG00000079419	**Ms4a6c**	2,91
ENSMUSG00000038379	**Ttk**	2,90

ENSMUSG00000034329	**Brip1**	2,88
ENSMUSG00000034349	**Smc4**	2,88
ENSMUSG00000023015	**Racgap1**	2,87
ENSMUSG00000073490	**Ifi207**	2,87
ENSMUSG00000052565	**H1f3**	2,87
ENSMUSG00000031262	**Cenpi**	2,87
ENSMUSG00000032783	**Troap**	2,86
ENSMUSG00000057191	**AB124611**	2,85
ENSMUSG00000036617	**Etl4**	2,84
ENSMUSG00000026285	**Pdcd1**	2,82
ENSMUSG00000006715	**Gmnn**	2,82
ENSMUSG00000026605	**Cenpf**	2,81
ENSMUSG00000022322	**Shcbp1**	2,80
ENSMUSG00000042265	**Trem1**	2,79
ENSMUSG00000037572	**Wdhd1**	2,78
ENSMUSG00000021485	**Mxd3**	2,78
ENSMUSG00000029082	**Bst1**	2,76
ENSMUSG00000012443	**Kif11**	2,76
ENSMUSG00000035373	**Ccl7**	2,75
ENSMUSG00000027115	**Kif18a**	2,75
ENSMUSG00000002602	**Axl**	2,74
ENSMUSG00000027496	**Aurka**	2,73
ENSMUSG00000035273	**Hpse**	2,73
ENSMUSG00000045932	**Ifit2**	2,72
ENSMUSG00000029816	**Gpnmb**	2,72
ENSMUSG00000015568	**Lpl**	2,71
ENSMUSG00000068617	**Efcab1**	2,71
ENSMUSG00000056888	**Glipr1**	2,70
ENSMUSG00000064347	**mt-Ta**	2,70
ENSMUSG00000027994	**Mcub**	2,70
ENSMUSG00000002944	**Cd36**	2,69
ENSMUSG00000028678	**Kif2c**	2,69
ENSMUSG00000000682	**Cd52**	2,69
ENSMUSG00000021176	**Efcab11**	2,68
ENSMUSG00000027360	**Hdc**	2,68
ENSMUSG00000028494	**Plin2**	2,67
ENSMUSG00000005397	**Nid1**	2,67
ENSMUSG00000041827	**Oasl1**	2,67
ENSMUSG00000048922	**Cdca2**	2,67
ENSMUSG00000051457	**Spn**	2,66
ENSMUSG00000102037	**Bcl2a1a**	2,65
ENSMUSG00000022548	**Apod**	2,64
ENSMUSG00000005087	**Cd44**	2,64
ENSMUSG00000079553	**Kifc1**	2,63
ENSMUSG00000031538	**Plat**	2,62
ENSMUSG00000039055	**Eme1**	2,62
ENSMUSG00000045382	**Cxcr4**	2,62

ENSMUSG00000036223	**Ska1**	2,62
ENSMUSG00000034773	**Hrob**	2,61
ENSMUSG00000097352	**C920009B18Rik**	2,60
ENSMUSG00000028391	**Wdr31**	2,60
ENSMUSG00000099974	**Bcl2a1d**	2,60
ENSMUSG00000028312	**Smc2**	2,60
ENSMUSG00000024659	**Anxa1**	2,59
ENSMUSG00000021886	**Gpr65**	2,58
ENSMUSG00000019987	**Arg1**	2,58
ENSMUSG00000101795	**Gm5835**	2,57
ENSMUSG00000021569	**Trip13**	2,57
ENSMUSG00000038943	**Prc1**	2,57
ENSMUSG00000027654	**Fam83d**	2,56
ENSMUSG00000034459	**Ifit1**	2,56
ENSMUSG00000040711	**Sh3pxd2b**	2,56
ENSMUSG00000026421	**Csrp1**	2,56
ENSMUSG00000031821	**Gins2**	2,55
ENSMUSG00000046295	**Ankle1**	2,55
ENSMUSG00000028551	**Cdkn2c**	2,54
ENSMUSG00000040212	**Emp3**	2,54
ENSMUSG00000025289	**Prdx4**	2,54
ENSMUSG00000036381	**P2ry14**	2,54
ENSMUSG00000007080	**Pole**	2,54
ENSMUSG00000021697	**Depdc1b**	2,53
ENSMUSG00000001025	**S100a6**	2,52
ENSMUSG00000044703	**Phf11a**	2,52
ENSMUSG00000039748	**Exo1**	2,52
ENSMUSG00000045954	**Cavin2**	2,51
ENSMUSG00000059089	**Fcgr4**	2,51
ENSMUSG00000002835	**Chaf1a**	2,50
ENSMUSG00000074802	**Gas2l3**	2,50
ENSMUSG00000022636	**Alcam**	2,50
ENSMUSG00000040528	**Milr1**	2,50
ENSMUSG00000029373	**Pf4**	2,48
ENSMUSG00000029322	**Plac8**	2,48
ENSMUSG00000101389	**Ms4a4a**	2,48
ENSMUSG00000023913	**Pla2g7**	2,48
ENSMUSG00000089782	**Btf3-ps1**	2,48
ENSMUSG00000029378	**Areg**	2,48
ENSMUSG00000027883	**Gpsm2**	2,47
ENSMUSG00000024590	**Lmnb1**	2,47
ENSMUSG00000000028	**Cdc45**	2,45
ENSMUSG00000028763	**Hspg2**	2,45
ENSMUSG00000024640	**Psat1**	2,45
ENSMUSG00000064349	**mt-Tc**	2,45
ENSMUSG00000033213	**AA467197**	2,45
ENSMUSG00000031756	**Cenpn**	2,45

ENSMUSG00000028108	**Ecm1**	2,44
ENSMUSG00000085939	**Cd63-ps**	2,44
ENSMUSG00000064368	**mt-Nd6**	2,44
ENSMUSG00000039814	**Xkr5**	2,44
ENSMUSG00000026228	**Htr2b**	2,43
ENSMUSG00000001517	**Foxm1**	2,43
ENSMUSG00000025498	**Irf7**	2,43
ENSMUSG00000081344	**Gm14303**	2,42
ENSMUSG00000030365	**Clec2i**	2,41
ENSMUSG00000031799	**Tpm4**	2,41
ENSMUSG00000015340	**Cybb**	2,41
ENSMUSG00000044080	**S100a1**	2,40
ENSMUSG00000039167	**Adgrl4**	2,40
ENSMUSG00000064372	**mt-Tp**	2,39
ENSMUSG00000030103	**Bhlhe40**	2,39
ENSMUSG00000024672	**Ms4a7**	2,39
ENSMUSG00000056054	**S100a8**	2,39
ENSMUSG00000043263	**Ifi209**	2,39
ENSMUSG00000044303	**Cdkn2a**	2,39
ENSMUSG00000026039	**Sgo2a**	2,38
ENSMUSG00000111118	**Gm6545**	2,38
ENSMUSG00000029910	**Mad2l1**	2,37
ENSMUSG00000054404	**Slfn5**	2,37
ENSMUSG00000031125	**3830403N18Rik**	2,37
ENSMUSG00000031146	**Plp2**	2,36
ENSMUSG00000022385	**Gtse1**	2,36
ENSMUSG00000020077	**Srgn**	2,36
ENSMUSG00000103377	**Gm37180**	2,36
ENSMUSG00000029561	**Oasl2**	2,35
ENSMUSG00000053038	**Gm6180**	2,35
ENSMUSG00000040658	**Dnph1**	2,35
ENSMUSG00000039899	**Fgl2**	2,35
ENSMUSG00000021714	**Cenpk**	2,35
ENSMUSG00000074896	**Ifit3**	2,35
ENSMUSG00000026873	**Phf19**	2,34
ENSMUSG00000082536	**Gm13456**	2,34
ENSMUSG00000036256	**Igfbp7**	2,34
ENSMUSG00000027074	**Slc43a3**	2,34
ENSMUSG00000020053	**Igf1**	2,33
ENSMUSG00000110275	**Gm5905**	2,33
ENSMUSG00000035352	**Ccl12**	2,33
ENSMUSG00000090272	**Mndal**	2,33
ENSMUSG00000039981	**Zc3h12d**	2,32
ENSMUSG00000023349	**Clec4n**	2,32
ENSMUSG00000067608	**Pcna-ps2**	2,32
ENSMUSG00000068101	**Cenpm**	2,32
ENSMUSG00000062488	**Ifit3b**	2,31

ENSMUSG00000056737	**Capg**	2,31
ENSMUSG00000033350	**Chst2**	2,31
ENSMUSG00000084349	**Rpl3-ps1**	2,31
ENSMUSG00000027555	**Car13**	2,31
ENSMUSG00000027800	**Tm4sf1**	2,31
ENSMUSG00000026335	**Pam**	2,30
ENSMUSG00000068744	**Psrc1**	2,29
ENSMUSG00000001542	**Ell2**	2,29
ENSMUSG00000004552	**Ctse**	2,29
ENSMUSG00000052776	**Oas1a**	2,28
ENSMUSG00000072620	**Slfn2**	2,28
ENSMUSG00000029516	**Cit**	2,28
ENSMUSG00000055555	**Ct55**	2,28
ENSMUSG00000005470	**Asf1b**	2,28
ENSMUSG00000028121	**Bcar3**	2,27
ENSMUSG00000035692	**Isg15**	2,27
ENSMUSG00000031304	**Il2rg**	2,27
ENSMUSG00000073418	**C4b**	2,25
ENSMUSG00000033721	**Vav3**	2,24
ENSMUSG00000027030	**Stk39**	2,24
ENSMUSG00000043483	**Gm6863**	2,24
ENSMUSG00000051235	**Gen1**	2,24
ENSMUSG00000021707	**Dhfr**	2,24
ENSMUSG00000034855	**Cxcl10**	2,24
ENSMUSG00000026622	**Nek2**	2,23
ENSMUSG00000056145	**AI504432**	2,23
ENSMUSG00000049134	**Nrap**	2,21
ENSMUSG00000072082	**Ccnf**	2,21
ENSMUSG00000020638	**Cmpk2**	2,21
ENSMUSG00000036181	**H1f2**	2,21
ENSMUSG00000028583	**Pdpn**	2,21
ENSMUSG00000028702	**Rad54l**	2,21
ENSMUSG00000027330	**Cdc25b**	2,21
ENSMUSG00000081603	**Gm14681**	2,20
ENSMUSG00000002985	**Apoe**	2,20
ENSMUSG00000025395	**Prim1**	2,20
ENSMUSG00000027203	**Dut**	2,20
ENSMUSG00000024066	**Xdh**	2,20
ENSMUSG00000041736	**Tspo**	2,20
ENSMUSG00000038252	**Ncapd2**	2,20
ENSMUSG00000021391	**Cenpp**	2,20
ENSMUSG00000030830	**Itgal**	2,20
ENSMUSG00000022945	**Chaf1b**	2,20
ENSMUSG00000028037	**Ifi44**	2,19
ENSMUSG00000086712	**Mexis**	2,19
ENSMUSG00000074364	**Ehd2**	2,19
ENSMUSG00000017861	**Mybl2**	2,19

ENSMUSG00000032690	**Oas2**	2,19
ENSMUSG00000054720	**Lrrc8c**	2,19
ENSMUSG00000040322	**Slc25a24**	2,18
ENSMUSG00000030142	**Clec4e**	2,18
ENSMUSG00000020185	**E2f7**	2,18
ENSMUSG00000029761	**Cald1**	2,18
ENSMUSG00000042029	**Ncapg2**	2,18
ENSMUSG00000037849	**Ifi206**	2,17
ENSMUSG00000053965	**Pde5a**	2,17
ENSMUSG00000020044	**Timp3**	2,17
ENSMUSG00000054203	**Ifi205**	2,17
ENSMUSG00000027322	**Siglec1**	2,16
ENSMUSG00000043091	**Tuba1c**	2,16
ENSMUSG00000041362	**Shtn1**	2,16
ENSMUSG00000030536	**Iqgap1**	2,16
ENSMUSG00000039470	**Zdhhc2**	2,15
ENSMUSG00000048612	**Myof**	2,15
ENSMUSG00000022881	**Rfc4**	2,15
ENSMUSG00000026879	**Gsn**	2,15
ENSMUSG00000047139	**Cd24a**	2,15
ENSMUSG00000025324	**Atp10a**	2,14
ENSMUSG00000020841	**Cpd**	2,14
ENSMUSG00000036103	**Colec12**	2,14
ENSMUSG00000050299	**Gm9843**	2,14
ENSMUSG00000021508	**Cxcl14**	2,13
ENSMUSG00000028480	**Glipr2**	2,13
ENSMUSG00000098090	**2700099C18Rik**	2,13
ENSMUSG00000024795	**Kif20b**	2,13
ENSMUSG00000025383	**Il23a**	2,13
ENSMUSG00000021493	**Pdlim7**	2,12
ENSMUSG00000051220	**Ercc6l**	2,12
ENSMUSG00000029086	**Prom1**	2,12
ENSMUSG00000032113	**Chek1**	2,11
ENSMUSG00000064367	**mt-Nd5**	2,11
ENSMUSG00000021696	**Elovl7**	2,11
ENSMUSG00000025494	**Sigirr**	2,10
ENSMUSG00000042284	**Itga1**	2,10
ENSMUSG00000083892	**Gm1848**	2,10
ENSMUSG00000020932	**Gfap**	2,09
ENSMUSG00000050410	**Tcf19**	2,08
ENSMUSG00000040855	**Reps2**	2,08
ENSMUSG00000037944	**Ccr7**	2,07
ENSMUSG00000069516	**Lyz2**	2,07
ENSMUSG00000005824	**Tnfsf14**	2,06
ENSMUSG00000034883	**Lrr1**	2,06
ENSMUSG00000037370	**Enpp1**	2,06
ENSMUSG00000042712	**Tceal9**	2,06

ENSMUSG00000083863	**Gm13341**	2,06
ENSMUSG00000085295	**4930430E12Rik**	2,05
ENSMUSG00000033644	**Piwil2**	2,05
ENSMUSG00000025351	**Cd63**	2,05
ENSMUSG00000050953	**Gja1**	2,04
ENSMUSG00000110344	**Gm45716**	2,04
ENSMUSG00000021360	**Gcnt2**	2,04
ENSMUSG00000060147	**Serpinb6a**	2,04
ENSMUSG00000022150	**Dab2**	2,04
ENSMUSG00000039209	**Rpl39l**	2,03
ENSMUSG00000054072	**Iigp1**	2,03
ENSMUSG00000106037	**Gm4332**	2,03
ENSMUSG00000031503	**Col4a2**	2,03
ENSMUSG00000052397	**Ezr**	2,03
ENSMUSG00000033082	**Clec1a**	2,02
ENSMUSG00000020641	**Rsad2**	2,02
ENSMUSG00000027009	**Itga4**	2,02
ENSMUSG00000035042	**Ccl5**	2,02
ENSMUSG00000029380	**Cxcl1**	2,02
ENSMUSG00000074785	**Plxnc1**	2,02
ENSMUSG00000032679	**Cd59a**	2,02
ENSMUSG00000025321	**Itgb8**	2,01
ENSMUSG00000001506	**Col1a1**	2,01
ENSMUSG00000069833	**Ahnak**	2,01
ENSMUSG00000103308	**Gm37800**	2,01
ENSMUSG00000040147	**Maob**	2,01
ENSMUSG00000060591	**Ifitm2**	2,01
ENSMUSG00000025059	**Gk**	2,01
ENSMUSG00000043421	**Hilpda**	2,00
ENSMUSG00000097654	**Gm26714**	2,00
ENSMUSG00000002068	**Ccne1**	2,00
ENSMUSG00000026355	**Mcm6**	2,00
ENSMUSG00000007872	**Id3**	2,00
ENSMUSG00000031198	**Fundc2**	2,00

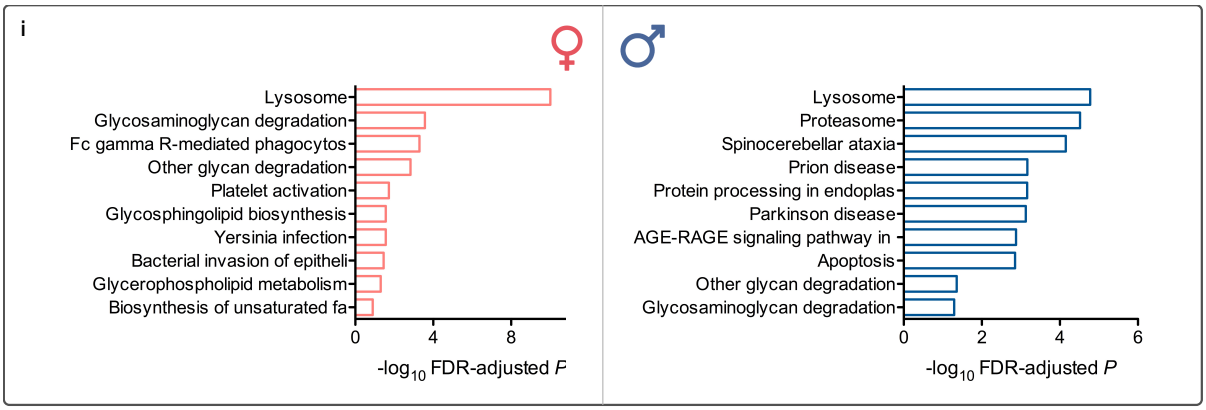

j

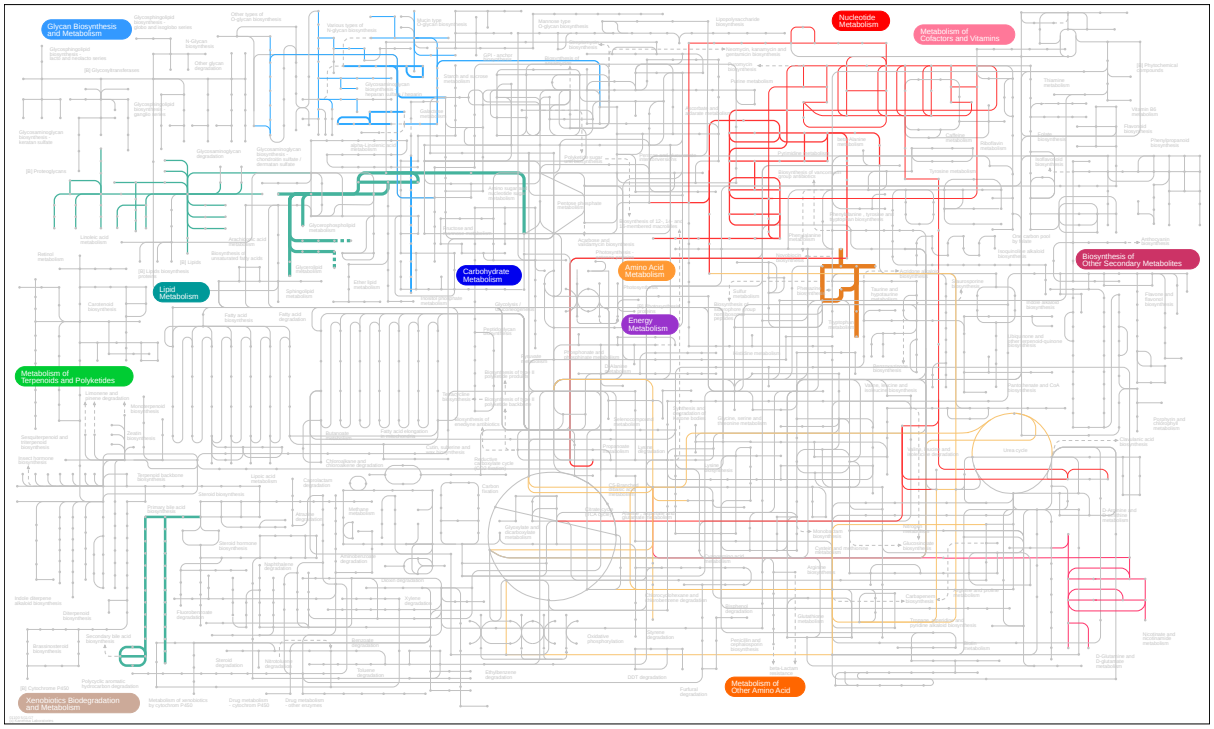
Glycan Biosynthesis and Metabolism
Nucleotide Metabolism
Metabolism of Cofactors and Vitamins
Carbohydrate Metabolism
Amino Acid Metabolism
Biosynthesis of Other Secondary Metabolites
Lipid Metabolism
Energy Metabolism
Metabolism of Terpenoids and Polyketides
Metabolism of Other Amino Acid
Xenobiotics Biodegradation and Metabolism

k

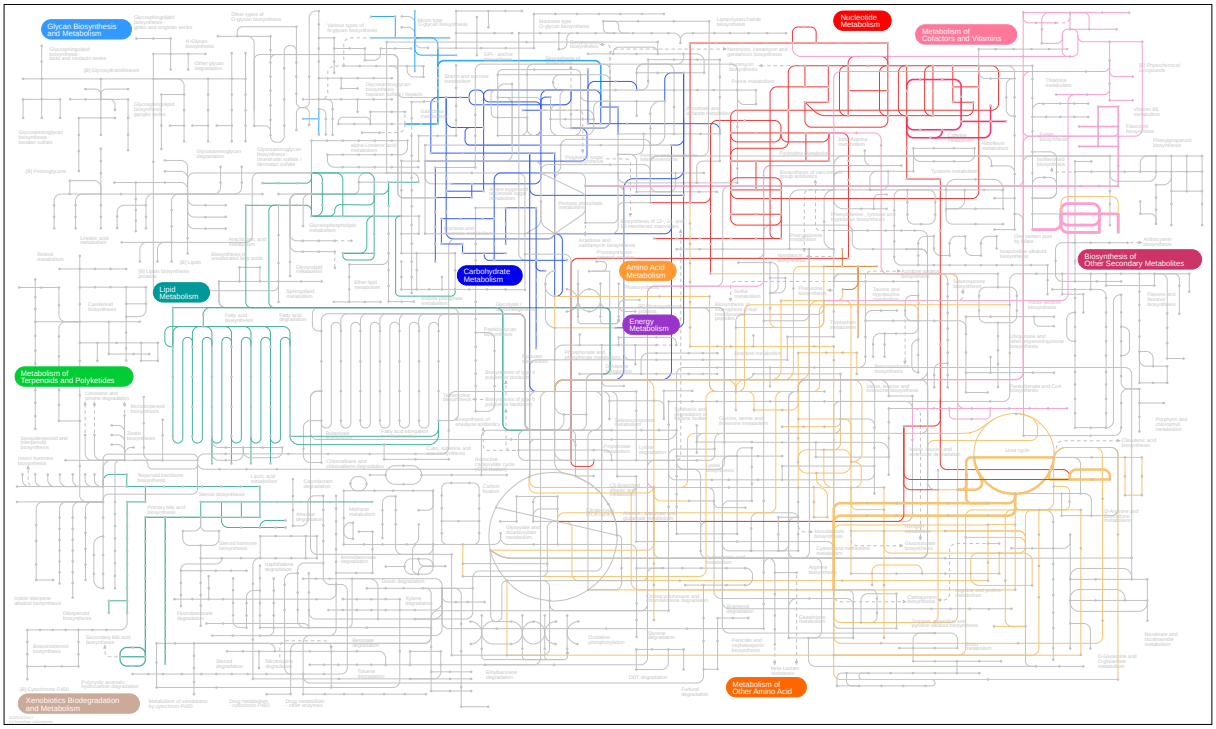
Glycan Biosynthesis and Metabolism
Nucleotide Metabolism
Metabolism of Cofactors and Vitamins
Carbohydrate Metabolism
Amino Acid Metabolism
Biosynthesis of Other Secondary Metabolites
Lipid Metabolism
Energy Metabolism
Metabolism of Terpenoids and Polyketides
Metabolism of Other Amino Acid
Xenobiotics Biodegradation and Metabolism

Supplementary Figure 3: Peripheral cell type accumulation in the CNS

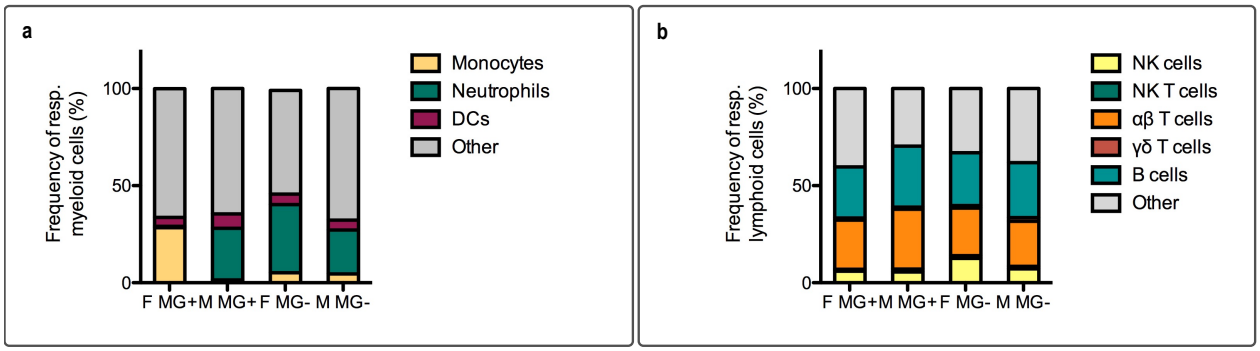

Supplementary Figure 3 | a-b, Changes in myeloid **(a)** and lymphoid **(b)** populations distribution of female and male Cx3Cr1creERT2 x iDTR- x eYFP (MG+) and Cx3Cr1creERT2 x iDTR+ x eYFP (MG-) mice three days after stroke.

Eidesstattliche Erklärung – Declaration on oath

Hiermit erkläre ich an Eides statt, dass ich die vorliegende Dissertation selbst verfasst und keine anderen als die angegebenen Quellen und Hilfsmittel verwendet habe.

I hereby declare, on oath, that I have written the present dissertation by my own and have not used other than the aknowledged resources and aids.

Hamburg, den 01.09.2023 Unterschrift